Submitted to The Astrophysical Journal
Preprint typeset using LaTeX style emulateapj

THE CENTRAL REGION OF BARRED GALAXIES: MOLECULAR ENVIRONMENT, STARBURSTS, AND SECULAR EVOLUTION

Shardha Jogee[1], Nick Scoville[2], & Jeffrey D. P. Kenney[3]

Submitted to The Astrophysical Journal

ABSTRACT

We study the molecular environment, the onset of starbursts, and secular evolution in the circumnuclear (inner 1–2 kpc) region of barred galaxies using a carefully selected sample of barred non-starbursts and starbursts, along with a panchromatic dataset made of high resolution CO (J=1–0) observations, optical, NIR, Hα, radio continuum, Brγ, and archival *HST* data. **(1)** We find that the molecular environment which has built up in the inner kpc of barred galaxies departs markedly from that present in the outer disk of galaxies. It involves molecular gas masses of 3×10^8 to 2×10^9 M$_\odot$, molecular gas surface densities of 500-3500 M$_\odot$ pc^{-2}, gas mass fractions of 10 to 30 %, and epicyclic frequencies of several 100 to several 1000 km s^{-1} kpc^{-1}. In this environment, gravitational instabilities can set in only at very high gas densities (few 100-1000 M$_\odot$ pc^{-2}), but once triggered, they grow on a short timescale of a few Myrs. This high density short timescale 'burst' mode may explain why the most intense starbursts tend to be in the central parts of galaxies. The molecular environment in the inner kpc of the ultra luminous infrared galaxy Arp 220 is a scaled up version of the one shown by barred starbursts, suggesting that interactions build up even more extreme conditions. **(2)** The barred starbursts and non-starbursts have circumnuclear SFRs of 3–11 and 0.1–2 M$_\odot$ yr^{-1}, respectively, although they host comparable amounts of molecular hydrogen in the inner few kpc. We suggest that some of the large variations in SFR per unit gas mass (SFR/$M_{\rm H2}$) are tied in to different stages of bar-driven inflow. In non-starbursts which are in the early stages of bar-driven inflow (henceforth type I non-starbursts), a large fraction of the circumnuclear gas is still along the large-scale stellar bar, has large non-circular kinematics and is not forming stars efficiently. In contrast, the starbursts and several non-starbursts (henceforth type II non-starbursts) seem to be in *later* stages of bar-driven inflow where their circumnuclear molecular gas is already concentrated within the inner kpc, inside the outer inner Lindblad resonance of the bar, and has predominantly circular motions. The higher SFR/$M_{\rm H2}$ in the starbursts may be related to the fact that their gas surface densities are larger (1000–3500 $M_\odot$ pc^{-2}) and close to the Toomre critical density over a large region. **(3)** In both barred non-starbursts and starbursts, the Q parameter reaches its minimum value of $\sim$ 1–2 in the region of star formation, despite an order of magnitude variation in the gas surface density and epicyclic frequency. This remarkable behavior strongly suggests that the onset of gravitational instabilities as characterized by Q plays an important role even in the inner kpc region. **(4)** We suggest that an episode of bar-driven inflow causes a barred galaxy to go through starburst and non-starburst phases typified by our sample. This may partly explain why no one-to-one correlation is seen between bars and central starbursts, even if a statistical correlation exists at the high luminosity end. The dynamical mass enclosed within the inner kpc radius of the barred galaxies in our sample is 6–30 $\times 10^9$ $M_\odot$ and can increase by several % over a Gyr for nominal bar-driven inflow rates. We present evidence that the inner kpc of selected sample galaxies are building compact stellar components which have disk-like properties and may belong to the class of pseudo-bulges (Kormendy 1993). We speculate that over its lifetime, a barred galaxy can experience numerous episodes of minor mergers and bar-driven gas inflows which can cause a buildup of the central mass concentration, bulge, and lead to secular evolution along the Hubble sequence.

1. INTRODUCTION

It is widely recognized today that non-axisymmetries such as large-scale stellar bars and general triaxialities facilitate the radial transfer of angular momentum and mass in disk galaxies, thus driving their dynamical and secular evolution. Recent observations (e.g., Ho et al. 1997; Knapen et al. 2000; Eskridge et al. 2000; Grosbol 2002) have compellingly shown that the majority (> 70 %) of nearby disk galaxies host large-scale stellar bars. It is widely believed that such bars efficiently drives gas from the outer disk into the inner kpc through a combination of gravitational torques and dissipative effects. In support of this picture, interferometric CO observations by Sakamoto et al.(1999) have demonstrated that barred galaxies tend to have larger molecular gas concentration within the inner kpc than unbarred galaxies. Several studies also show that very luminous starbursts tend to preferentially be in barred galaxies (Hunt & Malkan 1999; Hawarden et al. 1986; Mazzarella & Balzano 1986), but no strong correlations are seen in the Ho et al. (1997) sample which includes

[1]Space Telescope Science Institute, 3700 San Martin Drive, Baltimore, MD 21218
[2]Division of Physics, Mathematics, and Astronomy, MS 105-24, California Institute of Technology, Pasadena, CA 91125
[3]Yale University Astronomy Department, New Haven, CT 06520-8101

lower luminosity HII nuclei.

While correlations likely exist in a statistical sense between bars and starbursts, or between bars and large molecular gas concentrations, there are many poorly understood questions. For instance, no one-to-one correlation exists between the presence of a bar and a central starburst, and even barred spirals with apparently similar gas content within their circumnuclear (inner 1–2 kpc) region show a large variation in circumnuclear star formation rate (SFR; § 2). Furthermore, numerous secular evolutionary scenarios contend that bar-driven inflow can drive morphological evolution along the Hubble sequence (e.g., Friedli & Martinet 1993; Friedli & Benz 1995), but observational constraints on this process are only slowly accumulating.

In this study, we use a panchromatic dataset made of high resolution ($2''$; 100-200 pc) CO (J=1–0) observations, optical, NIR, Hα, radio continuum (RC), Brγ, and archival *HST* data in order to characterize the molecular environment, the onset of starbursts, and the dynamical evolution in the circumnuclear region of barred galaxies. Our sample consists of ten carefully selected nearby barred non-starbursts and starbursts, including some of the most luminous starbursts within 40 Mpc. This is a sizeable sample because high resolution ($2''$) interferometric CO observations require a heavy time investment. In fact, the interferometric observations for such a sample had to be carried out over a period of five years. Furthermore, high resolution (1–$2''$) CO observations of nearby galaxies have in the past often been limited to a few individual systems, and it is only in recent years that we have seen a systematic mapping of sizeable samples (10–12) of nearby galaxies (e.g., Baker 2000; Jogee 1999). Complementary surveys such as the $7''$ resolution BIMA CO(1–0) Survey of Nearby Galaxies (SONG; Regan et al. 2001; Helfer et al. 2001) or the NMA–OVRO $4''$ resolution CO(1–0) survey of galaxies (Sakamoto et al. 1999) are better suited for studying extended structures or the average properties within the inner 500 pc.

The main sections of the paper are as follows. § 2 outlines the sample selection and § 3 the properties of stellar bars in the sample galaxies. The imaging and interferometric CO observations are covered in § 4. § 6 highlights the extreme molecular environment which has built up in the inner kpc of barred galaxies and discusses its implication. In § 7, we estimate SFRs using different tracers such as Brγ, RC, and FIR luminosities, and use these values to estimate the SFR in the circumnuclear region. In § 8, we turn to a comparison of the circumnuclear molecular gas in the barred starbursts and non-starbursts with the overall goal of understanding why they have such different SFR/$M_{\rm H2}$ in the inner few kpc. In § 9, we push this investigation further by comparing the observed circumnuclear gas surface density to the critical density for the onset of gravitational instabilities. In § 10, we investigate where the molecular gas has piled up with respect to the dynamical resonances of the bar. In § 11, we discuss the results within the context of bar-driven secular evolutionary scenarios. For readers interested in specific galaxies, § 12 describes the molecular gas distribution and kinematics of individual galaxies. § 12 summarizes our main results.

2. SAMPLE SELECTION

In this study, we wish to investigate the properties of molecular gas in the circumnuclear region (inner 1–2 kpc) of barred galaxies, the parameters which control when they form stars, and the reasons for the large range in SFR/M_{H2} seen in the inner few kpc. In order to effectively address these questions, we will carry out high resolution ($2''$) interferometric CO observations (§ 2) of the sample galaxies. However, when selecting the sample prior to such observations, we necessarily have to use existing low resolution ($45''$) single dish CO luminosities (e.g., Young et al. 1995) as a first measure of the mass of cold molecular hydrogen (Dickman, Snell, & Schloerb 1986; Scoville & Sanders 1987). We avoided systems with very low CO luminosities as the high resolution interferometric CO observations would be too time-intensive. We obtain a measure of the massive SF rate within the same $45''$ aperture from the RC luminosity ($L_{\rm RC}$) at 1.5 GHz (e.g., Condon et al. 1990). Empirical evidence such as the FIR-RC correlation (Condon et al. 1982; Helou, Soifer, & Rowan-Robinson 1985) the Hα- RC correlation (Kennicutt 1983), as well as simple physical models (e.g., Condon 1992) suggest that the RC luminosity at 1.5 GHz is a good tracer of the massive SFR on sufficiently large scales. The FIR-radio correlation also appears to hold locally within individual galaxies at least on scales ≥ 1 kpc (Condon 1992).

We selected ten sample galaxies which satisfy the following criteria: **(i)** They lie in different parts of the $L_{\rm RC}/L_{\rm CO}$ versus $L_{\rm CO}$ plane (Fig. 1) such that they span a wide range in circumnuclear gas content and SFR per unit mass of gas. **(ii)** They have moderate and comparable distances (typically D=15 to 25 Mpc) so that the $2''$ interferometric CO observations (§ 2) can accurately resolve the gas distribution and kinematics on scales of 100-200 pc. (iii) They have moderate inclination (typically 30 to 55 deg) in order to minimize extinction problems and get a good handle on the gas kinematics. (iv) They have some complementary high resolution observations such as Brackett-γ fluxes (Puxley, Hawarden, & Mountain 1988, 1990), and 5 GHz RC observations (Saikia et al. 1994) for tracing the SF activity at resolutions comparable to that of the $2''$ interferometric CO observations. (v) We excluded major mergers with strong morphological distortions in the inner kpc region as the associated highly non-axisymmetric gas distributions and large non-circular motions often preclude an accurate dynamical analysis. This is discussed further in § 3.

Table 1 gives the general properties of the sample. Table 2 shows $L_{\rm CO}$, $L_{\rm RC}$, and the luminosities of different SF tracers within various apertures. Fig. 1 shows the sample galaxies plotted in the $L_{\rm RC}/L_{\rm CO}$ versus $L_{\rm CO}$ plane. The term 'starburst' is used in a multitude of ways in the literature: in some cases, a large SF luminosity alone is used to identify a star-forming region as a starburst, while in other cases the duration of the burst is also taken into account. In this work, the term circumnuclear starburst refers to a luminous and short-lived episode of SF in the inner kpc region. We adopt a working definition where the circumnuclear starbursts have a ratio ($L_{\rm RC}/L_{\rm CO}$) above 0.5, which corresponds to a gas consumption timescale ($M_{\rm H2}$/SFR) below 1 Gyr, under standard assumptions. The Milky Way has a (SFR/$M_{\rm H2}$) ratio above 10^{-9} yr^{-1}, and would be a non-starburst. The circumnuclear starbursts in our sample (NGC 470, NGC 2782, NGC 3504, NGC 4102, and NGC 4536) are marked on Fig. 1 and are amongst the most luminous starbursts within 40 Mpc. While they are selected on the basis of RC luminosities, the circumnuclear starbursts also have a large FIR luminosity, comparable to that of the prototypical starburst M82 which is marked for reference on Fig. 1. Four of the starbursts (NGC 470, NGC 2782, NGC 3504, and NGC 4102) in fact belong to Devereux's (1989) sample of the twenty brightest nearby ($15 < D < 40$ Mpc) circumnuclear starbursts selected on the basis of a high far-infrared luminosity ($L_{\rm FIR} > 2.9 \times 10^9 L_\odot$) and central 10 μm luminosity ($L_{10\mu{\rm m}} > 6 \times 10^8 L_\odot$).

Note that in Figure 1, *the SFR per unit mass of molecular gas in the central* $45''$ *spans more than an order of magnitude for a given total mass of molecular gas* . Can this range be due to the different distance of the sample galaxies causing the $45''$ beam to encompass regions of different sizes ? We believe this is unlikely because most of the SF activity is concentrated well inside the $45''$ beam, and most of the galaxies have comparable distances in the range 15–25 Mpc. In fact, a similar range in the SFR per unit mass of molecular gas is obtained if the central 10 micron luminosity (Giuricin et al. 1994; Devereux 1989) is used instead of the radio continuum to trace the SFR. It is also valid to ask whether variations in the CO-to-H_2 conversion factor χ between the galaxies might reduce the range in (SFR/$M_{\rm H2}$) on Fig. 1. We refer the reader to § 5 for a discussion on χ, but note here that the somewhat lower conversion factor in starbursts suggested by some studies (Aalto et al. 1994, 1995), would in fact *increase* rather than reduce the range in (SFR/$M_{\rm H2}$) in Fig. 1. Therefore, it appears that the range in SFR/$M_{\rm H2}$ within the sample is real.

3. STELLAR BARS AND TIDAL INTERACTIONS IN THE SAMPLE

Optical R-band images as well as NIR images which are less affected from extinction show evidence for large-scale stellar bars and oval distortions in all the sample galaxies. The latter are also classified as barred in the Third Reference Catalog of Bright Galaxies (RC3; de Vaucouleurs et al. 1991; Table 3). Figs. 2a-c illustrate the cases of NGC 3504, NGC 4314, and NGC 6951 where the large-scale bar is evident in the R-band or/and K-band image. In other cases such as NGC 4102, NGC 4536, or NGC 2782, there is less conspicuous evidence for a large-scale bar. In NGC 4102, both the K (Fig. 2d) and R-band images reveal a weaker oval distortion, with a surface brightness profile reminiscent of a lens (Jogee & Kenney 1996). Lenses may be dynamically related to chaotic stellar orbits in the bar region and in some systems they may be the remnants of a weakened or destroyed bar (e.g., Freeman 1996). In NGC 4536, the large inclination (66 deg) makes it difficult to clearly identify the stellar bar, but prominent spiral arms in the outer disk, appear to branch out from an oval structure, suggesting the presence of a large-scale stellar bar. Isophotal analysis of NIR images also indicate the presence of nested nuclear stellar bars in NGC 2782 (Jogee, Kenney, & Smith 1999; § 11) and NGC 4314 (Friedli et al. 1996; § 11).

The non-starburst NGC 3359 and NGC 4569 are interesting cases where the stellar bar may have been recently tidally triggered. Martin & Roy (1995) claim that the bar in NGC 3359 is younger than a Gyr, based on a comparisons of simulations (Friedli, Benz, & Kennicutt 1994) with properties of NGC 3359 such as the presence of HII regions along the bar and the abundance gradient profile which is steep inside the corotation resonance of the bar, but flattens sharply further out. The young bar may have been tidally induced by a nearby companion (Ball 1986). In the case of NGC 4569, the K-band isophotes (Fig. 6a) in the inner $45''$ (3.6 kpc) are significantly more elongated than in the outer disk. They suggest the presence of a boxy bulge in the inner $30''$ (2.9 kpc) radius, and a stellar bar-like feature at a P.A. of ~ 15 deg further out. Both bulge and bar show asymmetries: the bar is more elongated to the north than to the south, and the bulge isophotes show east-west asymmetries. Furthermore, the outer stellar disk has a warped appearance in the optical image reproduced in the Carnegie Atlas of Galaxies (Sandage & Bedke 1994). Although HI and optical properties of NGC 4569 were previously explained by ram pressure stripping (Kenney & Young 1989; Cayatte et al. 1994), the latter process only affects the diffuse atomic gas, but not the stellar component. Thus, a merger event or tidal interaction are also possible.

As stated in § 2, our sample excludes galaxies which are recent major mergers or/and have strong morphological distortions in the inner kpc region. While it is true that a correlation between starbursts and tidal interactions/mergers exist at the very high luminosity end (e.g., in bright Hickson Compact Group HII galaxies, ultra luminous infrared galaxies (ULIRGs)), it is *not* the purpose of our study to investigate correlations between starbursts and external environment. Thus, the exclusion of systems with strong morphological distortions is not a problem for our study. We still include in our sample galaxies which may be experiencing weaker interactions. In fact, all of the sample galaxies except for NGC 6951 show some evidence for tidal interaction in the recent past, or are in environments where they could potentially have interacted with or accreted other galaxies. This is illustrated in Table 3. NGC 470 is interacting with the large S0 galaxy NGC 474. NGC 2782 appears to have undergone a close, recent interaction with another smaller disk galaxy, and its properties have been modeled with an intermediate mass ratio (1:4) interaction by Smith (1994). NGC 3359 has a nearby companion. NGC 3504, NGC 4314, and NGC 4102 dwell in groups, while NGC 4569 and NGC 4536 are part of the Virgo cluster. As described above NGC 4569 shows several indications of a recent tidal disturbance. The galaxies NGC 2782 and NGC 470, with the largest mass-ratio interactions (1:4 and 1:1) are starbursts.

4. OBSERVATIONS

4.1. *CO (J=1->0) observations*

Table 4 describes the CO observations and channel maps. For seven sample galaxies (NGC 470, NGC 2782, NGC 3310, NGC 4102, NGC 4536, NGC 4569, and NGC 3359), $2''$ observations of the CO (J=1->0) line which has a rest frequency of 115.27 GHz, were made between 1995 and 2001 with the OVRO millimeter-wave interferometer (Padin et al. 1991). As of 1996, the array consists of six 10.4-m antennae with a primary HPBW of 65 $''$ at 115 GHz. The seven galaxies were observed in the low, equatorial, and high resolution configurations with projected baselines ranging from 15 to 242 m. Data were obtained simultaneously with an analog continuum correlator of bandwidth 1 GHz and a digital spectrometer setup which produced four independent modules that each have 32 channels with a velocity resolution of 10.4 km s^{-1}. For our observations, the modules were partially overlapping and covered a total bandwidth of 1200 km s^{-1} with 116 frequency channels. We corrected for temporal phase variations by interspersing integrations on the galaxy with observations of a phase calibrator (typically a quasar) every 20-25 minutes. Passbands were calibrated on the bright quasars 3C273, 3C84, and 3C345. The absolute flux scale, determined from observations of Uranus, Neptune, and 3C273, is accurate to 20%. The passband and flux calibration of the data were carried out using the Owens Valley millimeter array software (Scoville et al. 1993). We used the NRAO AIPS software to Fourier transform the calibrated uv data and deconvolve the channel maps with the 'CLEAN' algorithm as implemented in the AIPS tasks 'MX' and 'IMAGR'. Channel maps with both uniform and natural weighting were made for the galaxies. The naturally weighted maps capture more of the low signal-to-noise emission, but have lower spatial resolution.

4.2. *Optical observations*

We observed the ten sample galaxies using the Wisconsin Indiana Yale NOAO (WIYN) 3.5-m telescope at Kitt Peak National Observatory (KPNO), and the 0.9-m telescope at KPNO. On the WIYN telescope we used a 2048 x 2048 S2KB CCD with a plate scale of $0.2''$/pixel, and a field of view of $6.8'$x $6.8'$. On the 0.9-m, the 2048 x 2048 T2KA CCD had a plate scale of $0.68''$/pix, and field of view of $23.2'$ x $23.2'$. The galaxies were imaged with broad-band Harris $BVRI$ filters and narrow-band filters centered on the appropriately redshifted Hα+[N II] 6563 6583 Å emission lines. In order to subtract the stellar continuum light from the Hα+[N II] line images, continuum band images were taken using off-line filters centered on a wavelength $\sim$ 80 Å redward of the Hα+[NII] line. The continuum bandpass in this region is sufficiently close to the Hα+[NII] emission line that spectral color correction terms are generally negligible (Taylor et al. 1994). On nights where photometric conditions prevailed, galaxy exposures were interspersed with short exposures of spectrophotometric standards at airmasses similar to the galaxy exposure, in order to flux calibrate the Hα+[NII] observations. In a few cases, standard fields of Landolt stars (e.g., PG0918+029, PG1047+003, PG1323-086, WOLF 629, SA110-502) were observed throughout the night over a range of airmasses for extinction correction. The IRAF Package was used for data reduction. After bias-subtraction and flat-fielding, the images in each filter were registered using unsaturated field stars, combined, and cleaned free of cosmic rays. After sky subtraction, the off-line narrow-band image was subtracted from the on-line image to obtain continuum-free Hα+[NII] line images. The line images were flux calibrated using observations of spectrophotometric standards.

5. CIRCUMNUCLEAR MOLECULAR GAS CONTENT

The mass of molecular hydrogen ($M_{\rm H2}$) is estimated from the total flux using the relation (e.g., Scoville et al. 1987; Solomon et al. 1987; Kenney & Young 1989)

$$\frac{M_{\rm H2}}{(M_\odot)} = 1.1 \times 10^4 \; (\frac{\chi}{2.8 \times 10^{20}}) \; (D^2) \; (\int S_{\rm CO} dV) \quad (1)$$

where
- D is the distance in Mpc,
- $\int S_{\rm CO} dV$ is the integrated CO line flux in Jy km s^{-1}.
- χ is the CO-to-H_2 conversion factor, defined as the ratio of the beam-averaged column density of hydrogen to the integrated CO brightness temperature ($N(H_2)/I_{\rm CO}$).

Values of χ for molecular clouds in the Milky Way range from 1.8 to 4.5 $\times 10^{20}$ (K km $s^{-1})^{-1}$, based on different methods such as comparisons of the integrated ^{13}CO intensities with the visual extinction (e.g., Dickman 1975), observations of γ ray fluxes (e.g., Bloemen et al. 1984, 1986; Strong et al. 1988), and virial equilibrium considerations (e.g., Dickman et al. 1986; Scoville et al. 1987; Solomon et al. 1987). We assume in this paper the value of 2.8×10^{20} (K km $s^{-1})^{-1}$ obtained for the inner Galaxy by Bloemen et al. (1986).

The CO-to-H_2 conversion factor depends on many factors including the metallicity of the gas, the dust column density, the ambient radiation field, the physical conditions in the gas, and the optical thickness of the line. All the sample targets are massive spirals and they are likely to have solar or super-solar metallicities (Vila-Costas & Edmunds 1992); in this regime the CO line is probably optically thick, there is only a weak dependence of the CO-to-H_2 conversion factor on metallicity (e.g., Elmegreen 1989).

The use of a Milky Way conversion factor in the inner few kpc of galaxies with intense SF is somewhat uncertain. The gas may not be in or near virial equilibrium, and the molecular clouds can have different physical properties from Galactic clouds. For clouds in virial equilibrium χ depends on $\rho^{0.5}/T_{\rm B}$ (e.g., Scoville & Sanders 1987; Solomon et al. 1987), where $T_{\rm B}$ is the CO brightness temperature averaged over the cloud and ρ is the density. One might therefore argue that the effects of elevated temperatures and densities will partially offset each other in molecular clouds of starburst nuclei. On the other hand, multiple-line studies and radiative transfer modeling (e.g., Wall & Jaffe 1990; Helfer & Blitz 1993; Aalto et al. 1994, 1995) have suggested that the conversion factor in the centers of some starburst galaxies is lower than the Milky Way value by a factor of $\sim$ 3. However, given the absence of multiple-line studies or determinations of the CO-to-H_2 conversion factor in most of the galaxies in our sample, we adopt the Milky Way value, while bearing in mind the possible uncertainties.

Table 5 shows the CO flux and the mass of molecular hydrogen detected by the interferometric observations. In most galaxies we capture a large fraction (60 to 90 %) of the CO flux detected by single dish observations. We find massive gas concentrations $-$ 3×10^8 to 2×10^9 $M_\odot$ of molecular hydrogen –in the inner 2 kpc radius of the sample galaxies. In particular, many galaxies with different RC luminosities within the central $45''$ (e.g., NGC 6951 and NGC 4569 as compared to NGC 2782, NGC 3504, and NGC 4102) can have quite comparable circumnuclear molecular hydrogen content ($\sim 1-2\times 10^9$ $M_\odot$).

The distribution of the molecular gas as traced by the CO total intensity (moment 0) maps is shown for the starbursts and non-starbursts, respectively, in Figures 3a and 3b for the starbursts. The maps are drawn on a fixed linear scale and both the size of the synthesized beam and the position of the large-scale stellar bar are marked. Figs 3a-b reveal a wide variety of CO morphologies ranging from relatively axisymmetric annuli or disks (NGC 4102, NGC 3504, NGC 4536, NGC 470, and NGC 4314) to elongated double- peaked and spiral morphologies (starburst NGC 2782 and non-starbursts NGC 3351 and NGC 6951). We refer the reader to § 8 for a comparison of the molecular gas properties in the starbursts and non-starbursts, and to § 12 for a description of the individual galaxies in a case-by-case basis. But, first we highlight the remarkable molecular environment which has built up in the inner kpc of the sample galaxies.

6. THE EXTREME MOLECULAR ENVIRONMENT IN THE INNER KPC OF BARRED SPIRALS AND ITS IMPLICATIONS

The molecular environment which has developed in the circumnuclear region of the barred spirals differs markedly from that present in the outer disk of galaxies. We outline these marked differences in Table 6 and discuss how they impact the inner kpc.

(i) Gas densities and mass fraction: We compute the molecular gas surface densities ($\Sigma_{\rm gas-m}$) by deprojecting the moment 0 map and computing the azimuthally averaged surface density of molecular hydrogen ($\Sigma_{\rm H2}$) as a function of radius in the galactic plane, assuming a standard CO-to-H_2 conversion factor. We add in the contribution of He using $\Sigma_{\rm gas-m} = A_{\rm Z} \times \Sigma_{\rm H2}$, where $A_{\rm Z}$ is a numerical factor which depends on the metallicity. For the assumed solar metallicity (Z = 0.02, X=0.72, Y=0.26) $A_{\rm Z}$ = 1.36. The peak gas surface density $\Sigma_{\rm gas-m}$ in the inner kpc of these galaxies ranges from 500-3500 $M_\odot$ pc^{-2} (see § 8).

To estimate what fraction of the dynamical mass is in molecular form, we first calculate the total dynamical mass ($M_{\rm dyn}$) interior to radius R from the circular speed V_c :

$$M_{\rm dyn}(R) = \frac{V_{\rm c}^2(R)\ R\ \beta}{G} \qquad (2)$$

where G is the gravitational constant and β depends on the shape of the mass distribution. β=1 for a spherically symmetric mass distribution and is slightly lower for flattened configurations. For an exponential disk, we can overestimate the true dynamical mass by at most 1.3 if we assume β=1 (Binney & Tremaine 1987). We estimate $V_{\rm c}$ from the rotation curves derived from the CO spatial velocity plots and Hα spectroscopy (Jogee 1999). In regions where the gas shows evidence of non-circular motions in the spatial-velocity plots, estimates of $V_{\rm c}$ will be somewhat uncertain. We therefore make this estimate only for galaxies where the kinematics are relatively ordered and dominated by circular motions (§ 8).

In summary, we find that the inner kpc of the 11 barred spirals in our sample hosts peak molecular gas surface densities of 500-3500 M$_\odot$ pc^{-2} and molecular gas mass fractions of 10 to 30 %. *These densities are at least an order of magnitude higher than the typical average atomic and molecular gas surface densities (1-100 $M_\odot$ pc^{-2}) in the outer disk of normal spirals* (Deharveng et al. 1994; Kennicutt 1998), or the gas surface density (200 $M_\odot$ pc^{-2}) of a typical giant molecular cloud in the outer disk of the Milky Way (Scoville & Sanders 1987). Such large molecular gas surface densities and mass fraction in the inner kpc can *enhance the self gravity and clumpiness of the gas and produce stronger gravitational coupling between the gas and the stars* (e.g., Shlosman et al. 1989; Jog & Solomon 1984). The resulting two-fluid disk will be more unstable to gravitational instabilities than a purely stellar one-fluid disk (Jog & Solomon 1984; Elmegreen 1995) .

Furthermore, as the gas becomes more clumpy dynamical friction might become an increasingly important transport mechanism at low radii. For instance, in the case of a gas clump which has a mass M and a speed v at radius r, the timescale t_{df} on which dynamical friction operates is $\propto$ (r^2 v/M lnΛ), where lnΛ is the Coulomb logarithm (Binney & Tremaine 1987). Dynamical friction becomes quite effective for massive gas clumps at low radii: for M= 10^8 $M_\odot$, v $\sim$ 300 km s^{-1}, r=200 pc, t_{df} is as short as $\sim 3\times 10^6$ years.

(ii) Onset and growth of gravitational instabilities: For a thin differentially rotating gas disk, support against gravitational instabilities is provided by pressure forces on small scales, and by Coriolis forces from rotation on large scales. Gravitational forces only dominate above the Safronov (1960)/Toomre (1964) critical density ($\Sigma_{\rm crit}$) as described in detail in § 9. The Coriolis forces depend on the epicyclic frequency of oscillations κ which is a function of the circular speed $V_{\rm c}$:

$$\kappa = \sqrt{\frac{2V_{\rm c}}{R}(\frac{V_{\rm c}}{R} + \frac{dV_{\rm c}}{dR})}. \qquad (3)$$

We estimate κ from the CO and Hα rotation curves, bearing in mind that uncertainties exist in regions where there are non-circular motions. However, even uncertainties of a factor of a few do not change the basic finding of very high epicyclic frequencies κ of a few 100 to several 1000 km s^{-1} kpc^{-1}) in the inner 500 pc. These very high epicyclic frequencies coupled with the moderately large gas velocity dispersions (10-40 km s^{-1}) *cause the critical density ($\Sigma_{\rm crit}$) for the onset of gravitational instabilities to shoot up to several 100-1000 $M_\odot$ pc^{-2}. This is 1-2 orders of magnitude higher than the typical value of $\sim$ 10 $M_\odot$ pc^{-2} in the outer disk of spirals.* Although hard to trigger, once triggered, these instabilities have a short growth timescale ($t_{\rm GI}$) of a few Myrs for the most unstable wavelength:

$$t_{\rm GI} = \frac{\sigma}{\pi {\rm G}\ \Sigma_{\rm gas}} \qquad (4)$$

These considerations therefore imply that in the inner kpc gravitational instabilities can only set in at high gas densities, and these densities naturally lead to a rapid growth timescale. In other words, *the molecular environment and dynamical parameters of the inner kpc naturally force gravitational instabilities to set in and to grow in a "burst" mode defined by high density and short timescales.*

This may explain, at least in part, why the most intense starbursts tend to be found in the inner kpc of galaxies.

It is also important to note that the growth timescale (t_{GI}) of a few Myr in the inner kpc is comparable to the lifetime of an OB star. As a result, the fraction of molecular gas mass converted into stars before cloud complexes are disrupted by massive stars can be higher in the circumnuclear region than in the outer disk. The high pressure, high turbulence ISM may also favor more massive clusters as suggested by some authors (e.g., Elmegreen et al. 1993). It is relevant that 80 % of the sample galaxies show super star clusters.

(iii) ULIRGs as scaled-up local starbursts? In the circumnuclear region of the ULIRG Arp 220 (Scoville, Yun, & Bryant 1997), the conditions observed (Column 4 of Table 6) seem to be even more extreme than those in the inner kpc of the local barred starbursts (column 3 of Table 6). ULIRGs host higher surface densities of 10^4 $M_\odot$ pc^{-2}, velocity dispersion σ of 90 km s^{-1}, and epicyclic frequency κ of several 1000 km s^{-1} kpc^{-1}. Inspection of of Table 6 suggests that *the circumnuclear molecular environment of ULIRGs may be a scaled-up versions of that developed by the local starbursts in our sample.* In contrast to our sample galaxies (§ 3), ULIRGs are generally strongly interacting systems, often involving mergers of comparable mass spirals. This suggests that the strong interactions in the ULIRGs lead to even more extreme conditions in the inner kpc than bars do. It is possible that these interactions pile gas to very high densities in the inner kpc, produce larger turbulent linewidths and in some cases a deeper stellar potential (larger κ). The last two conditions would necessarily boost the critical density $\Sigma_{\rm crit}$ at which gravitational instabilities can set in, thereby ensuring the conditions for a super-starburst.

7. THE CIRCUMNUCLEAR SF RATE

When using the 45$''$ single dish CO map as a measure of the circumnuclear gas content (e.g., in § 2), it was appropriate to use the RC luminosity within a similar 45$''$ aperture as a measure of the circumnuclear SFR. The 45$''$ aperture corresponds to an aperture with a 2 kpc radius at the mean sample distance of 20 Mpc. However, now that we have obtained high resolution (2$''$) interferometric CO maps, it is important to estimate the star formation rate (SFR$_{\rm CO}$) within the radius ($R_{\rm CO}$) which encompasses most of the detected CO emission. We can then verify if the large range in SFR/$M_{\rm H2}$ seen within the sample when using 45$''$ averaged data persists even at higher resolution. $R_{\rm CO}$ is estimated by determining where the azimuthally averaged gas surface density falls below a few % of its peak value, and ranges from 500 to 1680 pc (Table 8).

We estimate SFR$_{\rm CO}$ within $R_{\rm CO}$ by considering an ensemble of SFRs derived from different tracers which each may offer a different advantage in terms of resolution, apertures, and extinction. For instance, a well-established physical framework exists linking Hα recombination lines to the UV continuum photons from massive young stars, but Hα fluxes can be strongly affected by extinction in the dusty circumnuclear region where gas densities reach several 100 to 1000 M$_\odot$ pc^{-2}. On the other hand, tracers such as the far-infrared or RC luminosity are less affected by extinction but their lower spatial resolution may not always enable us to estimate SFR within the radius $R_{\rm CO}$.

Sections (i) to (iii) below outline how we estimate SFRs from the global FIR luminosity, the Brγ luminosity, the non-thermal and thermal components of the RC emission which we denote, respectively, as SFR$_{\rm FIR}$, SFR$_{Br\gamma}$, SFR$_{RC-N}$, and SFR$_{RC-T}$. Table 7 summarizes the values and apertures for each tracer. We refer the reader to Appendix 1 for a more detailed description of the physical basis for each tracer.

(i) SFR based on the the global FIR luminosity (SFR$_{\rm FIR}$): The global FIR luminosity traces the massive SFR over the entire galaxy, under the assumption that most of FIR emission between 40 and 120 μm emanates from warm dust heated by massive stars. SFR$_{\rm FIR}$ was computed from

$$(\frac{\rm SFR}{M_\odot {\rm yr}^{-1}}) = 4.3 \times {\rm SFR}({\rm M} \geq 5{\rm M}_\odot) = \gamma \times (\frac{\rm L_{FIR}}{10^{10}{\rm L}_\odot}) \quad (5)$$

where SFR ($M \geq 5M_\odot$) is the rate of formation of stars with mass $M \geq 5M_\odot$. An extended Miller-Scalo IMF (Kennicutt 1983) with an upper mass cut-off $M_{\rm U}$ of 100 $M_\odot$ is assumed. We adopt γ= 3.9 (Condon 1992) following the assumptions in Appendix 1. As shown in Table 7, the global SFR ranges from 6 to 14 $M_\odot$ yr^{-1} for the starbursts and from 0.2 to 4 $M_\odot$ yr^{-1} for the non-starbursts. These values apply to the entire galaxy and therefore serve as an upper limit to the SFR in the circumnuclear region.

(ii) SFR based on the non-thermal and thermal component of the RC emission (SFR$_{RC-N}$, SFR$_{\rm RC-T}$): The thermal free-free emission from the photoionized HII regions and the non-thermal RC emission produced by relativistic electrons which are accelerated by supernova remnants are both related to the massive SFR as described in Appendix 1. The RC flux density at 1.5 and 4.9 GHz is dominated by non-thermal emission. We estimate the non-thermal fraction to be 0.88 at 1.5 GHz and 0.77 at 4.9 GHz following the approximation by Condon & Yin (1990) :

$$(\frac{S}{S_{\rm T}}) = 1 \ + \ 10 \times (\frac{\nu}{\rm GHz})^{0.1-\alpha} \quad (6)$$

where the non-thermal index α is $\sim$ 0.8. From the non-thermal component of the RC luminosity density ($L_{{\rm N}\nu}$), we estimate the star formation rate SFR$_{\rm RC-N}$ within the radius $R_{\rm RC}$ using

$$(\frac{SFR_{\rm RC-N}}{M_\odot {\rm yr}^{-1}}) = 4.3 \times 0.019 \times (\frac{\nu}{\rm GHz})^{\alpha} \ (\frac{L_{{\rm N}\nu}}{10^{20} \ {\rm WHz}^{-1}}) \quad (7)$$

This equation is derived in Appendix 1 and assumes the Galactic relationship between the supernova rate and the RC luminosity density. As shown in Table 7, SFR$_{\rm RC-N}$ applies to the region of radius R$_{\rm RC}$ which covers the inner 1-2 kpc, except for NGC 3359 and NGC 4314 where larger apertures apply. SFR$_{\rm RC-N}$ ranges from 3 to 14 $M_\odot$ yr^{-1} for the starbursts and from 0.1 to 2 $M_\odot$ yr^{-1} for the non-starbursts. When estimating SFRs in NGC 6951, we excluded the luminosity contribution from the inner 100 pc radius to avoid contamination from the Seyfert nucleus which is known to exist from optical line ratios (Munoz-Tunon et al. 1989)

We estimate the star formation rate ($\mathrm{SFR_{RC-T}}$) from the thermal component of the RC emission ($L_{\mathrm{T}\nu}$), following the assumptions in Appendix 1 :

$$(\frac{SFR_{\mathrm{RC-T}}}{M_{\odot}\mathrm{yr}^{-1}}) \;=\; 4.3 \times 0.176 \;\times (\frac{L_{\mathrm{T}\nu}}{10^{20}\ \mathrm{WHz}^{-1}}) \;\times (\frac{T_{\mathrm{e}}}{10^{4}\ \mathrm{K}})^{-0.45}\ (\frac{\nu}{\mathrm{GHz}})^{0.1} \quad (8)$$

$\mathrm{SFR_{RC-T}}$ is slightly lower than $\mathrm{SFR_{RC-N}}$, but the difference is only at the 5 % level. It is encouraging that the same trend is seen in $\mathrm{SFR_{RC-N}}$ as in $\mathrm{SFR_{FIR}}$: the starbursts have larger SFRs (3 to 14 $M_{\odot}$ yr^{-1}) than the non-starbursts (0.1 to 2 $M_{\odot}$ yr^{-1}). Figure 4 shows $\mathrm{SFR_{RC-N}}$ plotted against $\mathrm{SFR_{FIR}}$. We expect $\mathrm{SFR_{RC-N}}$ to be comparable to $\mathrm{SFR_{FIR}}$ and this turns out to be the case for all galaxies except NGC 2782 and NGC 3504, where $\mathrm{SFR_{RC-N}}$ is 10 to 30 % higher. This could be caused by a variety of reasons. The dust temperature and emissivities could be different from those assumed in Appendix 1, such that $\mathrm{SFR_{FIR}}$ underestimates the true global SFR. Another possibility is that part of the non-thermal RC emission is coming from starburst-driven outflows where the empirical Galactic relationship between the supernova rate and the RC luminosity density in star-forming regions assumed in Appendix 1 might not hold. In fact, in NGC 2782, the high (1″) resolution RC map (Saikia et al. 1994) shows that a large fraction of the RC emission emanates from double outflow shells which extend 850 pc away from the central starburst (Jogee et al. 1998). It is also possible that part of the non-thermal RC emission may be due to a hidden active nucleus, although there is no evidence from optical line ratios for an active nucleus in these two galaxies .

(iii) SFR based on Brγ fluxes ($SFR_{Br\gamma}$): The Brγ recombination line at 2.16 μm, under the assumptions listed in Appendix 1, traces Lyman continuum photons from massive stars. Published Brγ fluxes (e.g., Puxley et al. 1990) are only available for four starbursts NGC 2782, NGC 3504, NGC 4102, and NGC 4536 and for the non-starburst NGC 3351. As shown in Table 7, the radius $R_{Br\gamma}$ of the region over which Brγ observations were made varies between 500 to 1600 pc depending on the galaxy. $\mathrm{SFR}_{Br\gamma}$ is 1 to 6 $M_{\odot}$ yr^{-1} for the starbursts and 0.5 $M_{\odot}$ yr^{-1} for the non-starburst NGC 3351, as computed from :

$$(\frac{\mathrm{SFR}}{M_{\odot}\mathrm{yr}^{-1}}) = 11.97 \times 10^{-54}\ (\frac{N_{\mathrm{Ly}}}{\mathrm{s}^{-1}}) \quad (9)$$

$\mathrm{SFR_{RC-N}}$ is larger by a factor of 2 to 5 with respect to $\mathrm{SFR}_{Br\gamma}$ in the galaxies NGC 2782, NGC 3504, NGC 4102, and NGC 4536, where both SF rates are measured over comparable radii. It is likely that $\mathrm{SFR}_{Br\gamma}$ underestimates the true SFR as the Brγ data and ionization rate ($\mathrm{N_{Ly}}$) quoted by Puxley et al. (1990) have not been corrected for extinction at 2.2 μm. Dust within an internally dusty HII region can absorb Lyman continuum photons before they ionize any H atom, and dust along the line of sight can absorb part of the Brγ recombination photons.

Table 7 summarizes the SFR estimated ($\mathrm{SFR_{FIR}}$, $\mathrm{SFR}_{Br\gamma}$, SFR_{RC-N}, and SFR_{RC-T}) from the above tracers and the aperture over which it applies. From these values, we make a best estimate for $\mathrm{SFR_{CO}}$, the extinction-corrected SFR within the radius (R_{CO}) over which CO emission is detected in the moment maps. In the case of NGC 470, NGC 2782, NGC 4102, NGC 4536, and NGC 4569, we consider $\mathrm{SFR_{RC-N}}$ to be a reasonable estimate for $\mathrm{SFR_{CO}}$ since the RC maps show that most of the RC emission is concentrated within R_{CO}. For the remaining galaxies NGC 3504, NGC 3351, and NGC 4314, ($R_{\mathrm{RC}}/R_{\mathrm{CO}}$) is 0.6, 1.7, and 6.0 respectively. In NGC 3504, $\mathrm{SFR_{RC-N}}$ is a reasonable approximation for the SF rate within R_{CO} (1300 pc) because the Hα map shows that more than 90 % of Hα flux within R_{CO} originates from the inner 800 pc radius. In the case of NGC 3351, R_{CO} is $\sim$ 600 pc which is close to $R_{\mathrm{Br}\gamma} \sim$ 500 pc. We therefore adopt $\mathrm{SFR_{CO}}$ as 0.5 $M_{\odot}$ yr^{-1}. In the case of NGC 4314, we consider $\mathrm{SFR_{RC-N}} \sim 0.1$ $M_{\odot}$ yr^{-1} within $R_{\mathrm{RC}} \sim 3600$ pc as an upper limit to the SF rate within $R_{\mathrm{CO}} \sim 600$ pc.

Table 8 shows the resulting R_{CO}, $\mathrm{SFR_{CO}}$ and the mass of molecular hydrogen (M_{H2}) within this radius. As shown in Table 8, the resulting adopted *circumnuclear SFR ranges from 3 to 11 $M_{\odot}$ yr^{-1} in the starbursts and from 0.1 to 2 $M_{\odot}$ yr^{-1} in the non-starbursts.* It is evident that while non-starbursts such as NGC 4569 and NGC 6951 and starbursts such as NGC 4102, NGC 4536, and NGC 2782 all host several times 10^{9} $M_{\odot}$ of molecular hydrogen, their SFRs are substantially different. A similar comparison applies between the starburst NGC 470 and the non-starbursts NGC 3351 and NGC 4314 which host several times 10^{8} $M_{\odot}$ of molecular hydrogen.

8. COMPARISON OF MOLECULAR GAS IN THE STARBURSTS AND NON-STARBURSTS

The analysis in § 6 based on high resolution (2″) CO maps and different SF tracers confirms the suggestions in § 2 (based on lower resolution data) that *barred galaxies with comparable amount of molecular gas in the inner 1-2 kpc radius can show an order of magnitude range in the average SFR per unit mass of gas (SFR/M_{H2}) within this region.* Among galaxies which host several times 10^{9} $M_{\odot}$ of molecular hydrogen in the inner 2 kpc, starbursts such as NGC 4102, NGC 4536, and NGC 2782 have an average (SFR/M_{H2}) of order a few times 10^{-9} yr^{-1} while non-starbursts NGC 4569 and NGC 6951 have (SFR/M_{H2}) $\sim$ a few $\times 10^{-10}$ yr^{-1}. We now turn to a comparison of the circumnuclear molecular gas in the barred starbursts and non-starbursts with the overall goal of understanding why they have such different SFR per unit mass of gas (SFR/M_{H2}) in the inner few kpc.

While we focus here on a comparison of the starbursts and non-starbursts (Figs. 3,5,6,7), we refer any interested reader to § 11 and Figs 14–15 for a description of each *individual* galaxy. Figures 3a–b show a wide variety of molecular gas morphologies including relatively axisymmetric annuli or disks (starbursts NGC 4102, NGC 3504, NGC 4536, NGC 470, and non-starburst NGC 4314), elongated double- peaked and spiral morphologies (starburst NGC 2782 and non-starbursts NGC 3351 and NGC 6951), and highly extended distributions (non-starburst NGC 4569) In all of the sample galaxies (Figs. 3a–b) except for the non-starburst NGC 4569, the molecular gas is concentrated in the inner kpc radius. Figure 5 compares the spatial distribution of SF activity (shown as greyscale) and molecular gas (shown as CO contours) The x and y axes represent respectively, M_{H2} and (SFR/M_{H2}), as defined in

Table 8. In the case of NGC 4102, NGC 2782 and NGC 6951, we show the SF activity with existing high resolution ($1.0''$–$1.5''$) 1.49 and 4.89 GHz RC maps. Strictly speaking, in the case of NGC 6951, the RC map shows not just the star-forming ring of $4''$ (360 pc) radius, but also the Seyfert nucleus in the inner $1''$ (90 pc). For the remaining galaxies in Fig. 5, we use high resolution ($1.0'' - 1.5''$) Hα maps as there are no RC maps of resolution comparable to the CO. Our conclusions are given below.

8.1. *The Type I Non-Starburst NGC 4569*

The non-starburst NGC 4569 differs from the other sample galaxies in that it has a highly extended molecular gas distribution with complex kinematics and large linewidths of $\sim$ 150 km s^{-1}. We thus discuss its case separately. These properties of NGC 4569 are illustrated in Figs. 6a–d. A large fraction of the gas lies outside the inner kpc radius and extends out to a radius of 20 $''$ (1.7 kpc), at a similar P.A. ($\sim$ 15 deg) as the large-scale stellar bar (Figs. 6a–b). The extended gas in NGC4569 has highly non-circular kinematics, as shown by the spatial velocity plots along the kinematic major and minor axes (Figs. 6c–d). Along the kinematic major axis, velocities are generally positive (i.e., above the systemic value of -235 km s^{-1}) on the northeastern side, and negative on the southwest side. However, at a radius of $5''$ (400 pc), near the feature marked 'N1' in Fig. 6b, the velocities change from +100 km s^{-1} to a forbidden velocity of -75 km s^{-1}. This indicates the presence of non-circular motions caused by in-plane azimuthal streaming motions or/and vertical motions out of the plane.

As outlined in § 2.2, NGC 4569 shows signs of optical and NIR asymmetries suggestive of a recent tidal interaction or minor merger and it also hosts a large-scale stellar bar. Thus, we suggest that the extended gas in NGC 4569 which is generally elongated along the bar and shows strong streaming motions, is responding to gravitational torques from both the interaction and the (induced or spontaneous) stellar bar. *Taken together, the optical, NIR, and CO properties of NGC 4569 suggest it is in the early phases of bar-driven/tidally-driven gas inflow.* NGC 4569 is reminiscent of NGC 7479 which hosts large amounts of gas with non-circular kinematics along a large-scale stellar bar and show evidence for a minor merger (Laine & Heller 1999). However, the gas kinematics in NGC 4569 look more disturbed in the inner 400 pc than in NGC 7479.

There is intense SF in the central $2''$ (170 pc) radius, but the gas which is extended along the bar and has disturbed kinematics shows no appreciable SF. The properties of NGC 4569 stand in sharp contrast to the starburst NGC 4102, where most of the circumnuclear molecular gas has piled up in the inner $4''$ (340 pc) radius, shows predominantly circular kinematics, and is undergoing intense SF. The low SF efficiency in NGC 4569 may well be related to the fact that large velocity gradients and shear in gas streaming along the bar can prevent clouds from being self-gravitating. Additionally, gas moving in a bar potential can experience large tidal forces (Elmegreen 1979; Kenney & Lord 1991) and tidal heating (Das & Jog 1995) which slow down gravitational collapse. Several other galaxies show such low SF per unit mass of gas along their bars e.g., NGC 7723 (Chevalier & Furenlid 1978), NGC 1300, NGC 5383 (Tubbs 1982), NGC 7479 (Laine et al. 1999) or in M83 where the ratio of UV to CO luminosities is unusually low despite abundant CO (Handa, Sofue, & Nakai 1991).

In summary, we therefore suggest that the low SFR per unit gas mass of the non-starbursts NGC 4569 over the inner few kpc is due to the fact that *it is in the early stages of bar-driven/tidally-driven gas inflow, where most of its molecular gas has an extended distribution, highly non-circular kinematics and an associated large local shear which is not conducive to SF.* The barred galaxy NGC 7479 studied by Laine et al. (1999) may also be in this early evolutionary phase. In NGC 7479, only low levels of SF are seen along the bar despite the presence of several $\times 10^9$ $M_\odot$ of molecular gas in a dust lane along the bar (Laine et al. 1999). This gas shows large non-circular motions, a large velocity gradient, and a projected velocity gradient of at least 100 km s^{-1} (Laine et al. 1999). We shall henceforth use the term **'Type I non-starburst'** to denote this kind of system, where a large fraction of the molecular gas is still inflowing towards the inner kpc (generally along the leading edges of the bar), exhibiting large non-circular motions and not forming stars efficiently.

8.2. *The Starbursts and Type II Non-Starbursts*

The remaining starbursts (NGC 4102, NGC 3504, NGC 4536, NGC 470) and non-starbursts (NGC 6951, NGC 3351, NGC 4314) in our sample do not show such extreme kinematics or extended gas distributions as NGC 4569. In all of them, the molecular gas detected is concentrated within the inner kpc radius and the velocity field in the inner 500 pc radius is generally dominated by circular motions, with occasional weaker non-circular components (see § 11 for details). Most of the circumnuclear molecular gas seems to have reached the inner kpc radius of the bar and only a small fraction of it seems to be still inflowing along the stellar bar. The latter gas component shows up in the form of faint gas streams which extend out and intersect the dust lanes on the leading edges of the large-scale bar and show non-circular motions. Such gas streams are seen in clearly in non-starburst NGC 6951 (Fig. 15a–b) and also at fainter levels in NGC 3351 (Fig. 15c–d), NGC 4314 (Fig. 15e–f), and starburst NGC 4102 (Fig. 14a–b). We conclude that in contrast to NGC 4569, the remaining barred starbursts and non-starbursts seem to be *in significantly later stages of bar-driven inflow where most of the molecular has already settled into the inner kpc of the barred potential and no longer shows extreme non circular motions.* We henceforth refer to these kind of non-starbursts as **'Type II non-starbursts'.**

What is the difference between the starbursts and Type II non-starbursts? To answer this question, we use the two-dimensional distribution of SF and gas in Fig. 5, as well as the azimuthally averaged gas and SFR surface densities in Fig. 7a–b. Fig. 7a shows the radial variation of the deprojected azimuthally-averaged molecular gas surface density ($\Sigma_{\rm gas-m}$) derived in § 5. In order to display meaningful values, quantities are plotted starting at a radius $\geq$ half the size of the synthesized CO beam which is typically $2''$ or 150 pc. Fig. 7b plots the azimuthally-averaged molecular gas surface density SFR per unit area (Σ_{SFR}) in the galactic plane as a function of radius. *We find that the starbursts show larger gas surface densities*

(1000-3500 $M_\odot$ pc^{-2}) in the inner 500 pc radius compared to the Type II non-starbursts for a given CO-to-H_2 conversion factor. In Fig. 7a, the Type II non-starbursts have peak $\Sigma_{\rm gas-m}$ reaching only 500-950 $M_\odot$ pc^{-2}. We also note from Fig 6a and 6b that in the central 600 pc radius, $\Sigma_{\rm gas-m}$ and Σ_{SFR} follow each other more closely in the case of the starbursts.

Is the presence of apparently higher gas surface densities in the starbursts a real effect? We can rule out artifacts caused by resolution effects since we have similar linear resolution (in pc) for starbursts and non-starbursts with comparable circumnuclear molecular gas content (e.g., NGC 4102, and NGC 3504 versus NGC 6951, or NGC 2782 and NGC 4536 versus NGC 4569). Another concern is that the higher $\Sigma_{\rm gas-m}$ in the starbursts may be due to an increase in CO emissivity caused by the higher temperatures associated with the intense SF. However, potential variations in CO emissivity cannot fully account for the observed differences in $\Sigma_{\rm gas-m}$ since CO peaks do not coincide with the Hα and RC peaks in several galaxies e.g., NGC 6951, NGC 2782, and NGC 3351 (Fig. 5). Thus, we consider the possibility that a large fraction of the molecular gas in the starbursts truly has a higher surface density than in the non-starbursts. This difference of a factor of 3–4 in $\Sigma_{\rm gas-m}$ can in turn lead to *large* differences in the SF *if the gas in the starbursts is above a critical density for SF while a large part of the gas in the non-starbursts is sub-critical.* We address this possibility quantitatively in § 9 by comparing $\Sigma_{\rm gas-m}$ to different theoretical critical densities which are believed to be relevant for the onset of SF.

9. THEORETICAL MODELS FOR SF APPLIED TO CIRCUMNUCLEAR STARBURSTS AND TYPE II NON-STARBURSTS

Numerous theoretical models have been applied to the outer disks of galaxies in order to explain the observed SF activity. An overview is presented in Appendix 2 where the instability criteria are summarized for several theoretical models. In this section, we compare the observed circumnuclear gas surface density $\Sigma_{\rm gas-m}$ to the critical density relevant for the onset of SF with the overall goal of understanding some of the differences between the starbursts and Type-II non-starbursts. In particular, we consider theoretical scenarios which assume that the onset of gravitational or axisymmetric instabilities (Safronov 1960; Toomre 1964; Goldreich & Lynden-Bell 1965a; Elmegreen 1979) is relevant for the growth of clouds and the onset of SF. Such models have achieved a fair degree of empirical success in the outer disks of Sa-Sc spirals, gas-rich E and S0s s (Kennicutt 1989; Eder 1990; Kennicutt 1998).

For a thin differentially rotating gas disk, support against gravitational instabilities is provided by pressure forces on small scales, and by Coriolis forces from rotation on large scales. One can show that axisymmetric instabilities set in when the gas surface density $\Sigma_{\rm gas}$ exceeds a critical density such that the Safronov (1960)/Toomre (1964) Q parameter falls below 1, where

$$\mathrm{Q} = \frac{\Sigma_{\rm crit}}{\Sigma_{\rm gas}} = \frac{\alpha\kappa\ \sigma}{\pi\ \mathrm{G}\ \Sigma_{\rm gas}} \leq 1 \tag{10}$$

Here, ω is the angular frequency, $\Sigma_{\rm gas}$ is the gas surface density, σ is the gas velocity dispersion, κ is the epicyclic frequency, and G is the gravitational constant. For an infinitely thin disk, α is 1, but for disks of finite thickness, α is somewhat larger (Larson 1985). Empirically, Kennicutt (1989) found that α is ~ 0.7 in the outer disks of Sc spirals. A two-fluid disk made of both gas and stars is always more unstable and will have a lower α than a purely gaseous or stellar one-fluid disk (Jog & Solomon1984; Elmegreen 1995).

We discuss the gravitational instability models in the context of the type II non-starbursts NGC 4314, NGC 3351, and NGC 6951, and the starbursts NGC 4102, NGC 4536 and NGC 3504. We cannot apply these simply axisymmetric models to other sample galaxies as they have highly non-axisymmetric gas distributions (e.g., the starburst NGC 2782 and Type I non-starburst NGC 4569) and non-circular kinematics (e.g., NGC 4569). We ignore the contribution of atomic HI because we have limited high resolution HI data for our sample galaxies and furthermore, molecular hydrogen is believed to dominate the ISM in the inner kpc of spirals (e.g., Scoville & Sanders 1987; Tacconi & Young 1986).

A more vicious problem is to get a good estimate for the velocity dispersion σ in the central ($2''$), especially when the $2''$ CO beam encompasses a steeply rising rotation curve. In the latter case, beam smearing artificially increases the observed σ and to a lesser degree impacts κ and $\Sigma_{\rm gas}$ in ways that depend on the intrinsic intensity and velocity field (Jogee 1999). Given that corrections for beam-smearing are model-dependent and not necessarily unique, we decide not to apply any such corrections, and instead perform the instability analyses (Fig. 8) only for radii exceeding $2''$ where the effect of beam-smearing is much less severe. In non-starbursts and starbursts alike, we therefore present results over radii of $\sim 2''$–$8''$ (Fig. 8). The lower limit of $2''$ corresponds to 180 pc for NGC 6951, NGC 4102 and NGC 4536, and to 100 pc for NGC 4314 and NGC 3351. Our results are summarized below.

(i) Type II non-starburst NGC 4314: In NGC 4314, HII regions are concentrated within an annulus between a radius of $5''$ and $7''$ (240 and 400 pc) where $\Sigma_{\rm gas}$ is $\sim$ 800 $M_\odot$ pc^{-2} (Fig. 8). Interior to this annulus, there are no HII regions although $\Sigma_{\rm gas}$ drops by only a factor of 2-3 (Fig 8). This lack of SF activity is not an artifact caused by extinction in the *H*α image or by resolution effects since neither the *J-K* image (Friedli et al. 1996) nor the high resolution *HST* images (Benedict et al. 1996) show elevated levels of dust or young stars at $r < 250$ pc. Thus, SF appears truly suppressed interior to the annulus of HII regions. The instability analysis (Fig. 8) shows that *Q reaches its lowest value, between 1 and 2, in the star-forming annulus* between r=$5''$ and $7''$ (240 and 400 pc) and it rises sharply at lower and higher radii. At $r \geq 7''$ where we cannot measure σ, we adopted a lower limit of 10 km s^{-1} based on the fact that a relatively constant value of 10 to 6 km s^{-1} has been measured in the outer disks of spirals (e.g., Dickey et al. 1990). Thus, values estimated for Q at $r \geq 7''$ outside the SF annulus are *lower* limits and the true rise in Q is likely to be even sharper than shown in Fig. 8. Interior to the star-forming annulus, between r = $2''$ and $5''$ (100 to 240 pc), Q increases by more than a factor of 3, indicating highly sub-critical gas densities. It is unlikely that this rise in Q is primarily due to beam-smearing because the observed σ increases by at most 1.5 interior to the SF annulus. (The mean value of $\sigma = 25$ km s^{-1} inside the SF ring and 15 km s^{-1} in the ring).

(ii) Type II non-starburst NGC 3351: In NGC 3351, the SF activity is concentrated within an annulus between a radius of 6″ and 9″ (300 and 450 pc) where $\Sigma_{\rm gas}$ is $\sim$ 550 $M_\odot$ pc^{-2} (Fig. 8). At lower radii, between 2″ and 6″ (100 and 450 pc), there is a large amount of molecular gas and $\Sigma_{\rm gas}$ shows no significant change. Yet no HII regions are seen (Fig. 8). The absence of observed SF activity at $r < 6''$ is not caused by extinction since near-infrared K-band observations of NGC 3351 show several hot spots (likely due to young K supergiants) in the ring of HII regions, but a relatively smooth distribution suggestive of older stars further in (Elmegreen et al. 1997). We find that in NGC 3351 Q *reaches its minimum value of* $\sim$ *1.5 in the annulus of HII regions* between a radius of 6″ and 9″ (300 and 450 pc; Fig 8). Further in, between a radius of 2″ and 6″ (100 and 450 pc), Q rises sharply to ~ 6 suggesting sub-critical gas densities. We again note that this increase in Q by a factor of > 3 is not primarily due to beam-smearing since the observed σ does not show a similar increase. σ has a mean value of 20 km s^{-1} in the SF ring and 25 km s^{-1} inside it.

(iii) Type II non-starburst NGC 6951: In NGC 6951, a similar trend in the Q parameter exists. The massive CO peaks at a radius of 6″ (550 pc) host a local molecular gas surface density of 2000 $M_\odot$ pc^{-2} and an azimuthally averaged $\Sigma_{\rm gas}$ of 1000 $M_\odot$ pc^{-2} (Fig. 8). Yet, the CO peaks are not associated with SF either in Hα and RC maps. Instead, SF is concentrated in a ring of radius $\sim 3''$ (300 pc). Kohno et al. (1999) find that Q is close to 1 in the star-forming annulus.

(iv) The starbursts NGC 4102, NGC 4536: The circumnuclear SF in the starbursts NGC 4102 and NGC 4536 is distributed over a wide annulus between 100 and 700 pc. Although the ground-based $H\alpha$ or RC images (e.g., Fig. 5) may give the misleading impression that Sf extends all the way into the center, *HST* images of both galaxies show a smooth distribution of old stars within the central 100 pc (1″) radius. Adopting the same approach for the starbursts NGC 4102 and NGC 4536 as for the non-starbursts, we perform the instability analysis from $r \sim 2''$–$8''$ (Fig. 8). As before, we exclude the central $r \sim 2''$ radius where the effect of beam smearing is severe. We also exclude larger radii ($r > 8''$) where there are faint gas streams which connect to the large-scale dust lanes on the leading edges of the bar because the Toomre analysis is not valid for such non-axisymmetric gas distributions.

The instability analysis (Fig. 8) shows that in the starbursts NGC 4102 and NGC 4536, the Toomre Q parameter remains $\sim$ 1-2 from $r \sim 2''$–$8''$ (200–700 pc) in the region of SF despite a factor of 2–3 variation in σ and a factor of 10 variation in both the gas surface density ($\Sigma_{\rm gas}$) and the epicyclic frequency (κ). Indeed, between a radius of 200 and 700 pc, σ ranges from 40 to 15 km s^{-1}, $\Sigma_{\rm gas}$ from 2200 to 200 $M_\odot$ pc^{-2}, and κ from 1500 to 200 km s^{-1} kpc^{-1}. A value of $Q \sim 1$ is also found in the starburst NGC 3504 by Kenney et al (1993). Furthermore, inspection of Fig. 8 shows that the $Q \sim$ 1-2 annulus spans $\sim$ 450 pc (e.g., 250–700 pc) in the starbursts NGC 4102 and NGC 4536, but only $\sim$ 150 pc (e.g., 300–450 pc) in the non-starbursts NGC 4314 and NGC 3351. It thus appears that the annulus over which Q remains $\sim$ 1-2 is 3 times wider in the starbursts than in the non-starbursts suggesting that the former host a larger amount of gas which is close to the critical density.

(v) Overall trends: The analyses in § (i)–(iv) suggest a striking result: *the Toomre Q parameter remains* $\sim$ *1-2 in the region of SF despite the large dynamic range in molecular gas properties, namely a factor of a few variation in* σ *and an order of magnitude variation in the gas surface density* ($\Sigma_{\rm gas}$) *and the epicyclic frequency* (κ). It is true that the analyses involve many uncertain quantities such as the CO-to-H_2 conversion factor and should, therefore, be taken with a grain of salt. However, with such a large variation in quantities such as $\Sigma_{\rm gas}$ and κ, Q could easily have ended up having almost any value, and the fact that it remains close to 1 can hardly be fortuitous. Instead, the evidence presented strongly suggests that the onset of gravitational instabilities as characterized by Q plays an important role in controlling the onset of SF in the inner kpc of spirals. At first sight, this may seem surprising since large-scale gravitational instabilities have been invoked for the collapse of atomic gas into molecular clouds within the outer disk of galaxies, but molecular gas in the inner kpc is already in the form of clouds. However, large-scale gravitational instabilities may be relevant for SF even in the inner kpc because they help to aggregate molecular clouds into large complexes where the clouds can thereafter grow through local processes involving accretion and collisions (e.g., Kwan 1979; Scoville et al. 1986; Gammie, Ostriker, & Jog 1991; Elmegreen 1990).

The results presented in § (i)–(iv) also suggest at least a partial explanation for the differences in SFR per unit mass of gas between the non-starbursts and starbursts. In both Type II non-starbursts and starbursts, the Q parameter reaches its minimum value of $\sim$ 1–2 in the annuli of SF. However, the annulus over which Q remains $\sim$ 1-2 is three times wider in the starbursts than in the non-starbursts, suggesting that *starbursts host a larger amount of gas which is close to the critical density.* Inside and outside the annuli of SF, the Type II non-starbursts host large gas concentrations where gas densities are well below $\Sigma_{\rm crit}$ ($Q >> 2$), and SF appears inhibited.

10. RELATIONSHIP BETWEEN THE DYNAMICAL RESONANCES OF THE BAR AND THE CIRCUMNUCLEAR GAS DISTRIBUTION

In order to develop a coherent picture for bar-driven evolution of disk galaxies, we need to understand how gas behaves in a barred potential and what controls its circumnuclear distribution. The high resolution (100-200 pc) CO data in this survey can set important constraints on the distribution of molecular gas within the inner kpc of a bar.

A barred potential is made up of different families of periodic stellar orbits characterized by a (conserved) Jacobi energy, $E_{\rm J}$, a combination of energy and angular momentum (e.g., Binney & Tremaine 1987). The most important families are those aligned with the bar major axis (so-called x_1 orbits) or with its minor axis (x_2 orbits) (Contopoulos & Papayannopoulos 1980). The x_1 family extends between the center and the bar's corotation radius. If the central mass concentration of a bar is large enough, it can also develop one or more inner Lindblad resonances (ILRs). In the case of a single ILR, the x_2 family appears between the center and the ILR, while if two ILRs exist it appears between the inner ILR (IILR) and outer ILR (OILR).

The abrupt change in orientation by $\pi/2$ at each resonance is restricted to (collisionless) stellar orbits. The gas-populated orbits can change their orientation only gradually due to shocks induced by the finite gas pressure. Therefore, the gas response to bar torquing leads to the formation of large-scale offset shocks and a subsequent gas inflow. Large scale stellar bars efficiently drives gas from the outer disk down to kpc scales through a combination of gravitational torques and dissipative effects. In the inner few 100 pc, we expect the gas inflow to stall because shocks associated with the bar weaken, and gravitational torques in the vicinity of ILRs may even reverse (e.g., Combes & Gerin 1985; Shlosman et al. 1989; Athanassoula 1992)

The exact locations and even the number of ILRs can be inferred reliably from non-linear orbit analysis (e.g., Heller & Shlosman 1996) based on the knowledge of the galactic potential. We use two approximate empirical methods based on the epicyclic approximation and on the shape of the dust lanes. In the epicyclic approximation, we write the potential of a weak stellar bar as the linear sum of an axisymmetric term and a smaller non-axisymmetric term, and use the epicycle theory to solve the equations of motion of a star. At the ILRs, there is a match between the natural frequency of radial oscillations (κ), and the forcing frequency (Ω - $\Omega_{\rm p}$) :

$$\Omega = \Omega_{\rm p} \pm \kappa/2 \tag{11}$$

where Ω is the angular frequency, $\Omega_{\rm p}$ is the bar pattern speed. A kinematic diagnostic for the presence of ILRs is that the peak of (Ω - $\kappa/2$) should exceed $\Omega_{\rm p}$. We get an upper limit for $\Omega_{\rm p}$ by assuming the corotation resonance (where Ω= $\Omega_{\rm p}$) lies at or beyond the end of the bar (e.g., Combes & Elmegreen 1993). We estimate Ω and κ from the CO and Hα rotation curves as described in § 5, bearing in mind that uncertainties exist in regions where there are non-circular motions. Upper limits on $\Omega_{\rm p}$ range from 43 to 115 km s^{-1} kpc^{-1} within the sample galaxies (Table 9; Figs. 9a–b). The peak of (Ω - $\kappa/2$) is well above the upper limit on $\Omega_{\rm p}$, implying that at least one ILR exists in the starbursts NGC 4102, NGC 4536, and NGC 3504, and in the non-starbursts NGC 4314, NGC 6951, and NGC 3351. We use the upper limit on $\Omega_{\rm p}$ in Fig. 9a–b to derive upper and lower limits, respectively, for the radius of the OILR ($R_{\rm OILR}$) and IILR ($R_{\rm IILR}$). These are shown in Table 9. A comparison of $R_{\rm OILR}$ with the azimuthally-averaged molecular gas surface density $\Sigma_{\rm gas-m}$ (Fig. 7a) shows that *the starbursts and Type II non-starbursts have their peak gas surface density and most of their circumnuclear gas inside or very near the OILR of the stellar bar*. Similar results are reported in studies of individual systems (e.g., Sofue 1991; Kenney et al. 1992; Knapen 1995a,b; Jogee 1999, 2001; Jogee et al. 2002a,b).

The afore-described kinematic estimates for the location of the OILR depend sensitively on the radial variation of Ω and κ and can carry large uncertainties. We therefore obtain independent estimates based on the morphology of circumnuclear dust lanes which trace the loci of shocks. In the presence of x_2 orbits associated with ILRs, the two dust lanes which are associated with the leading edges of a bar do not cross the center of the galaxy, but are offset along the bar minor axis, in the direction of x_2 orbits (e.g., Athanassoula 1992; Byrd et al 1994; Piner et al. 1995; Combes 1996). The separation of the offset dust lanes provides a lower limit to $2 \times R_{\rm OILR}$. Figs. 10a-c illustrate the case for the type II non-starburst NGC 6951. The large-scale stellar bar of NGC 6951 has a semi-major axis of $28''$ (5.2 kpc; Fig. 10a) and two relatively straight dust lanes are visible on its leading edge (Fig. 10b). As they approach the circumnuclear region, these dust lanes do not cross the center of the galaxy, but instead are offset along the bar minor axis. These dust lanes connect to the spiral-shaped CO arms where the two CO peaks lie almost along the minor axis of the stellar bar (Fig. 10c) The CO and dust morphology are consistent with the accumulation of gas near the OILR. Similar pairs of offset dust lanes are seen in the starbursts NGC 3504 and NGC 4102, and in the type II non-starbursts NGC 3351 and NGC 4314.

The CO data reveal large gas concentrations inside the OILR, but do not enable us to determine whether the gas has flown past the IILR since the CO resolution (100-200 pc) is comparable to $R_{\rm IILR}$. However, we note that the *HST* images of many sample galaxies (e.g., NGC 4102, NGC 3504, NGC 4536, NGC 4314, NGC 3351, NGC 6951) show that SF does not extend inside the central 100 pc radius or so; this may potentially be due to the IILR blocking further gas inflow. It is interesting that NGC 2782 which hosts a nuclear stellar bar (§ 11; Jogee et al. 1999) is the only starburst where the *HST* images show SF peaking at the center.

11. BAR-DRIVEN SECULAR EVOLUTIONARY SCENARIOS

In this penultimate section, we speculate on potential evolutionary connections between the barred starbursts and non-starbursts in our sample, and discuss possible scenarios for bar-driven dynamical evolution.

The evidence presented in § 10 (based on the dynamical frequencies and dust morphologies) suggest that the starbursts and type II non-starbursts have piled up most of their circumnuclear gas inside or near the OILR of the large-scale stellar bar. In contrast, the Type I non-starburst such as NGC 4569 has an extended gas distribution extending out to $r \sim$2 kpc (§ 7), with a large fraction of the gas still inflowing along the bar and exhibiting large non-circular motions.

We suggest that a barred galaxy would show up as a Type I non-starburst in the early stages of bar-driven inflow where large amounts of gas are still along the bar, experiencing shocks, torques, and large non-circular motions. A schematic illustration is shown in Fig. 11. Examples of such systems might be NGC 4569 (§ 7; this work), NGC 7479 (§ 7; Laine et al. 1999), NGC 7723 (Chevalier & Furenlid 1978), NGC 1300, and NGC 5383 (Tubbs 1982). During this phase, SF is suppressed or highly inefficient due to large velocity gradients, shear, and tidal forces (Elmegreen 1979) in the gas along the bar. *The low SFR/$M_{\rm H2}$ along a strong bar, as typified by the Type I non-starburst, is fundamental in enabling a bar to efficiently* *increases the central mass concentration in the inner kpc of galaxies.* It is only when the gas inflow rate along the bar exceeds the SFR over the same region, that an efficient mass buildup happens. Available estimates of gas inflow rates along large-scale stellar bars range from 1 to 4 $M_{\odot}$ yr^{-1} (Quillen et al. 1995; Laine, Heller, & Shlosman 1998; Regan, Teuben, & Vogel 1997). If we assume a conservative net inflow rate of 1 $M_{\odot}$ yr^{-1} along the bar into the inner kpc radius, then over 1 Gyr a bar can increase the dynamical mass in the inner kpc by 1 $\times 10^{9}$ $M_{\odot}$ or a few %. For instance, in our sample galaxies the dynamical mass (§ 5) enclosed within r=1 kpc ranges from 6–30 $\times 10^{9}$ $M_{\odot}$ (Fig. 12), and would increase by 6–30 %. In practice, the mass buildup may be slower due to starburst-driven gas outflows which can be $\sim$ 1–a few $M_{\odot}$ yr^{-1} (e.g., Jogee et al. 1998 for the starburst NGC 2782; Heckman, Armus, & Miley 1990).

In the later stages of bar-driven inflow, a barred galaxy likely goes through a Type II non-starburst and possibly a starburst phase (Fig. 11). As suggested by § 8 and 10, after gas crosses the OILR it settles into a more axisymmetric distribution with predominantly circular motions. Theoretically, such a behavior is expected in the vicinity of ILRs where shocks associated with the bar weaken, and gravitational torques weaken or even reverse (e.g., Combes & Gerin 1985; Shlosman et al. 1989; Athanassoula 1992). The instability analysis in § 8 suggests that gas concentrations which build up near the ILRs will undergo SF once the gas densities exceed the Safronov (1960)/Toomre (1964) critical density $\Sigma_{\rm crit} = (\alpha\kappa\sigma/\pi G)$. In the inner kpc, the very high epicyclic frequency (several 100–1000 km s^{-1} kpc^{-1}) will naturally force $\Sigma_{\rm crit}$ to be high (e.g., several 100-1000 M$_{\odot}$ pc^{-2}), thereby enabling SF to occur only at high gas densities. Under this scenario, *some type II non-starbursts are pre-starbursts* which may eventually become starbursts (Fig. 11) if the gas density subsequently becomes super-critical.

The intense starbursts in our samples with circumnuclear SFRs of 3–11 M$_{\odot}$ yr^{-1} will build compact young stellar disks or annuli inside the OILR. The interplay between the SFR, the outflow rate driven by starburst winds or jets, and the molecular gas supply will eventually determine how massive such compact stellar components will be. Thus, the inner kpc where the bulge is usually present, can witness the birth of compact stellar components which form from the cold dissipative gas component and are therefore relatively flat initially. *These compact stellar components may belong to the class of so-called pseudo-bulges* (Kormendy 1993) whose light distribution and kinematics are more consistent with a disk than with a spheroidal bulge component. Several studies have in fact reported that the central light distribution of many late type galaxies are better represented by an exponential disk-like component than an $r^{1/4}$ profile (e.g., de Jong 1996; Courteau, de Jong, & Broeils 1996)

As a typical starburst in our sample converts its molecular gas reservoir into such a compact disky stellar component, *it is expected to transition into a Type II non-starburst* as the gas density in part of the wide gas annulus will soon becomes sub-critical. One possible outcome is that SF shuts off first at lower radii (where $\Sigma_{\rm crit}$ is higher, the instability growth timescale $t_{\rm GI} \sim Q/\kappa$ is shorter, and $\Sigma_{\rm SFR}$ is higher) such that we end up with a newly-built compact disky stellar component lying inside a thin star-forming gas ring. In our own sample, the type II non-starburst NGC 3351 may provide a beautiful example of this process. Inside its thin CO ring, NGC 3351 hosts a central stellar component which has a high ratio of rotational to random motions (Kormendy 1983) Isophotal fits to the K and R band images of NGC 3351 (Fig. 13) shows that this central component has an ellipticity and P.A similar to those of the outer disk. Both the light distribution and kinematics would suggest that a compact stellar component with disk-like properties has built up in the central r=6$''$ (300 pc) of NGC 3351. Thus, in this framework *some type II non-starbursts may also be post-starbursts hosting a compact disky stellar component* (Fig. 11). It should be noted that vertical instabilities (e.g., Sellwood 1993; Merritt & Sellwood 1994), vertical ILRs associated with the bars (Combes et al. 1990), or even the destruction of the bar (Hasan & Norman 1990; Norman, Sellwood, & Hassan 1996) can scatter stars in the initially flat disky component to large scale heights, thereby enhancing or building a stellar bulge.

The overall schematic picture (Fig. 11) which emerges is that an episode of bar-driven gas inflow causes a barred galaxy to go through successive phases from a Type I non-starburst to a type II non-starburst which, under the right conditions, can undergo a starburst that will eventually return to a type II non-starburst. This picture would naturally explain why a *one-to-one* correlation is not seen between bars and powerful central starbursts although in a statistical sense relatively luminous starbursts tend to be preferentially barred compared to normal galaxies (Hunt & Malkan 1999; Hawarden et al. 1986; Mazzarella & Balzano 1986). Over its lifetime, a disk galaxy can undergo numerous episodes of bar-driven gas inflow characterized by these phases and gradually build up its central mass concentration and bulge, provided an adequate gas supply is maintained inside the corotation radius of the bar. This can be achieved by accreting gas-rich satellites in a barred disk galaxy or/and by externally inducing a new bar whose corotation radius encloses pre-existing gas reservoirs at large radii. Minor (1:10) to moderate (1:4) mass-ratio tidal interactions and mergers provide a natural way of doing both (Fig. 11) and are believed to be frequent over the last 7 Gyrs (z=0–1) (Jogee et al. 2003; Mobasher et al. 2004).

While many such secular evolutionary scenarios have been suggested whereby successive bar-driven inflow transform galaxies from late to early Hubble types in the direction of increasing bulge-to-disk ratios (Friedli & Benz 1995; Friedli & Martinet 1993; Kormendy 1993; Hasan & Norman 1990; Pfenniger & Norman 1993), numerous key questions within this framework remain controversial and unclear. How do the bar size, strength, and pattern speeds evolve over a galaxy's lifetime taking into account the interaction of the bar with the dark matter halo (Athanassoula 2002, 2003; Weinberg & Katz 2002; Bournaud & Combes 2002)? Can bars with a range of initial strengths lead to a large enough central mass concentration in the inner 100–200 pc to cause their own self destruction, and if bar dissolution does happen can the dynamically hot disk left behind undergo recurrent bar formation as a result of gas accretion episodes (e.g., Hasan & Norman 1990; Norman, Sellwood, & Hassan 1996; Pfenniger & Norman 1993; Bournaud & Combes 2002; Athanassoula 2002, 2003)?

12. INDIVIDUAL GALAXIES

The molecular gas distribution and kinematics of individual starbursts and non-starbursts are described below. Figures 14a–j and 15a–f show the total intensity (moment 0) and intensity-weighted velocity (moment 1) maps. Spatial-velocity plots are shown for selected cases when they can better represent complex kinematics.

12.1. *The Starbursts*

NGC 4102, NGC 4536, NGC 3504, and NGC 470: Within the inner kpc radius of the starbursts NGC 470, NGC 4102, NGC 3504, and NGC 4536, the molecular gas distribution (Figs. 14a–h) observed in *the sky plane* looks relatively symmetric about the line of nodes and is elongated along that position angle with an aspect ratio consistent with projection effects caused by the inclination of the galaxies. This implies that within the galactic plane of these four starbursts, most of the circumnuclear molecular gas has a relatively axisymmetric distribution of 300-600 pc radius. The moment 1 isovelocity contours (Figs. 14a–h) in the the inner 500 pc radius trace the characteristic spider diagram, suggesting the gas motions are predominantly circular. Several starbursts (NGC 4102, NGC 4536) show faint gas streams which extend from the relatively axisymmetric gas concentrations and curve along the leading edges of the large-scale stellar bar, connecting to the large-scale dust lanes. The gas streams show non-circular motions and are likely inflowing along the bar into the inner kpc region.

NGC 2782 : The starburst galaxy NGC 2782 differs in several respects from the other starbursts. The CO morphology in the sky plane is non-axisymmetric, double peaked and bar-like in the inner kpc radius (Fig. 14i–j). Since the galaxy has a low inclination of $\sim$ 30 deg, this elongated morphology is not due to projection effects but more likely reflects the intrinsic gas distribution in the galactic plane. Jogee et al. (1999) have presented evidence that the CO properties are consistent with the molecular gas responding to a nuclear stellar bar of radius $\sim$ 1.3 kpc, identified via isophotal analysis of NIR images. The CO bar-like feature in NGC 2782 is offset in a leading sense with respect to the nuclear stellar bar and shows some non-circular kinematics (Jogee et al. 1999). The nuclear stellar bar appears to be fueling gas from the CO lobes at a kpc radius into the central 200 pc radius where resides a powerful central starburst, forming stars at a rate $\geq 3\ M_{\odot}$ yr^{-1} (Jogee et al. 1998). It is striking that NGC 2782 is the only starburst in our sample where *HST* images show SF peaking at the center. In contrast, the other starbursts do not show evidence for strong nuclear stellar bars and their *HST* images shows that SF does not extend into the inner 100 pc region.

12.2. *The Non-Starbursts*

NGC 6951: In NGC 6951, there are two CO peaks at a radius of $6''$ (550 pc) lying nearly perpendicular to the large-scale stellar bar whose P.A. is 85 deg (Fig. 3b or 10a). Fainter emission around the peaks form two spiral-shaped streams which extend out and curve along the dust lanes on the leading edge of the large-scale bar. The molecular gas at the CO peaks and in the spiral streams shows complex non-circular motions (Figs. 15a–b). In NGC 6951, NGC 3351, and NGC 4314 the CO peaks lie near the OILR of the large-scale stellar bar (§ 9).

NGC 3351: In NGC 3351, the CO emission shows two peaks at a radius of $\sim$ 7" (350 pc). As in NGC 6951, the two CO peaks lie nearly perpendicular to the large-scale stellar bar whose P.A. is 110 deg (Fig. 3b). The CO emission around the peaks appears to connect to the dust lanes which lie on the leading edge of the bar. The isovelocity contours curve near the CO peaks, suggesting non-circular streaming motions (Fig. 15c–d). Interior to the CO peaks, the spatial velocity plot along the kinematic minor axis, where we are sensitive to the radial in-plane motion, and vertical out-of-plane motion, shows complex non-circular kinematics.

NGC 4314: In NGC 4314, most of the gas is concentrated in a multiple-peaked relatively circular ring of radius $5''$–$7''$ (240 and 400 pc). Two faint CO spurs extend from the ring and intersect the dust lanes which lie on the leading edge of the large-scale stellar whose P.A. is 143 deg (Fig. 3b). Non-circular motions of 10 to 65 km s^{-1} are detected in the CO spurs (Fig. 15e–f). The CO peaks lie near the OILR of the large-scale stellar bar (§ 9). Furthermore, inside the clumpy CO ring, ground-based (Friedli et al. 1996) and *HST* (Benedict et al. 1993) images of NGC 4314 reveal a nuclear stellar bar of radius $4''$ (200 pc) at a position angle of -3 to -12 deg. In contrast to NGC 2782, the CO emission in NGC 4314 is not primarily concentrated along the nuclear stellar bar, but instead forms a clumpy ring at the end of the nuclear bar. The reason for such different gas and SF distributions in the two nuclear bars may be an evolutionary in nature. In the case of NGC 4314, we may be seeing gas which is outside the corotation of a nuclear bar that formed earlier and the gas is thus experiencing an outward torque (Jogee et al. in prep.; Friedli & Martinet 1993). Conversely, in NGC 2782 we may be witnessing the early decoupling phase of a nuclear stellar bar induced by gas inside the OILR of the large-scale bar.

NGC 4569: NGC 4569 (Figs. 6a–d) differs from the above three non-starbursts in that it has a highly extended molecular gas distribution with complex kinematics and large linewidths of $\sim$ 150 km s^{-1}. A large fraction of the gas lies outside the inner kpc radius, extends out to a radius of 20 $''$ (1.7 kpc), at a similar position angle as the large-scale stellar bar (Figs. 6a–b). This gas has highly non-circular kinematics, as shown in the spatial velocity plots along the kinematic major and minor axes (Figs. 6c–d). Along the kinematic major axis, velocities are generally positive (i.e., above the systemic value of -235 km s^{-1}) on the northeastern side, and negative on the southwest side. However, at a radius of $5''$ (400 pc), near the feature marked 'N1' in Fig. 12b, the velocities change from +100 km s^{-1} to a forbidden velocity of -75 km s^{-1}. This indicates the presence of non-circular motions caused by in-plane azimuthal streaming motions or/and vertical motions out of the plane. As discussed in § 7, the CO properties of NGC 4569 could be consistent with the early phases of bar-driven/tidally-driven gas inflow. NGC 4569 is reminiscent of NGC 7479 which hosts large amounts of gas with non-circular kinematics along a large-scale stellar bar and shows evidence for a minor merger (Laine & Heller 1999). However, the gas kinematics in NGC 4569 look more disturbed in the inner 400 pc than in NGC 7479.

NGC 3359: In NGC 3359, the interferometric observations captured less than 30 % of the single dish flux, in contrast to the other sample galaxies (Table 5). The moment 0 map of NGC 3359 in Fig. 4b shows a very patchy CO distribution made up of a few clumps which lie away from the center. The present observations indicate that there is no bright centrally peaked CO distribution in the inner 500 pc of NGC 3359. The missing single dish flux may come from extended gas and/or diffuse low surface brightness CO in the central regions. As discussed in § 2, several authors have proposed that the large-scale stellar bar in NGC 3359 is young and may have been tidally triggered and it is possible that there are significant amounts of gas further out along the bar. To resolve this issue, future interferometric observations of a larger field of view, using a more compact array configuration needs to be carried out.

13. SUMMARY AND CONCLUSIONS

There is now mounting evidence that bars, whether spontaneously or externally triggered, efficiently drive gas from the outer region into the circumnuclear (inner 1–2 kpc) region of galaxies, and that barred galaxies have on average larger molecular gas concentration within the inner kpc than unbarred galaxies (Sakamoto et al. 1999). We use a panchromatic dataset made of high resolution (100-200 pc) CO (J=1→0) observations, optical, NIR, Hα, RC, Brγ and archival *HST* data, and a carefully selected sample of barred non-starbursts and starbursts in order to tackle further perennial questions. What kind of molecular environment is built in the circumnuclear region of a barred galaxy in terms of gas densities, mass fraction, and dynamical parameters? What factors control the onset of SF in the gas and can they account for the large range in SFR per unit mass of molecular gas seen in the circumnuclear region? Is there evidence for stellar components such as pseudo-bulges or bulges being built as a result of bar-driven inflow, in accordance with secular evolutionary scenarios? Our results are summarized below.

(1) The molecular environment which has developed in the circumnuclear region of the barred spirals *differs markedly* from that present in the outer disk of galaxies. It includes molecular gas masses of 3×10^8 to 2×10^9 M$_\odot$, molecular gas surface densities of 500-3500 M$_\odot$ pc^{-2}, gas mass fractions of 10 to 30 %, and epicyclic frequencies of several 100 to several 1000 km s^{-1} kpc^{-1}. In this environment characterized by a high epicyclic frequency and moderate velocity dispersions of 10 to 40 km s^{-1}, gravitational instabilities set in only at very high gas densities (few 100-1000 M$_\odot$ pc^{-2}), but once triggered, they grow rapidly on a timescale of a few Myrs. This high density short timescale 'burst ' mode favored by molecular environment in the inner kpc may explain why the most intense starbursts tend to be in the central parts of galaxies. Furthermore, the high pressure, high turbulence ISM can lead to the formation of clouds with high internal dispersion and mass, and hence may favor the formation of massive clusters as suggested by Elmegreen et al (1993). The molecular environment in the inner kpc of the ultra luminous infrared galaxy Arp 220 is a scaled up version of the one shown by barred starbursts in our samples suggesting that interactions build up even more extreme conditions.

(2) We find a good correlation between the circumnuclear SFR estimated from RC data and the global FIR luminosity for most galaxies. The barred starbursts and non-starbursts have circumnuclear SFRs of 3 to 11 and 0.1-2 M$_\odot$ yr^{-1} respectively in the inner kpc, although they host comparable amounts of molecular hydrogen, assuming a standard CO-to-H$_2$ conversion factor. Thus, barred galaxies with comparable amount of molecular gas in the inner 1-2 kpc radius can show an order of magnitude range in the average SFR per unit mass of gas (SFR/$M_{\rm H2}$) within this region. We suggest that some of this range can be understood in terms of different stages of bar-driven inflow:

(i) A non-starburst like NGC 4569 (which we denote as a *type I non-starburst*) which is in the *early stages of bar-driven inflow* has a highly extended molecular gas distribution where *a large fraction of the gas is still along the large-scale stellar bar, showing large non-circular kinematics and not forming stars efficiently.* The low SF efficiency in this gas is likely due to the large velocity gradients and shear. Several other galaxies studied by others such as NGC 7479 (Laine et al. 1999), NGC 7723 (Chevalier & Furenlid 1978), NGC 1300, and NGC 5383 (Tubbs 1982) may be in a similar phase.

(ii) The other non-starbursts (which we denote as *type II non-starbursts)* and starbursts seem to be in *later* stages of bar-driven inflow as their circumnuclear molecular gas is already concentrated within the inner kpc radius and the velocity field is dominated by circular motions. The higher SFR/$M_{\rm H2}$ in the starbursts compared to the type II non-starbursts may be related to the fact that their gas surface densities are larger (1000–3500 $M_\odot$ pc^{-2}) and close to the Toomre critical density over a large region. Conversely, in the type II non-starbursts, the gas appears to be supercritical only over a narrow region outside of which there are gas-rich regions with sub-critical gas densities and no appreciable SF.

(3) In both Type II non-starbursts and starbursts, the Q parameter reaches its minimum value of $\sim$ 1–2 in the region of SF despite the large dynamic range in molecular gas properties, namely a factor of a few variation in σ and *an order of magnitude variation in the gas surface density* ($\Sigma_{\rm gas}$) *and the epicyclic frequency* (κ). This remarkable behavior strongly suggests that the onset of gravitational instabilities as characterized by Q plays an important role in controlling the onset of SF even in the inner kpc region. For ($\Sigma_{\rm crit} = \alpha\kappa\sigma/\pi G$), the value of 0.7 for α found by Kennicutt (1989) in the outer disk of spirals works well in the circumnuclear region too.

(4) We present evidence that the starbursts and type II non-starbursts have piled up most of their circumnuclear gas inside or near the OILR of the large-scale stellar bar. The evidence is based on dynamical frequencies computed under the epicyclic approximation, as well as on circumnuclear dust morphologies. We estimate upper limits for the bar pattern speed in the range of 43 to 115 km s^{-1} kpc^{-1} and an OILR radius of > 500 pc for most of the sample galaxies.

(5) The dynamical mass enclosed within the inner kpc radius of the barred galaxies in our sample is 6–30 $\times 10^9$ $M_\odot$ and can increase by several % over a Gyr for nominal bar-driven inflow rates. Intense starbursts such as those in our sample with SFR of 3–11 $M_\odot$ yr^{-1} in the inner kpc will build compact relatively flat stellar components (annuli or disks) inside th OILR of the large-scale bar. *Such compact stellar components may belong to the class of so-called pseudo-bulges* (Kormendy 1993) whose light distribution and kinematics are more consistent with a disk than with a spheroidal bulge component. We present evidence for such pseudo-bulge components in our sample.

(6) We suggest that an episode of bar-driven inflow causes a barred galaxy to go through starburst and non-starburst phases as typified by our sample. This would naturally explain why a *one-to-one* correlation is not seen between bars and central starbursts, although statistically relatively luminous starbursts tend to be preferentially barred . We speculate that over its lifetime, a barred galaxy experiences numerous episodes of minor mergers and bar-driven /tidally-driven gas inflow which lead to a gradual buildup of its central mass concentration, bulge, and secular evolution along the Hubble sequence.

14. ACKNOWLEDGMENTS

Support for this work was generously provided by NSF grant AST 99-81546, and a grant from the K. T. and E. L. Norris Foundation. SJ also acknowledges support from the National Aeronautics and Space Administration (NASA) under LTSA Grant NAG5-13063 issued through the Office of Space Science, a Grant-in-Aid of Research from Sigma Xi (The Scientific Research Society), an AAUWEF Fellowship, and a Zonta International Amelia Earhart Fellowship. We thank D. Friedli, F. Combes, R. B. Larson, C. Martin, R. Kennicutt, J. H. Knapen, I. Shlosman, K. Sheth, and B. Elmegreen for discussions and comments of earlier versions of the manuscript. We thank the staff and observers at the Owens Valley Radio Observatory for their support, D. J. Saikia and A. Pedlar for kindly providing the 5 GHz RC maps.

15. APPENDIX 1 : ESTIMATING THE SFR FROM DIFFERENT TRACERS

We describe below how different tracers such as the the global FIR luminosity, the Hα recombination line at 6563 Å, the Brγ recombination line at at 2.16 μm, and the non-thermal component of the RC emission at 1.49 GHz can provide estimates of the SF rate. We focus here on the physical basis and assumptions behind the methods.

(i) SFR from the global FIR luminosity (SFR$_{\rm FIR}$)
The FIR emission of spiral galaxies is believed to be emission mostly from heated dust. A two component model made up of a warm dust component in clouds which is heated by massive stars, and a cooler cirrus dust component which is heated by the general interstellar radiation field (Helou 1986; Lonsdale-Perrson & Helou 1987) is generally assumed. Stars more massive than 5 $M_\odot$ are believed to be important for heating the dust (Devereux & Young 1990).

A fraction β of the emission from heated dust appears in the FIR band between 40 and 120 μm (Helou et al. 1988). For typical dust temperatures and emissivities, β is of order 2/3 (Helou et al. 1988; Condon 1992). If most of this emission comes from warm dust heated by massive stars rather than from dust heated by old stars, then the FIR luminosity is a good tracer of massive SFR. The FIR luminosity can be a more reliable tracer of the SFR than NIR/optical recombination lines in dusty regions, especially if the massive stars are dust embedded. Following Hunter et al. (1986) and Condon (1992), and assuming an extended Miller-Scalo IMF (Kennicutt 1983), with an upper mass cut-off $M_{\rm U}$ of 100 $M_\odot$, and assuming the SFR is constant over the lifetimes ($\sim$ few $\times 10^7$ years) of massive ($M \geq 5 M_\odot$) stars, one finds :

$$(\frac{\rm SFR}{M_\odot {\rm yr}^{-1}}) = 4.3 \times {\rm SFR(M \geq 5M_\odot)} = \gamma \times (\frac{\rm L_{FIR}}{10^{10}{\rm L_\odot}}) \quad (12)$$

For the assumed dust temperature and emissivities γ =3.9 (Condon 1992). Other studies which assume different dust properties or use synthesis models quote a range of values for γ, e.g., γ =5.2 (Hunter et al. 1986), γ =2.2 (Lehnert & Heckman), γ =1.7 (Kennicutt 1998).

(ii) SFR from the Hα recombination line at 6563 Å (SFR$_{H\alpha}$): In HII regions, UV Lyman continuum photons (of wavelengths λ < 912 Å) from OB stars ionize the surrounding hydrogen atoms which subsequently recombine to produce Hα and Brγ emission lines. Assuming ionization-bounded and internally dust-free HII regions, an extended Miller-Scalo IMF (Kennicutt 1983) between 0.1 and 100 $M_\odot$, a mass range of 10 to 100 $M_\odot$ for massive stars, case B recombination, electron temperatures and densities of 10^4 K and 10^4 cm^{-3}, one gets the relation between the massive SFR averaged over 10^7 years, and the number of Lyman continuum photons per second (N$_{\rm Ly}$):

$$(\frac{\rm SFR(M \geq 10M_\odot)}{M_\odot {\rm yr}^{-1}}) = 1.9 \times 10^{-54}\ (\frac{N_{\rm Ly}}{\rm s^{-1}}) \quad (13)$$

The total SF rate (SFR) and the Hα luminosity are then related by (Kennicutt 1983) :

$$\begin{aligned}(\frac{\rm SFR}{M_\odot {\rm yr}^{-1}}) &= 6.3 \times {\rm SFR(M \geq 10M_\odot)} \\ &= (\frac{L(H\alpha)}{7 \times 10^{41}\ {\rm ergs\ s^{-1}}}) \quad (14)\end{aligned}$$

The advantage of using Hα as a SFR tracer is that a clear physical basis exists connecting Hα recombination lines to massive young stars, and Hα observations are easily made over large field of views of tens of arcminutes, covering an entire galaxy. However, in the gas-rich circumnuclear regions and underestimate the true SFR. For a typical gas-to-dust ratio in spirals, the visual extinction $A_{\rm V}$ reaches 1 magnitude for column densities of the order of $2-4 \times 10^{21}$ H atoms cm^{-2} or gas densities of the order of 15 to 30 $M_\odot$ pc^{-2}.

(iii) *SFR from Brγ recombination line at 2.16 μm:* For a case B recombination, electron temperatures and densities of 10^4 K and 10^4 cm^{-3}, and a dust free nebula, one expects 70 Brγ photons per Lyman continuum photon (e.g., Puxley et al. 1990). Brγ fluxes, being in the NIR, have extinctions reduced by a factor of $\sim$ 10 compared to Hα. As shown in Table 5, four starburst galaxies in our sample, as well as the non-starburst galaxy NGC 3351 have published Brγ fluxes (Puxley et al. 1988; Puxley et al. 1990).

(iv) SFR from the non-thermal component of the RC emission (SFR$_{\rm RC-N}$) : Compared to the Hα and Bγ photons, the RC emission is less directly related to the SFR. However, there is empirical evidence such as the FIR-radio correlation in a variety of systems (Condon et al 1982 ;Helou et al. 1985) and a radio-Hα correlation (Kennicutt 1983), which support the use of RC as a tracer of massive SFR. The RC emission from spiral galaxies is generally made up of thermal and a non-thermal components.

The thermal component is due to free-free emission from HII regions photoionized by massive stars. At high enough frequencies where the opacity is $\ll 1$, the thermal RC luminosity is proportional to the number of ionizing Lyman continuum photons (assuming a dust-free nebula). Under these conditions, the thermal luminosity density ($L_{\rm T\nu}$ at 1.49 GHz can be related to the massive SFR using the relations in Condon (1992) and Kennicutt (1983):

$$(\frac{\rm SFR(M \geq 5M_{\odot})}{M_{\odot}{\rm yr}^{-1}}) = 0.176 \times (\frac{L_{\rm T\nu}}{10^{20}\ {\rm WHz}^{-1}}) \times (\frac{T_{\rm e}}{10^4{\rm K}})^{-0.45} (\frac{\nu}{\rm GHz})^{0.1} \quad (15)$$

The non-thermal component of the RC is due to synchrotron emission produced by relativistic electrons which are accelerated by Type II and Ib supernovae remnants (SNRs) from massive stars. At 1.49 GHz, the non-thermal component dominates over the thermal one. The non-thermal flux density ($\rm S_N$) or luminosity density ($L_{\rm N\nu}$) falls steeply with frequency as $\nu^{-\alpha}$ where α is on average ~ 0.8 at 1.49 GHz (Gioia et al. 1982; Condon 1983). It can be related to the massive SFR by assuming that all massive stars with mass M $\geq 8M_{\odot}$ produce supernovae which can accelerate the relativistic electrons. Assuming the Milky Way empirical relation between $L_{\rm N\nu}$ at 1.49 GHz and the supernovae rate ($\upsilon_{\rm SN}$) (Condon & Yin 1990), an extended Miller-Scalo IMF with an upper mass cut off $M_{\rm U}$ of 100 $M_{\odot}$, it follows that

$$(\frac{\rm SFR(M \geq 5M_{\odot})}{M_{\odot}{\rm yr}^{-1}}) = 0.019 \times (\frac{\nu}{\rm GHz})^{\alpha} (\frac{L_{\rm N\nu}}{10^{20}\ {\rm WHz}^{-1}}) \quad (16)$$

In order to apply this equation to the sample galaxies, we need to separate the non-thermal ($S_{\rm N}$) and thermal ($S_{\rm T}$) components from the total RC flux density (S) at 1.49 GHz. One way to do this is to fit power laws to continuum data at different frequencies and extrapolate the fit to 1.49 GHz, but this can lead to large errors in $S_{\rm T}$, since the non-thermal spectrum may steepen at higher frequencies (Carlstrom & Kronberg 1991; Condon 1992). Therefore, we adopted a mean thermal fraction $< S_{\rm T}/S >$ given by the approximation of Yin & Condon (1990) and Condon (1992), based on the FIR-Radio and FIR-Hα correlation. The mean scatter in this relation is a factor of 2.

$$(\frac{S}{S_{\rm T}}) = 1 + 10 \times (\frac{\nu}{\rm GHz})^{0.1-\alpha} \quad (17)$$

16. APPENDIX 2 : THEORETICAL SCENARIOS FOR CLOUD GROWTH AND THE ONSET OF SF

Theoretical ideas proposed in the last forty years for cloud growth and the onset of SF include the onset of gravitational or axisymmetric instabilities (Safronov 1960; Toomre 1964; Goldreich & Lynden-Bell 1965a; Elmegreen 1979) the growth of shearing perturbations (e.g., Elmegreen 1993), the swing amplification of shearing spiral-shaped instabilities (Goldreich & Lynden-Bell 1965b; Jog 1992), cloud collisions (e.g., Kwan 1979; Scoville, et al. 1986; Gammie et al. 1991; Elmegreen 1990). and magnetic instabilities (Parker 1966) We focus on the first three theoretical scenarios which have achieved a fair degree of empirical success. Key concepts and instability criteria are summarized.

16.1. *Gravitational instabilities*

For a thin differentially rotating gas disk, support against gravitational instabilities is provided by pressure forces on small scales, and by Coriolis forces from rotation on large scales. From the dispersion relation,

$$\omega^2 = \kappa^2 - 2\pi\ {\rm G}\ \Sigma_{\rm gas}\ |{\rm k}| + {\rm k}^2\ {\rm v}_{\rm s}^2 \quad (18)$$

one can show that axisymmetric instabilities set in when the gas surface density $\Sigma_{\rm gas}$ exceeds a critical density such that the Safronov (1960)/Toomre (1964) Q parameter falls below 1, where

$$\rm Q = \frac{\Sigma_{crit}}{\Sigma_{gas}} = \frac{\alpha\kappa\ \sigma}{\pi\ G\ \Sigma_{gas}} \leq 1 \quad (19)$$

Here, ω is the angular frequency, k is the wavenumber given by ($2\ \pi/\lambda$), $v_{\rm s}$ is the sound speed, $\Sigma_{\rm gas}$ is the gas surface density, σ is the gas velocity dispersion, κ is the epicyclic frequency, and G is the gravitational constant.

For an infinitely thin disk, α is 1, but for disks of finite thickness, α is somewhat larger (Larson 1985). Empirically, Kennicutt (1989) found that α is ~ 0.7 in the outer disks of Sc spirals. A two-fluid disk made of both gas and stars is always more unstable and will have a lower α than a purely gaseous or stellar one-fluid disk (Jog & Solomon 1984; Elmegreen 1995)

Large-scale instabilities such as gravitational instabilities (Elmegreen 1979; Jog & Solomon 1984; Larson 1985) or swing amplification (Goldreich & Lynden-Bell 1965b) can help to aggregate interstellar gas into large complexes. Molecular clouds can thereafter grow through local processes involving accretion and collisions (e.g., Kwan 1979; Scoville et al. 1986).

The overall timescale on which molecular clouds grow ($\rm t_{CL}$) is expected to be only somewhat larger than the growth timescale ($\rm t_{GI}$) for the most unstable wavelength (Larson 1988). For small Q, $\rm t_{GI}$ is given by:

$$t_{\rm GI} = \frac{\sigma}{\pi {\rm G}\ \Sigma_{\rm gas}} \approx \frac{\rm Q}{\kappa} \quad (20)$$

16.2. *Shearing Instabilities*

In order for appreciable cloud growth to occur, the gravitational perturbations must grow significantly before shearing forces disrupt the layer. The Oort A constant describes the local shear rate where

$$A = \frac{-R}{2}\ \frac{d\Omega}{dR} = \frac{1}{2}\ (\Omega - \frac{dV}{dR}) \tag{21}$$

Gravitational perturbations grow at a rate given by $(\pi \mathrm{G}\Sigma_{\rm gas}/\sigma)$, and the total growth factor from times -1/A to 1/A scales as $\mathrm{e}^{2\pi \mathrm{G}\Sigma_{\rm gas}/\sigma \mathrm{A}}$. Appreciable growth of shearing perturbations occurs when the gas density exceeds the critical shear density (e.g., Elmegreen 1993; Hunter, Elmegreen, & Baker 1998), and the shear S criterion is less than 1 :

$$\Sigma_{\rm shear} = \frac{2.5\ A\ \sigma}{\pi\ \mathrm{G}} \tag{22}$$

and

$$\mathrm{S} = \frac{\Sigma_{\rm shear}}{\Sigma_{\rm gas}} = \frac{2.5\ \mathrm{A}\ \sigma}{\pi\ \mathrm{G}\ \Sigma_{\rm gas}} \leq 1 \tag{23}$$

The S and Q criteria converge to similar critical densities for a flat rotation curve where $\kappa \sim 1.4\Omega$, and 2.5 $A \sim 1.3\Omega$.

16.3. *Swing Amplification*

Another process which could be relevant to the growth of density fluctuations in differentially rotating gas disks is swing amplification. Even if Q is above Q_O, this does not stabilize a gas disk against non-axisymmetric ($m \geq$ 2) instabilities. Shearing disturbances and loosely wound spiral density waves can be amplified by swing amplification. This process requires the disk to be cold and the disturbance to be loose. The X parameter is a measure of how tight the disturbance is:

$$\mathrm{X} = \frac{\mathrm{k_c\ R}}{\mathrm{m}} = \frac{2\pi\ \mathrm{R}}{\mathrm{m}\ \lambda_{\rm c}} = \frac{\mathrm{R}\ \kappa^2}{2\ \pi\ \mathrm{m\ G}\ \Sigma_{\rm gas}} \tag{24}$$

A necessary and sufficient condition for swing amplification to work for m=2 modes is Q $\leq$ 3 and X $\leq$ 3. For Q between 1.5 to 2, amplifications factors ranging from 5 to 30 are typically achieved for m=2 modes (Goldreich and Lynden-Bell 1965; Julian and Toomre 1966).

REFERENCES

AAalto, S., Booth, R. S., Black, J. H., Koribalski, B., Wielebinski, R. 1994, A&A, 286, 365
Aalto, S., Booth, R. S., Black, J. H., & Johansson, L. E. B. 1995, A&A 300, 369.
Athanassoula, E. 1992, MNRAS, 259, 345
Athanassoula, E; 2002, ApJL, 569, 83
Athanassoula, E. 2003; , MNRAS, 341, 1179
Baker, A. J. 2000, Ph.D. thesis
Ball, R. 1986, ApJ, 307, 453
Benedict, G. F., Smith, B. J., and Kenney, J. D. P., 1996, AJ, 111, 1861
Binney, J., & Tremaine, S. 1987, Galactic Dynamics, ed. Ostriker, J. P. (Princeton, N. J.: Princeton University Press)
Bloemen, J. B. G. M., Caraveo, P. A., Hermsen, W., Lebrun, F., Maddalena, R. J., Strong, A. W., & Thaddeus, P. 1984, A&A, 139, 37.
Bloemen, J. B. G. M., Strong, A. W., Mayer-Hasselwander, H. A., Blitz, L., Cohen, R. S., Dame, T. M., Grabelsky, D. A., Thaddeus, P., Hermsen, W., & Lebrun, F. 1986, A&A, 154, 25
Bournaud, F., & Combes, F. 2002, A&A, 392, 83
Byrd, G., Rautiainen, P., Salo, H., Buta, R., & Crocher, D. A. 1994, AJ, 108, 476
Cayatte, V., van Gorkom, J. H., Balkowski, C. & van Gorkom, J. H. 1994 AJ, 107, 1003
Chevalier, R. A., & Furenlid, I. 1978, ApJ, 225, 67
Combes, F., & Gerin, M. 1985, A&A, 150, 327
Combes, F., Debasch, F., Friedli, D., & Pfenniger, D. 1990, A&A, 233, 82
Combes, F. & Elmegreen, B. G. 1993, A&A, 271, 391
Combes, F. 1996, in Proceedings of the Les Houches School, Starbursts: Triggers, Nature, and Evolution, ed. B. Guiderdoni & A. Kembhavi (Berlin: Springer-Verlag; Les Ulis: EDP Sciences), 175.
Condon, J. J., Condon M. A., Gisler, G., Puschell, J. J. 1982, ApJ, 252, 102
Condon, J. J., Helou, G., Sanders, D. B., & Soifer, T. B. 1990, ApJS, 73, 359
Condon, J. J., & Yin, Q. F. 1990, ApJ, 357, 97
Condon, J. J. 1992, ARAA, 30, 575
Condon, J. J., Anderson, E., & Broderick, J. J. 1995, AJ, 109, 2318
Contopoulos, G. & Papayannopoulos, T. 1980, A&A 92, 33
Courteau, S., de Jong, R. S., Broeils, A. H. 1996, ApJ 457, L73.
Das, M. & Jog, C. J. 1995, ApJ, 451, 167
de Blok, W. J. G., McGaugh, S. S., & van der Hulst, J. M. 1996, MNRAS, 283, 18
de Blok, W. J. G. & McGaugh, S. S. 1997,
de Vaucouleurs, G., de Vaucouleurs, A., Corwin Jr., H. G., Buta, R. J., Paturel, G., & Fouque, P. 1991, Third Reference Catalogue of Bright Galaxies (New York: Springer) (RC3)
Deharveng, J. M., Sasseen, T. P., Buat, V., Bowyer, S., Lampton, M., & Wu, X. 1994, A&A, 289, 715
Devereux, N. A. 1989, ApJ, 346, 126
Devereux, N. A & Young, J. S. 1990 ApJ, 359, 42
De Jong, R. S. 1996, A&A 313, 45
Dickey, J. M., Hanson, M. M., & Helou, G. 1990, ApJ, 352, 522
Dickman, R. L. 1975, ApJ, 202, 50
Dickman, R. L., Snell, R. L., & Schloerb, F. P. 1986, ApJ, 309, 326
Eder, J. A. 1990, Ph.D. thesis, Yale University
Elmegreen, B. G. 1982, ApJ, 253, 655
Elmegreen, B. G. 1989, ApJ, 338, 178
Elmegreen, B. G. 1990, ApJ, 357, 125
Elmegreen, B. G., Kaufman, M., & Thomasson, M. 1993, ApJ, 412, 90
Elmegreen, B. G., 1993, in SF in Stellar Systems, ed. G. Tenorio-Tagle, M. Prieto & F. Sanchez (Cambridge: Cambridge University Press), 381
Elmegreen, B. G. 1995, MNRAS, 275, 944
Elmegreen, D. M., Chromey, F. R., Santos, M., & Marshall, D. 1997, AJ, 114, 1850
Freeman, K. C. 1996, in ASP Conference Series, Vol. 91, Proceedings of IAU Colloquium 157, Barred Galaxies, ed. R. Buta, D. A. Crocker, & B. G. Elmegreen (San Francisco: ASP), 230
Friedli, D., & Martinet, L. 1993, A&A, 277, 27
Friedli, D. & Benz, W. 1995, A&A, 268, 65
Friedli, D. & Benz, W., & Kennicutt, R. 1994, ApJ, 430, L105
Friedli, D., Wozniak, H., Rieke, M., & Bratschi, P. 1996, A&AS, 118, 461
Gammie, C. F., Ostriker, J. P., & Jog, C. J. 1991, ApJ. 378, 565
Giovanelli, R. & Haynes, M. P. 1983, AJ, 88, 881
Goldreich, P., & Lynden-Bell, D. 1965a, MNRAS, 130, 125
Goldreich, P., & Lynden-Bell, D. 1965b, MNRAS, 130, 125
Grosbol, P. J. 1985, A&AS, 60, 261
Grosbol, P. 2002, in ASP Conf. Series, Disks of Galaxies: Kinematics, Dynamics, & Perturbations eds. E. Athanassoula & A. Bosma, in print
Guiricin, G., Tamburni, L., Mardirossin, F., Mezzetti, M., & Monaco, P. 1994, ApJ, 427, 202
Handa, T., Sofue, Y., & Nakai, N. 1991, in Proceeding of IAU Symposium 146, Dynamics of Galaxies and Their Molecular Cloud Distributions, ed. F. Combes and F. Casoli (Dordrecht: Kluwer), 156
Hasan, H., & Norman, C. 1990, ApJ, 361, 69
Hasan, Pfenniger, & Norman 1993
Hawarden, T. G., Mountain, C. M., Leggett, S. K., & Puxley, P. J. 1986 MNRAS, 221, 41Athanassoula, E. 1992, MNRAS, 259, 345
Heckman, T. M., Armus, L., & Miley, G. K. 1990, ApJS, 574, 833
Helfer, T. T., & Blitz, L. 1993, ApJ, 419, 86
Helfer et al. 2001, ApJS, 276, 1131
Heller, C. H., & Shlosman, I. 1996
Helou, G., Soifer, B. T., & Rowan-Robinson, M. 1985, ApJ, 298, L7
Ho, L. C., Filippenko, A. V., & Sargent, W. L. W. 1997, ApJ, 487, 591

Hunt, L. K., & Malkan, M. A. 1999, ApJ, 516, 660

Hunter, D. A., Gillett, F. C., Gallagher, J. S., Rice, W. L., & Low, F. J. 1986, ApJ, 303, 171.

Hunter, D. A. & Plummer, J. D. 1996, ApJ, 462, 732

Hunter, D. A., Elmegreen, B. G., & Baker, A. L. 1998

Impey, C. and Bothun, G. 1989, ApJ, 341, 341, 89

Jog, C. J., & Solomon, P. M. 1984, ApJ, 276, 127

Jog, C. J. 1992, ApJ, 390, 378

Jogee, S., & Kenney, J. D. P. 1996, in ASP Conference Series, Vol. 91, Proceedings of IAU Colloquium 157, Barred Galaxies, ed. R. Buta, D. A. Crocker, & B. G. Elmegreen (San Francisco: ASP), 230

Jogee, S., Kenney, J. D. P., & Smith, B. J. 1998, ApJL, 494, L185

Jogee, S. 1999, Ph.D. thesis, Yale University

Jogee, S., Kenney, J. D. P., & Smith, B. J. 1999, ApJ, 526, 665

Jogee, S. 2001, in Proceedings of Rinberg Workshop, Starbursts Near and Far, eds L. Tacconi & D. Lutz (Heidelberg: Springer-Verlag), 182 (astro-ph/0201202)

Jogee, S., Baker, A. J., Sakamoto, K., Scovile, N. Z., & Kenney, J. D. P. 2001, ASP Conf. Series, Vol. 249, The Central kpc of Starbursts and AGN: The La Palma Connection, eds. J. H. Knapen, J. E. Beckman, I. Shlosman, & T. J. Mahoney (San Francisco: ASP), 612 (astro-ph/0201209)

Jogee, S., Knapen, J. H., Laine, S., Shlosman, I., Scoville, N. Z., & Englmaier, P. 2002a, ApJL, 570, L55 (astro-ph/0201208)

Jogee, S., Shlosman, I., Laine, S., Knapen, J. H., Englmaier, P., Scoville, N. Z., & Wilson, C. D. 2002b, ApJ, Aug 10 issue (astro-ph/0202270)

Jogee, S., & GEMS/GOODS collaboration 2003 IAU Symposium 216, Maps of the Cosmos.

Julian, W. H., & Toomre, A. 1966, ApJ, 146, 810.

Kenney, J. D. P., & Young, J. S. 1989, ApJ, 344, 171

Kenney, J. D. P., & Lord, S. D. 1991, ApJ, 381, 118

Kenney, J. D. P., Wilson, C. D., Scoville, N. Z., Devereux, N. A., & Young, J. S. 1992, ApJ, 395, L79

Kenney, J. D. P., Carlstrom, J. E., & Young, J. S. 1993, ApJ, 418, 687

Kennicutt, R. C., Jr. 1983, ApJ, 272, 54

Kennicutt, R. C., Jr. 1989, ApJ, 344, 685

Kennicutt, R. C., Jr., 1998, ApJ, 498, 541

Knapen, J. H., Beckman, J. E., Heller, C. H., Shlosman, I., & De Jong, R. S. 1995, ApJ, 454, 623

Kohno, K., Kawabe, R., & Vila-Vilar, B. 1999, ApJ, 511, 157

Kormendy, J. 1983, ApJ, 265, 632

Kormendy, J. 1993, in Proceedings of IAU Symposium 153, Galactic bulges, ed. H. DeJonghe and H. J. Habing, (Dordrecht: Kluwer), 209

Kwan, J. 1979, ApJ, 229, 567

Laine, S., Kenney, J. D. P., Yun, M. S., & Gottesman, S. T. 1999, ApJ, 511, 709

Laine, S. & Heller, C. H. 1999, MNRAS, 308, 557

Larson, R. B. 1985, MNRAS, 214, 379

Mobasher, M., Jogee, S., Dahlen, T., de Mello, D., Lucas, R. A., Conselice, C. J., Grogin, N. A., & Livio M. 2004, ApJL, 600/2, 74 (astro-ph/0309066)

Munoz-Tunon, C., Vilchez, J. M., Castaneda, H. O., & Beckman, J. E. 1989, Ap&SS, 157, 165

Maiolino, R., Ruiz, M., Rieke, G. H., & Papadopulos, P. 1997, ApJ, 485, 552

Martin, P. 1995, AJ, 109, 2428

Martin P., & Roy, R. 1995, ApJ, 445, 161

Merritt, D., & Sellwood, J. A. 1994, ApJ, 425, 551

Munoz-Tunon, C., Vilchez, J. M., Castaneda, H. O., & Beckman, J. E. 1989, Ap&SS, 157, 165

Norman, C. A., Sellwood, J. A., & Hasan, H. 1996, ApJ, 462, 114.

Padin, S., Scott, S. L., Woody, D. P., Scoville, N. Z., Seling, T. V., Finch, R. P., Giovanine, C. J., & Lawrence, R. P. 1991, PASP, 103, 461

Parker, E. N. 1966, ApJ, 145, 811

Pfenniger, D. & Norman, C. 1993, ApJ, 409, 91

Piner, B., Glenn, S., James, M., & Teuben, P. J. 1995, ApJ, 449, 508

Puxley, P. J., Hawarden, T. G., & Mountain, C. M. 1988, MNRAS, 234, 29

Puxley, P. J., Hawarden, T. G., & Mountain, C. M. 1990, ApJ, 364, 77.

Quillen, A. C., Frogel, J. A., Kenney, J. D. P., Pogge, R. W., & DePoy, D. L. 1995, ApJ, 441, 549

Regan, M. W., Vogel, S. N., & Teuben, P. J. 1997, ApJ, 482, L143

Regan, M. W. et al. 2001, ApJ, 561, 218

Safronov, V. S. 1960, Annales d'Astrophys, 23, 979

Saha, A., et al. 1996. ApJ, 466, 55

Saikia, D. J., Pedlar, A., Unger, S. W., & Axon, D. J. 1994, MNRAS, 270, 46

Sakamoto, K., Scoville, N. Z. , Yun, M. S., Crosas, M., Genzel, R. et al. 1999, ApJ, 514, 68

Sandage, A. & Bedke, J., 1994, The Carnegie Atlas of Galaxies (Washington D. C.: Carnegie Institute of Washington)

Schweizer, F., & Seitzer, S. 1988, ApJ, 328, 88

Scoville, N. Z., Sanders, D. B., & Clemens, D. P. 1986, ApJ, 310, L7

Scoville, N. Z., Yun, M. S., Clemens, D. P., Sanders, D. B., & Waller, W. H. 1987, ApJS, 63, 821

Scoville, N. Z., & Sanders, D. B. 1987, in Interstellar Processes, ed. D. J. Hollenbach and H. A. Thronson (Dordrecht: Reidel), 21

Scoville, N. Z., Carlstrom, J. E., Chandler, C. J., Phillips, J. A., Scott, S. L., Tilanus, R. P. J., & Wang, Z. 1993, PASP, 105, 1982

Scoville, N.Z., Yun, M.S., & Bryant, P.M. 1997, ApJ, 484, 702

Sellwood, J. A, 1993, in Proceedings of IAU Symposium 153, Galactic bulges, ed. H. DeJonghe and H. J. Habing, (Dordrecht: Kluwer), 391

Shaw, M. A., Axon, D., Probst, R., Gatley, I. 1995, MNRAS, 274, 369.

Shlosman, I., Frank, J., and Begelman, M. C. 1989, Nature, 338, 45

Smith, B. J. 1994, AJ, 107, 1695

Soifer, B. T., Boehmer, L., Neugebauer, G., & Sanders, D. B. 1989, AJ 98, 766

Solomon, P. M., Rivolo, A. R., Barrett, J., & Yahil, A. 1987, ApJ, 319, 730

Strong, A. W., Bloemen, J. B. G. M., Dame, T. M., Grenier, I. A., Hermsen, W., Lebrun, F., Nyman, L.-A., Pollock, A. M. T., & Thaddeus, P. 1988, A&A, 207, 1

Tacconi, L. J., & Young, J. S. 1986, ApJ, 308, 600

Taylor, C. L., Brinks, E., Pogge, R. W., & Skillman, E. D. 1994, AJ, 107, 971

Toomre, A. 1964, ApJ, 139, 1217

Tubbs, A. D. 1982, ApJ, 255, 458

Tully, R. B. 1988, 'Nearby Galaxies Catalog' (Cambridge: Cambridge University Press)

van den Bergh, S. 1976, ApJ, 206, 883

van der Hulst, J. M., Skillman, E. D., Smith, T. R., Bothun, G. D., McGaugh, S. S., & de Blok, W. J. G. 1993, AJ, 106, 548

van Zee, L., Haynes, M. P., Salzer, J. J., Broeils, A. H. 1996, AJ, 112, 129

van Zee, L., Haynes, M. P., Salzer, J. J., Broeils, A. H. 1997, AJ, 113, 1618

Vila, M. B., Pedlar, A., Davies, R. D., Hummel, E., & Axon, D. J. 1990, MNRAS, 242, 379

Vila-Costas, M. B., & Edmunds, M. G. 1992, MNRAS, 259, 121

Wall, W. F., & Jaffe, D. T. 1990, ApJ, 361, L45

Wilson, C. D., Scoville, N. Z., & Rice, W. 1991, AJ, 101, 1293

Wozniak, H., Friedli, D., Martinet, L., Martin, P., Bratschi, P., 1995, A&AS 111, 115.

Young, J. S., & Scoville, N. Z. 1991, ARAA, 29, 581

Young, J. S., Xie, S., Tacconi, L., Knezek, P., Viscuso, P., Tacconi-Garman, L., Scoville, N., Schneider, S. et al. 1995, ApJS, 98, 219

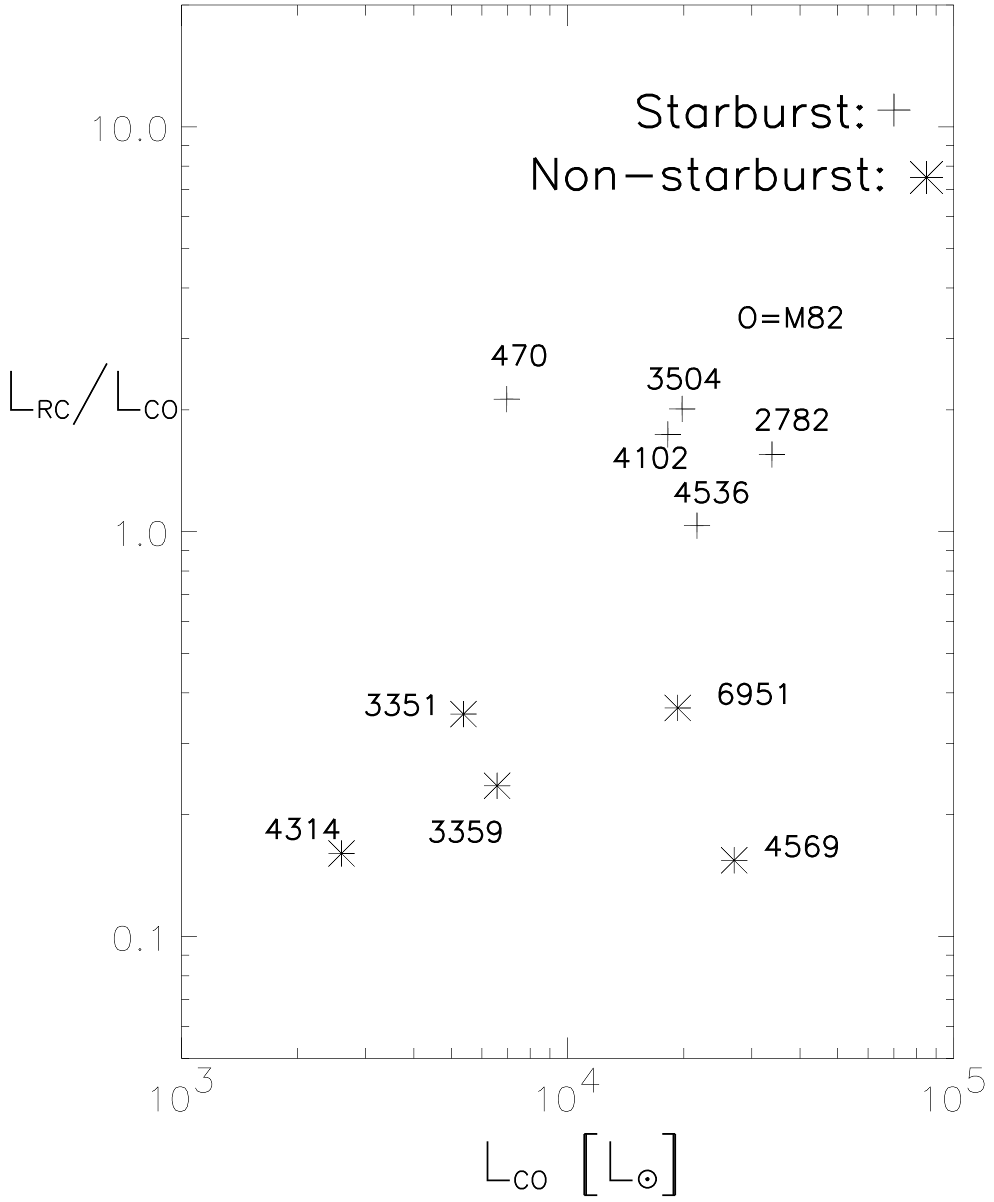

Fig. 1— The sample of barred starbursts and non-starbursts: L_{RC} is the RC luminosity at 1.49 GHz and $L_{\rm CO}$ is the single dish CO luminosity. Both are measured in the central 45″ diameter or inner 1-2 kpc radius. The galaxies in our sample (designated by their NGC numbers) as well as the prototypical starburst M82 are plotted. Note that for a given L_{CO}, the star formation rate per unit mass of molecular hydrogen as characterized by L_{RC}/L_{CO} can vary by an order of magnitude.

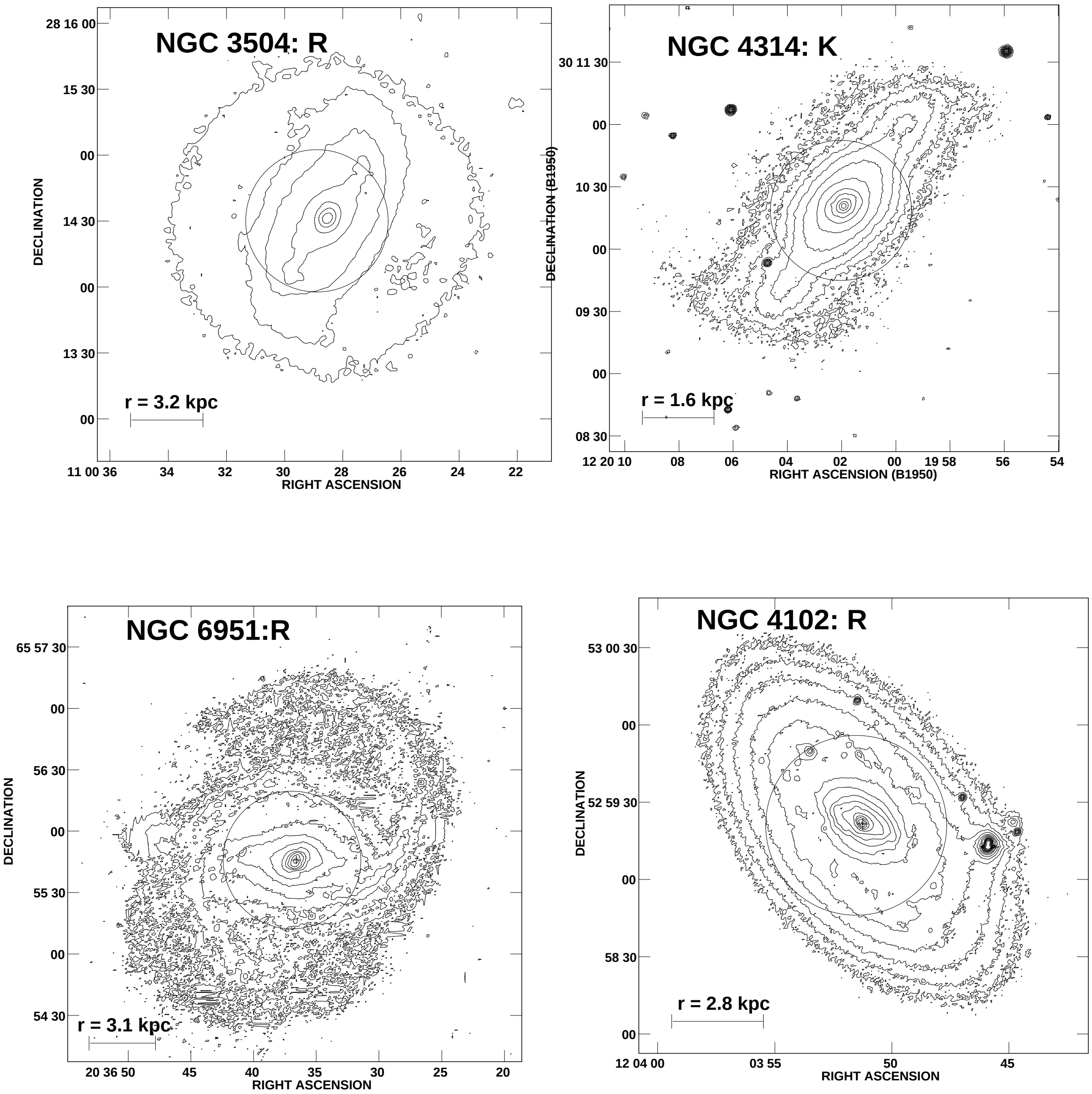

Fig. 2— Evidence for large-scale stellar bars/oval distortions: (a) R-band image of NGC 3504 **(b)** K-band image of NGC 4314, **(c)** R-band image of NGC 6951, and **(d)** the R-band image of NGC 4102. These images illustrate the large-scale stellar bars and oval distortions in typical sample galaxies. The dotted circle shows the OVRO CO(1–0) half power beam width (65″) at 115 GHz and illustrates the region where molecular gas is mapped.

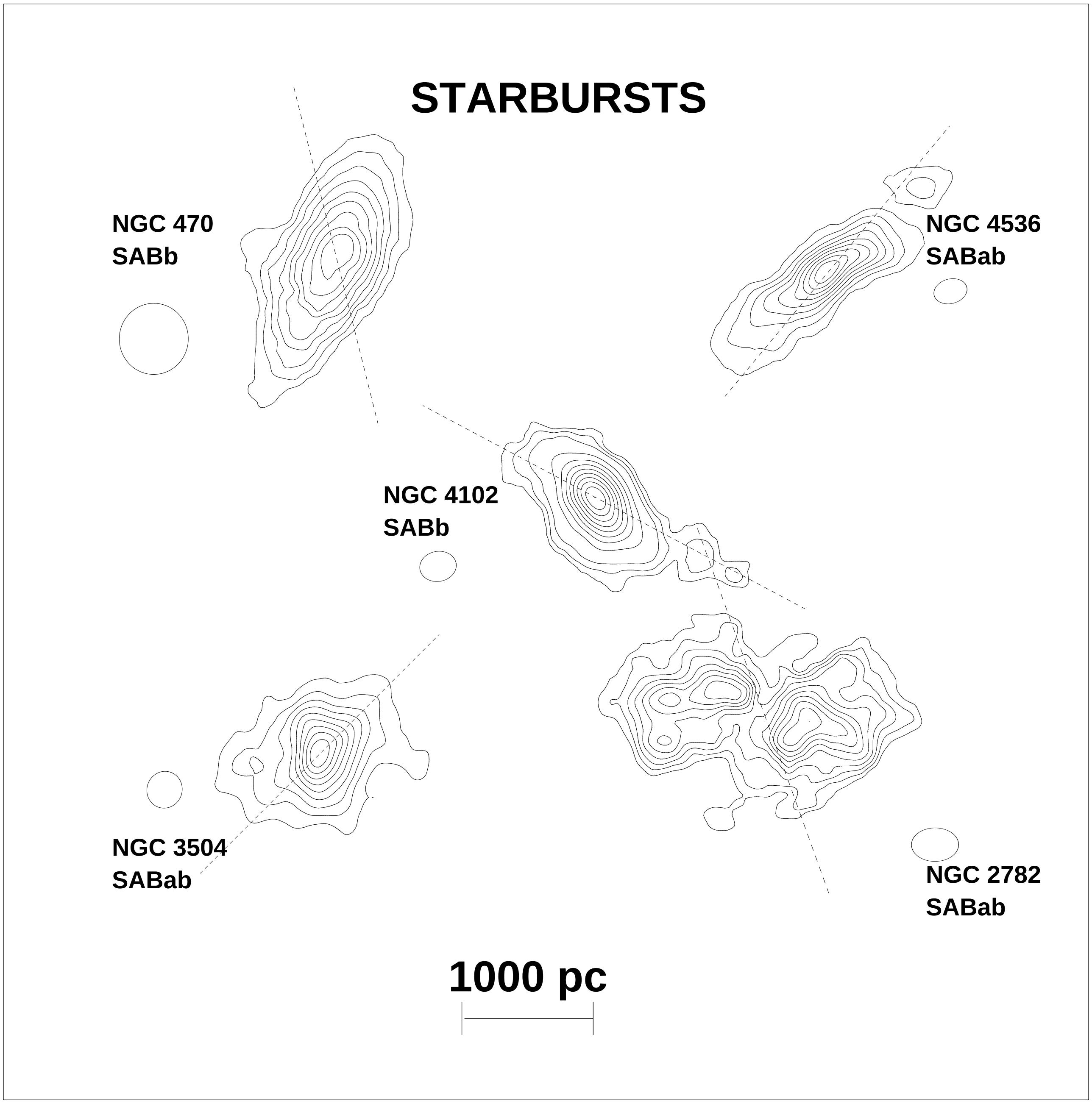

Fig. 3— The circumnuclear molecular gas morphology: The CO total intensity (moment 0) maps of barred starbursts and non-starbursts are shown. The size of the synthesized beam is shown next to each map. The dotted line shows the position angle of the large-scale stellar bar/oval. There is a wide variety of circumnuclear CO morphologies including relatively axisymmetric annuli or disks (starbursts NGC 4102, NGC 3504, NGC 4536, and non-starbursts NGC 4314), elongated double- peaked and spiral morphologies (starburst NGC 2782 and non-starbursts NGC 3351 and NGC 6951), and extended distributions elongated along the bar (non-starburst NGC 4569). The relationship between the gas distribution and the resonances of the bar is discussed in § 10 and Fig. 9.

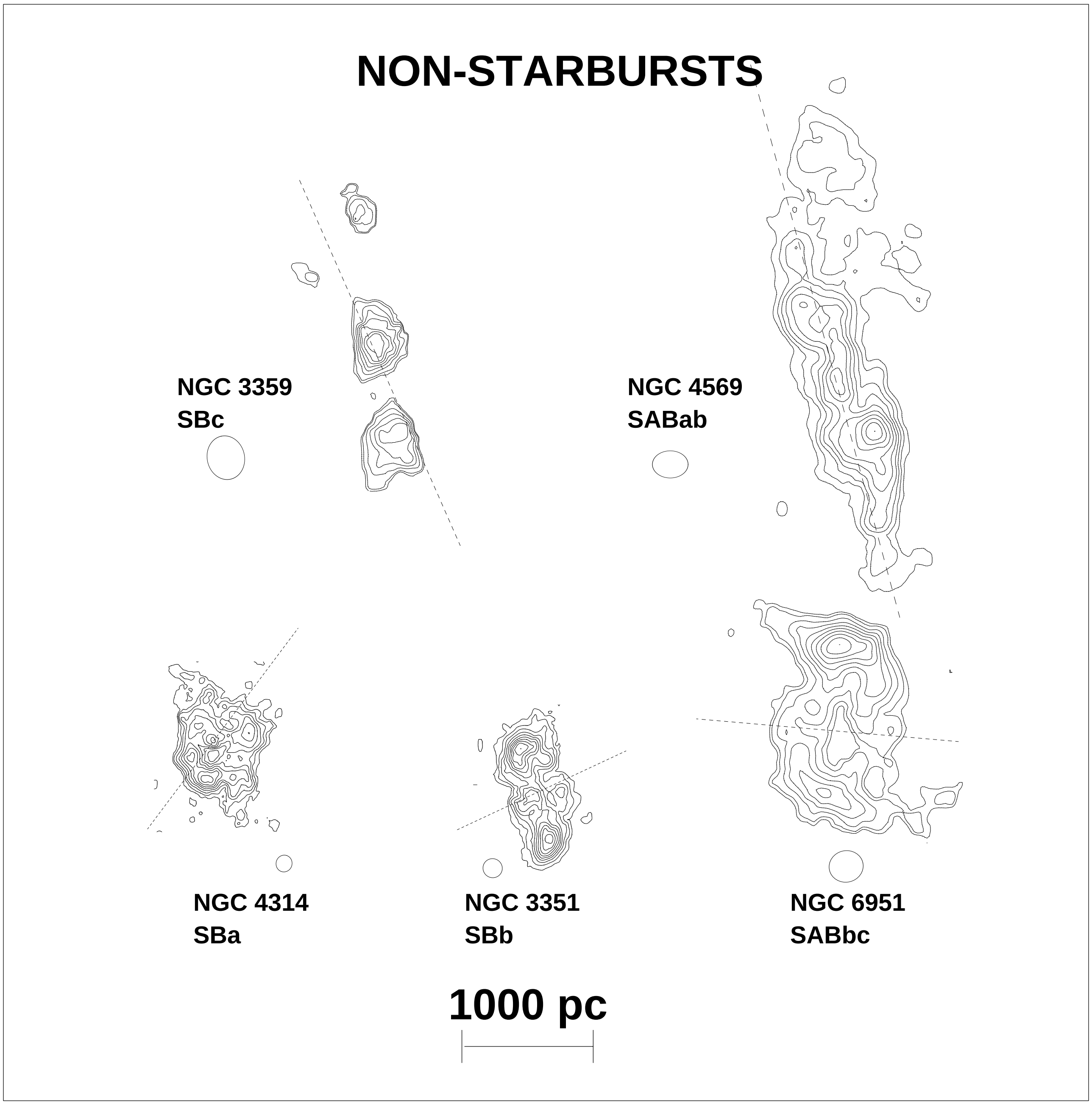
NON-STARBURSTS
NGC 3359
SBc
NGC 4569
SABab
NGC 4314
SBa
NGC 3351
SBb
NGC 6951
SABbc
1000 pc

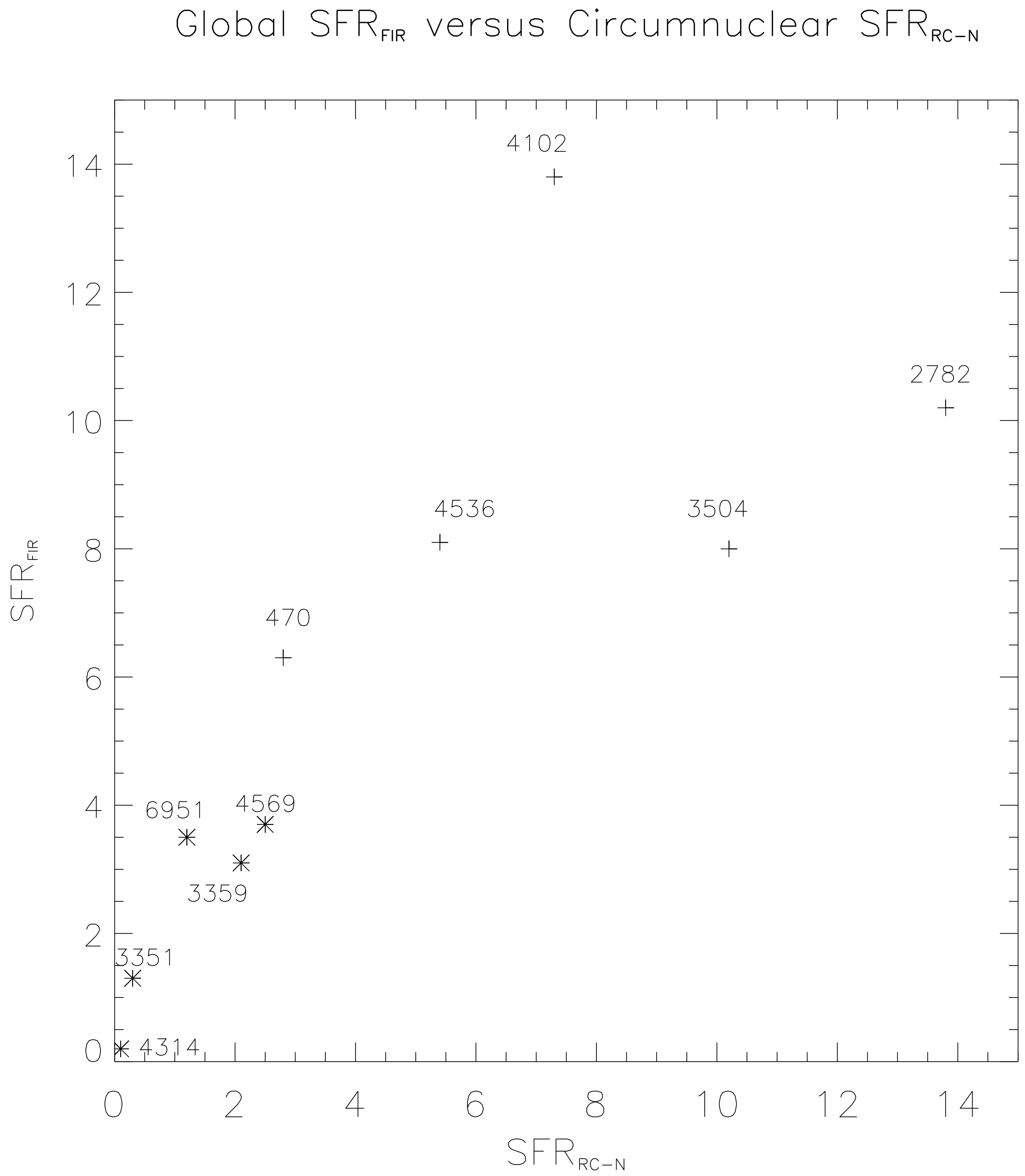

Fig. 4— A comparison of the SFRs estimated from different tracers: The star formation rate (SFR_{RC-N}) estimated from the non-thermal RC in 45″ is plotted against the star formation rate(SFR_{FIR}) estimated from the total FIR luminosity. SFR_{RC-N} is less than SFR_{FIR} as expected, except in NGC 2782 and NGC 3504, where SFR_{RC-N} is 10 to 30 % higher.

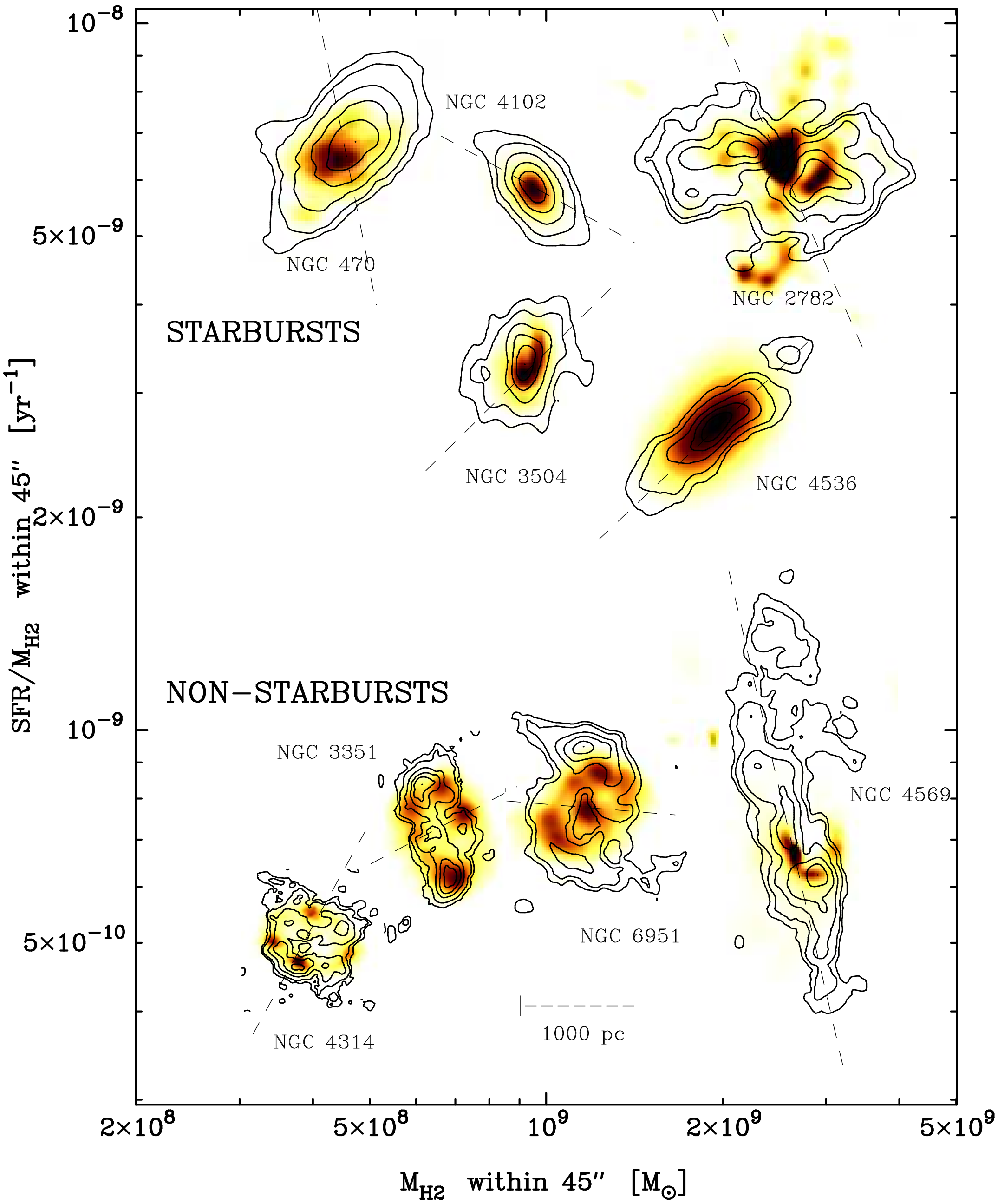

Fig. 5— Distribution of molecular gas and SF in the barred starbursts and non-starbursts: In the SFR/M_{H2} versus M_{H2} plane, the CO intensity (contours) is overlaid on the 1.5 or 4.9 GHz radio continuum map (greyscale) of NGC 4102, NGC 2782, and NGC 6951 and on the Hα map for the other galaxies. The greyscale traces the star formation activity and in the case of NGC 6951, it also shows the Seyfert 2 nucleus in the inner 100 pc. The Hα and RC maps have a resolution of $1.0 - 1.5''$. The synthesized CO beam is typically $2''$ or 100–200 pc. The dotted line is the P.A. of the large-scale stellar bar/oval.

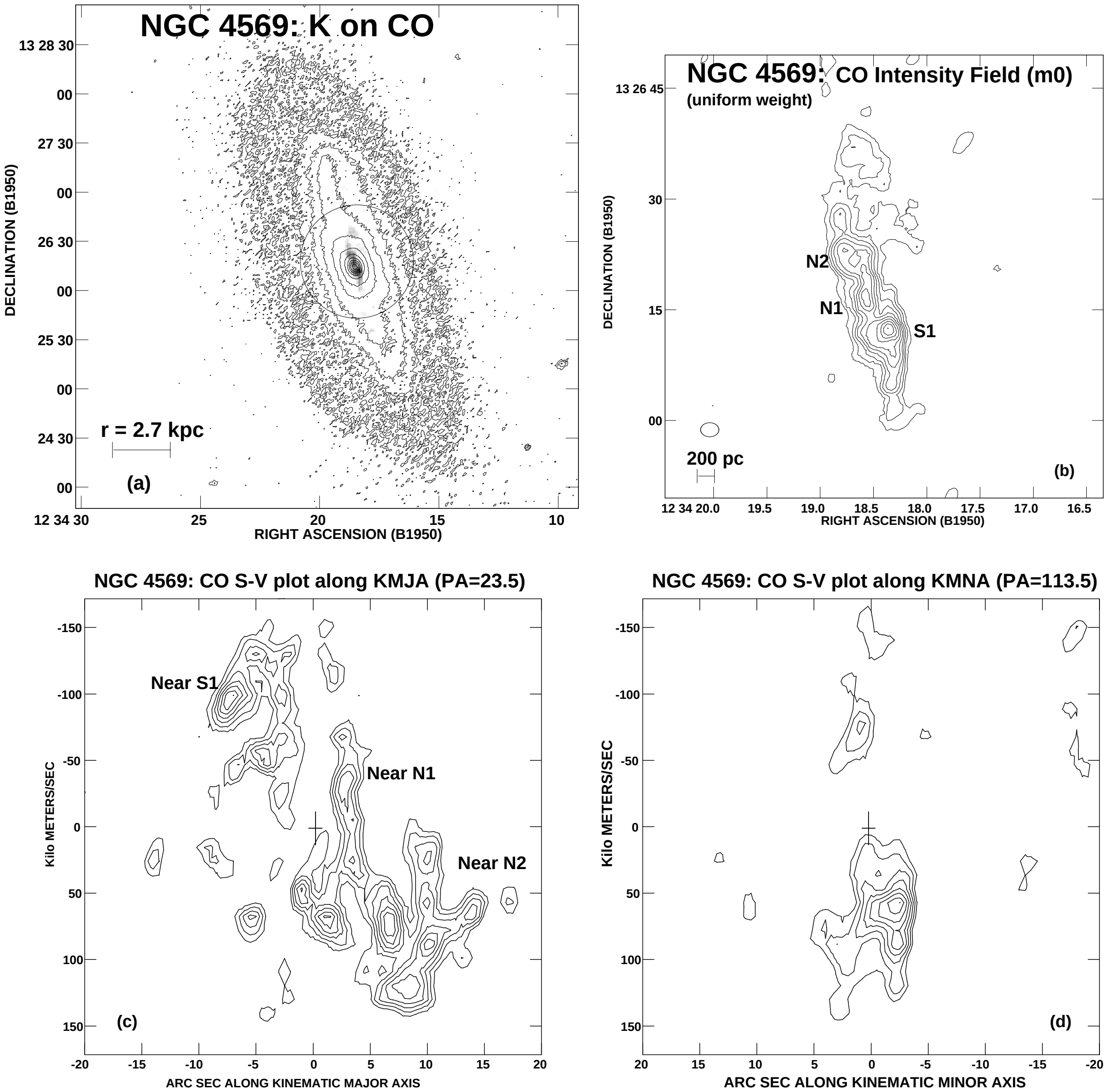

Fig. 6— Gas distribution and kinematics in NGC 4569: (a) The *K*-band image (contours) with a field of view of 5′ (25.9 kpc) shows an asymmetric stellar bar. The overlaid circle shows the 65″ half power beam width of the CO interferometric observations. The CO distribution inside the beam is shown in greyscale. **(b)** The uniformly weighted (2.65″ × 2.01″ or 223 × 169 pc) CO total intensity map in the central 6″ (5.0 kpc) shows an extended molecular gas distribution in NGC 4569. The gas extends out to a large (20 ″ or 1.7 kpc) radius, and is elongated along the direction of the large-scale stellar bar. **(c), (d)** show the spatial velocity plots along the kinematic major and minor axes. The molecular gas extends out to a 2 kpc radius and shows very disturbed kinematics. Along the kinematic major axis, velocities are generally positive (i.e above the systemic value) on the northeastern side. However, at a radius of 5″ (400 pc), near the feature marked 'N1' in (b), the velocities change from $\sim +100$ km s^{-1} to a forbidden velocity of -75 km s^{-1}.

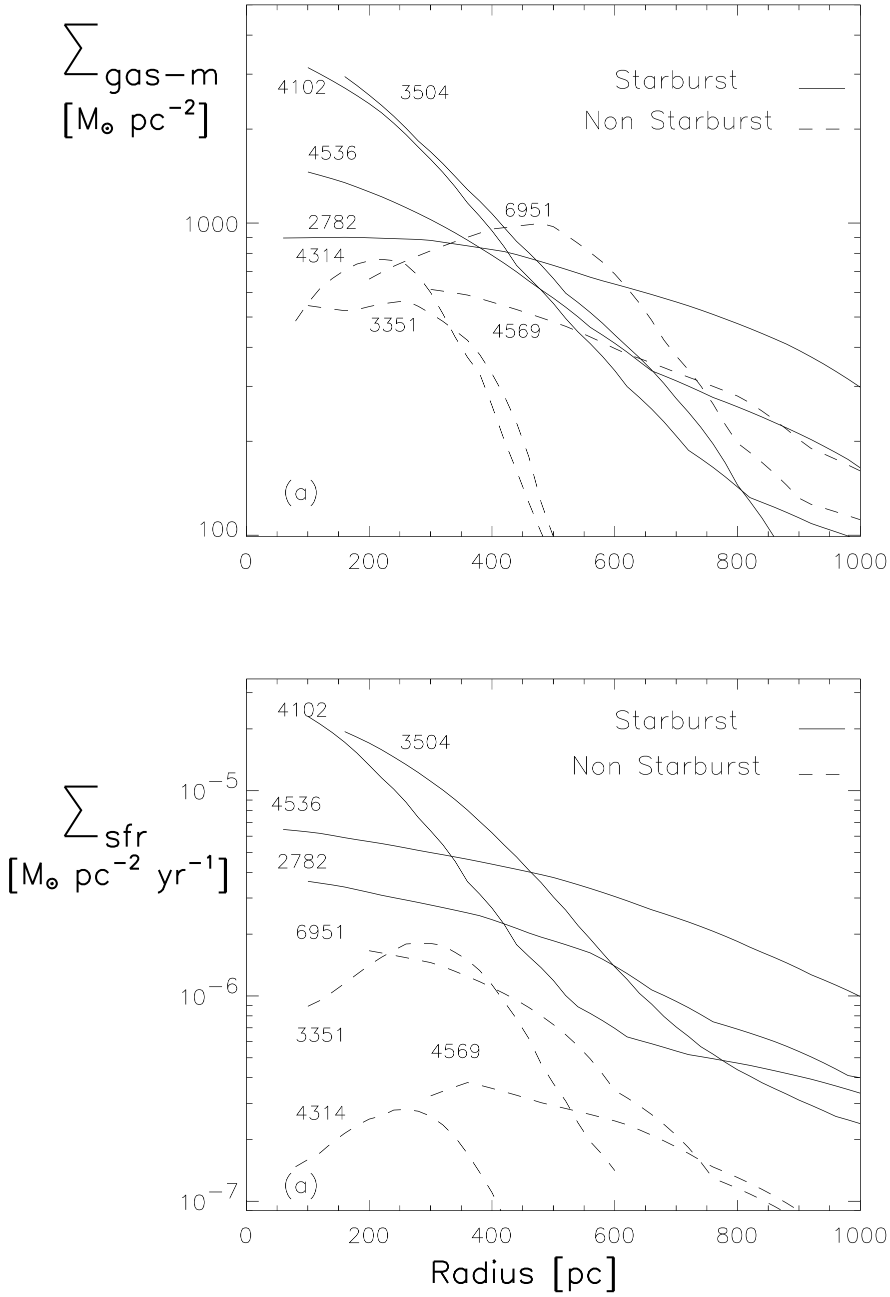

Fig. 7— **(a), (b)** show the azimuthally averaged molecular gas surface density (Σ_{gas}) and the SFR per unit area (Σ_{SFR}). The extinction-corrected profiles are convolved to a similar resolution of 100-200 pc for all the galaxies. Quantities are plotted starting at a radius $\geq$ half the size of the synthesized beam (typically 2$''$ or 150 pc). Most of the starbursts have developed larger molecular gas surface densities (1000-3500 $M_\odot$ pc^{-2}) in the inner 500 pc radius than the non-starbursts, for a given CO-to-H$_2$ conversion factor. In the inner 500 pc radius of the starbursts, both $\Sigma_{\rm gas-m}$ and Σ_{SFR} increase towards the center.

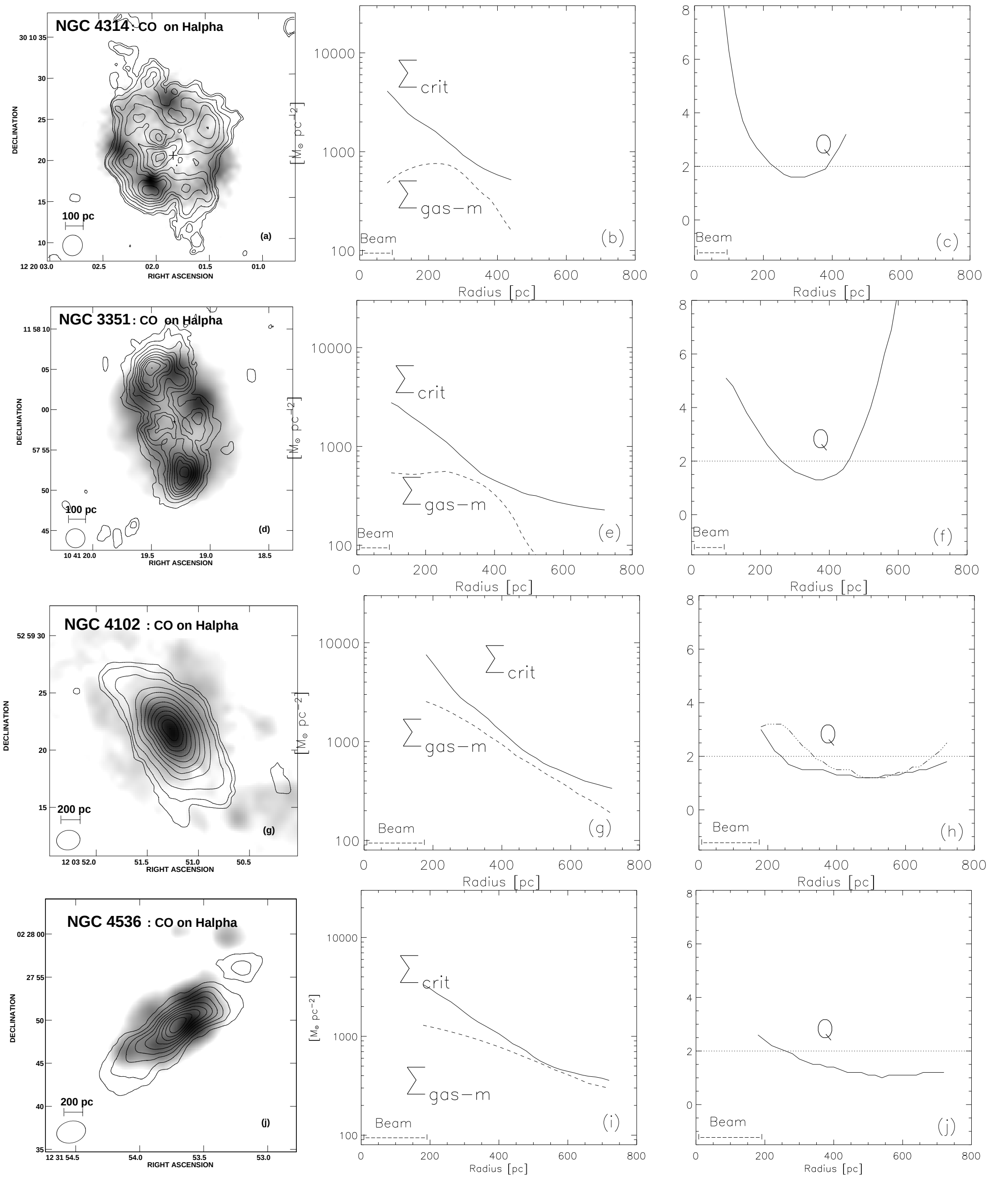

Fig. 8— Comparison of the gas density with the Toomre critical density in the non-starbursts and starbursts: Column 1: The CO distribution (contours) on the Hα (greyscale) for the non-starbursts NGC 4314 and NGC 3351, and the starbursts NGC 4102 and NGC 4536. **Column 2:** The molecular gas surface density $\Sigma_{\rm gas-m}$ and the critical density ($\Sigma_{\rm crit}$ $=\alpha\kappa\sigma/\pi G$) for the onset of gravitational instabilities assuming α =1. Quantities are plotted starting at a radius equal to the CO beam size ($\sim 2''$). **Column 3:** The Toomre Q parameter ($\Sigma_{\rm crit}/\Sigma_{\rm gas}$). The horizontal line denotes the value of Q in the outer disk of spirals where Kennicutt (1989) finds α =0.7. In the non-starbursts NGC 4314 and NGC 3351, HII regions are concentrated in a gas-rich annulus of radius 350 pc ($7''$) while further in, the star formation activity drops sharply despite large gas surface densities above 400 $M_\odot$ pc^{-2}. In these non-starbursts, Q reaches its lowest value (1–2) in the ring of HII regions while at lower radii Q increases to $\sim$ 6, suggesting sub-critical gas densities. In the starbursts NGC 4102 and NGC 4536, Q remains remarkably close to 1–2 over a wide region, between a radius of 250 to 700 pc, although the gas surface density and the epicyclic frequency both vary by nearly an order of magnitude.

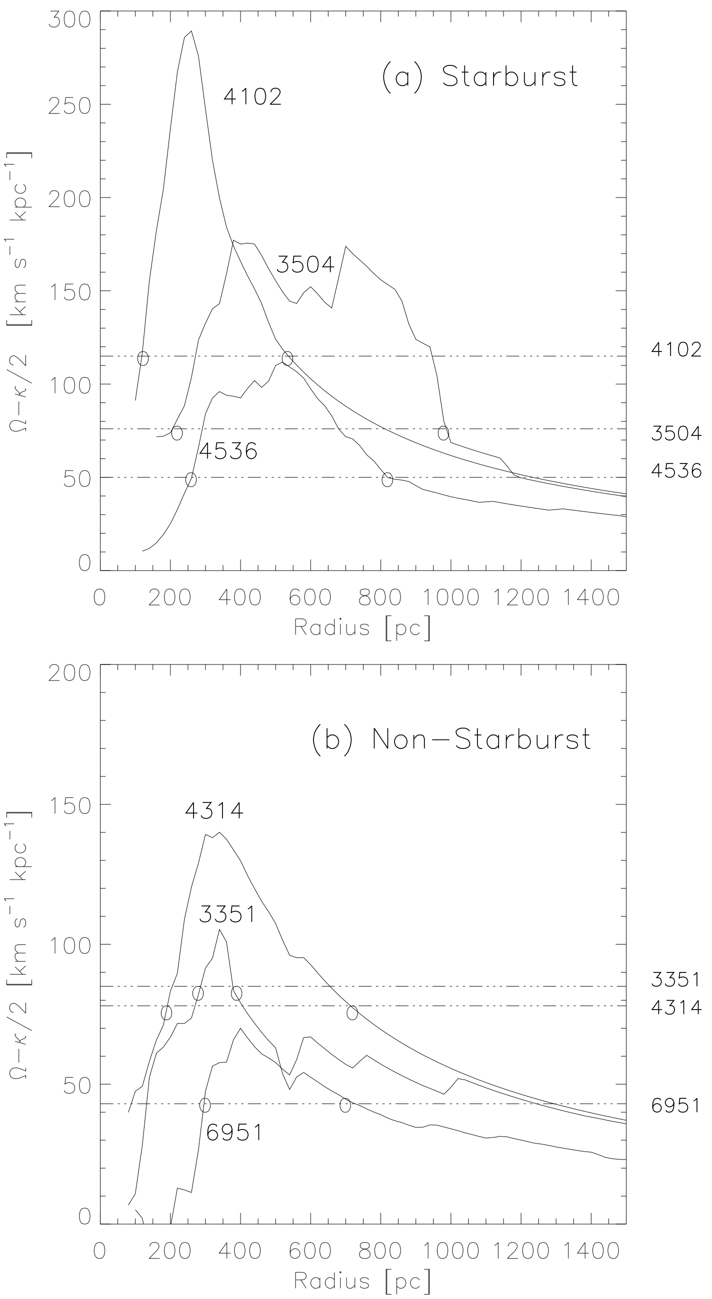

Fig. 9— Inner Lindblad resonances in the barred starbursts and non-starbursts: [Ω - $\kappa/2$] is plotted against radius for select **(a)** starbursts and **(b)** non-starbursts. The bar pattern speed Ω_p is drawn as horizontal lines and estimated by assuming that the corotation resonance is near the end of the large-scale stellar bar (see Table 9). Under the epicycle theory for a weak bar, the intersection of [Ω - $\kappa/2$] with Ω_p defines the locations of the ILRs. In these systems, the circumnuclear gas is concentrated inside the outer ILR of the large-scale stellar bar/oval.

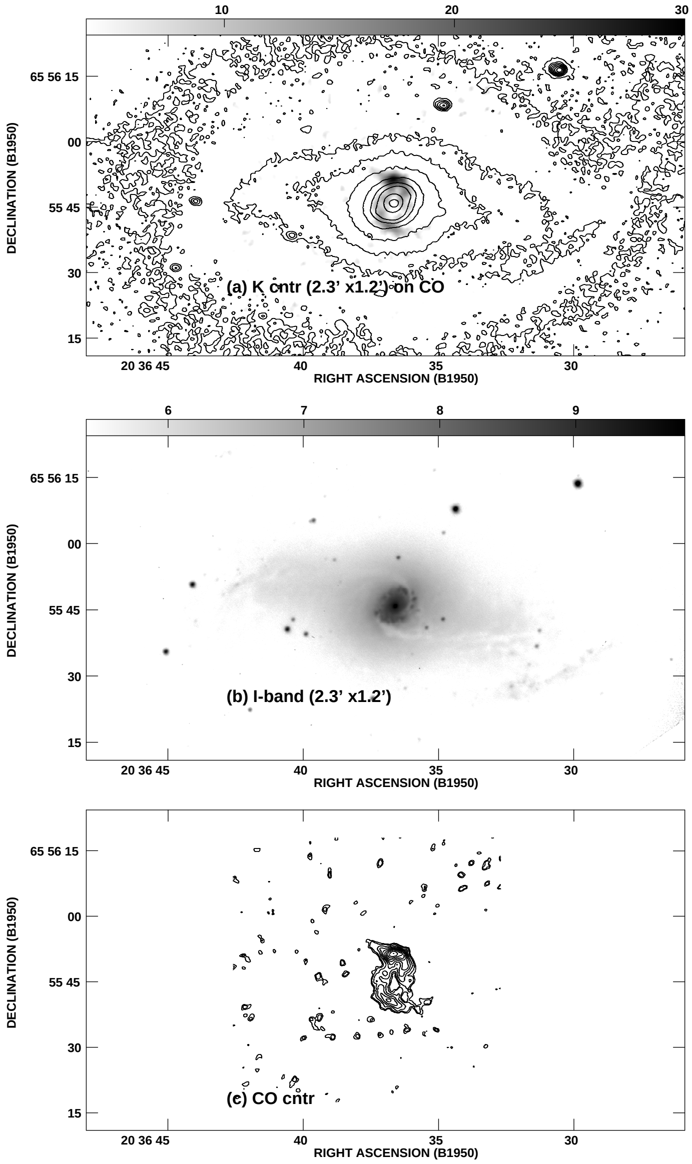

Fig. 10— Relationship between the large-scale stellar bar, large-scale dust lanes, and circumnuclear CO morphology in NGC 6951: (a) The K-band image (contours) of NGC 6951 with a $2.3' \times 1.2'$ (12.7×6.9 kpc) field of view shows the inner region of the large-scale stellar bar which has a semi-major axis of $28''$ (5.2 kpc). The circumnuclear CO (J=1->0) total intensity map (greyscale) is superposed, but note that its half power beam is only $65''$ (6.1 kpc). **(b) *I*-band image with the same field of view as the K-band image in (a). Two relatively straight dust lanes extend along the major axis of the large-scale stellar bar and are offset towards its leading edge. These dust lanes do not cross the center of the galaxy, but rather cross the bar minor axis and connect to a ring of star formation of radius $\sim 4''$ (380 pc). (c)** The CO (J=1->0) total intensity map (contours) is displayed on the same scale as (a) and (b) to facilitate comparisons. NGC 6951 has two spiral-shaped CO arms where the emission peaks at a radius r $\sim 6''$ (570 pc). The two CO peaks lie almost along the minor axis of the bar and the CO arms connect to the two relatively straight dust lanes on the leading edge of the large-scale stellar bar. The CO and dust morphology are consistent with the piling up of gas near the OILR.

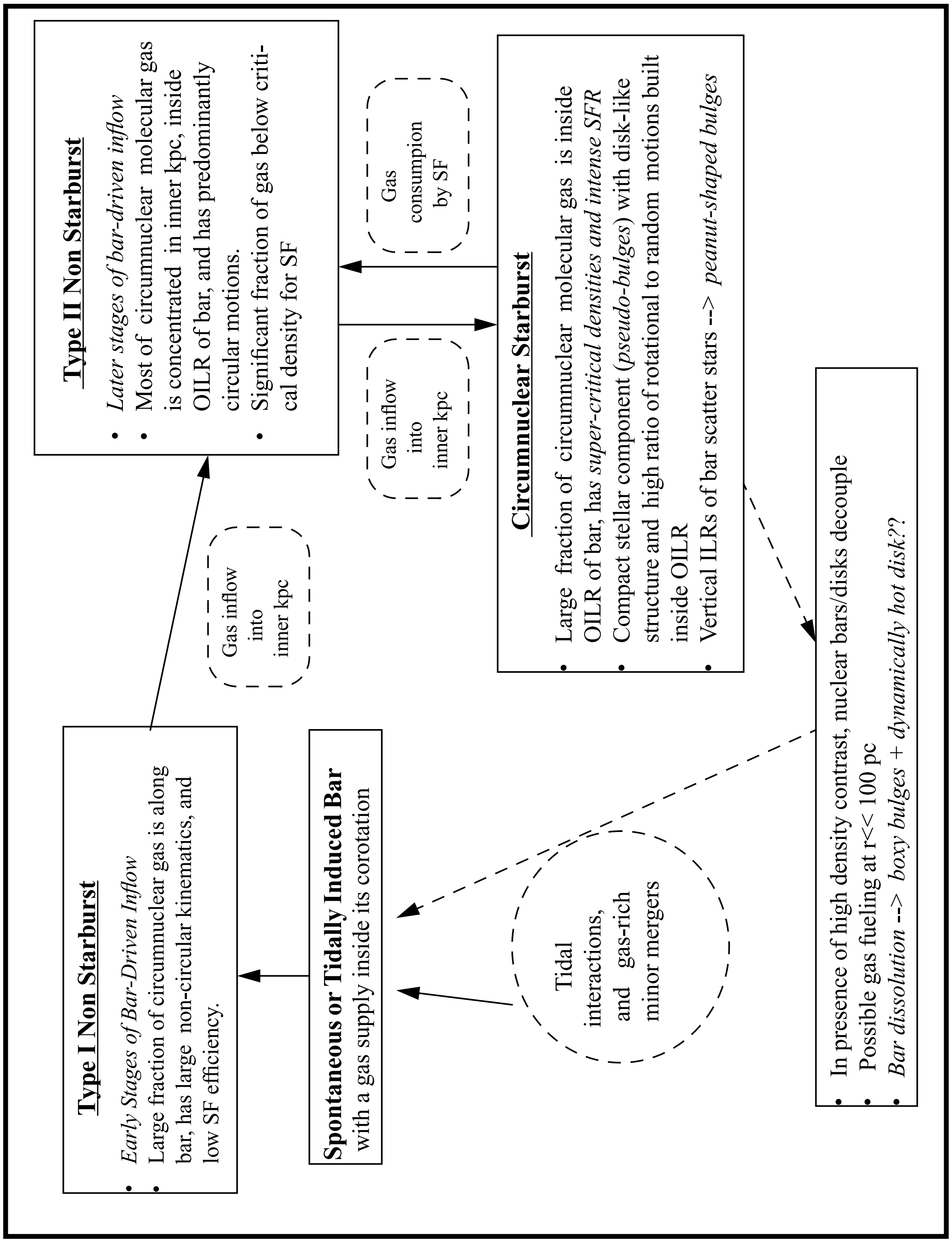

Fig. 11— Bar-Driven Secular Evolution: This figure sketches possible scenarios for bar-driven dynamical evolution and postulates potential evolutionary connections between the barred starbursts and non-starbursts in our sample. We suggest that a strongly barred galaxy would show up as a Type I non-starburst in the early stages of bar-driven inflow where large amounts of gas are still inflowing along the bar, have large non-circular motions, and are not forming stars efficiently. In the later stages where most of the circumnuclear gas has piled up inside the OILR of the bar, we may see a Type II non-starburst or even a circumnuclear starburst if most of the gas exceeds a critical density. The latter seems well represented by the Toomre value in our sample. Pseudo-bulges (Kormendy 1993) or compact stellar components with disk-like properties can be built in the inner kpc, as seen in our sample galaxy NGC 3351. Over its lifetime, a disk galaxy can undergo numerous episodes of bar-driven gas inflow and gradually build up its central mass concentration and bulge, provided an adequate gas supply is maintained inside the corotation radius of the bar. However, if the central mass concentration becomes large enough, bar dissolution may occur, leaving behind a dynamically hot disk. It is as yet unclear if tidal interactions and gas-rich accretions can lead to viable recurrent bar formation in such a disk.

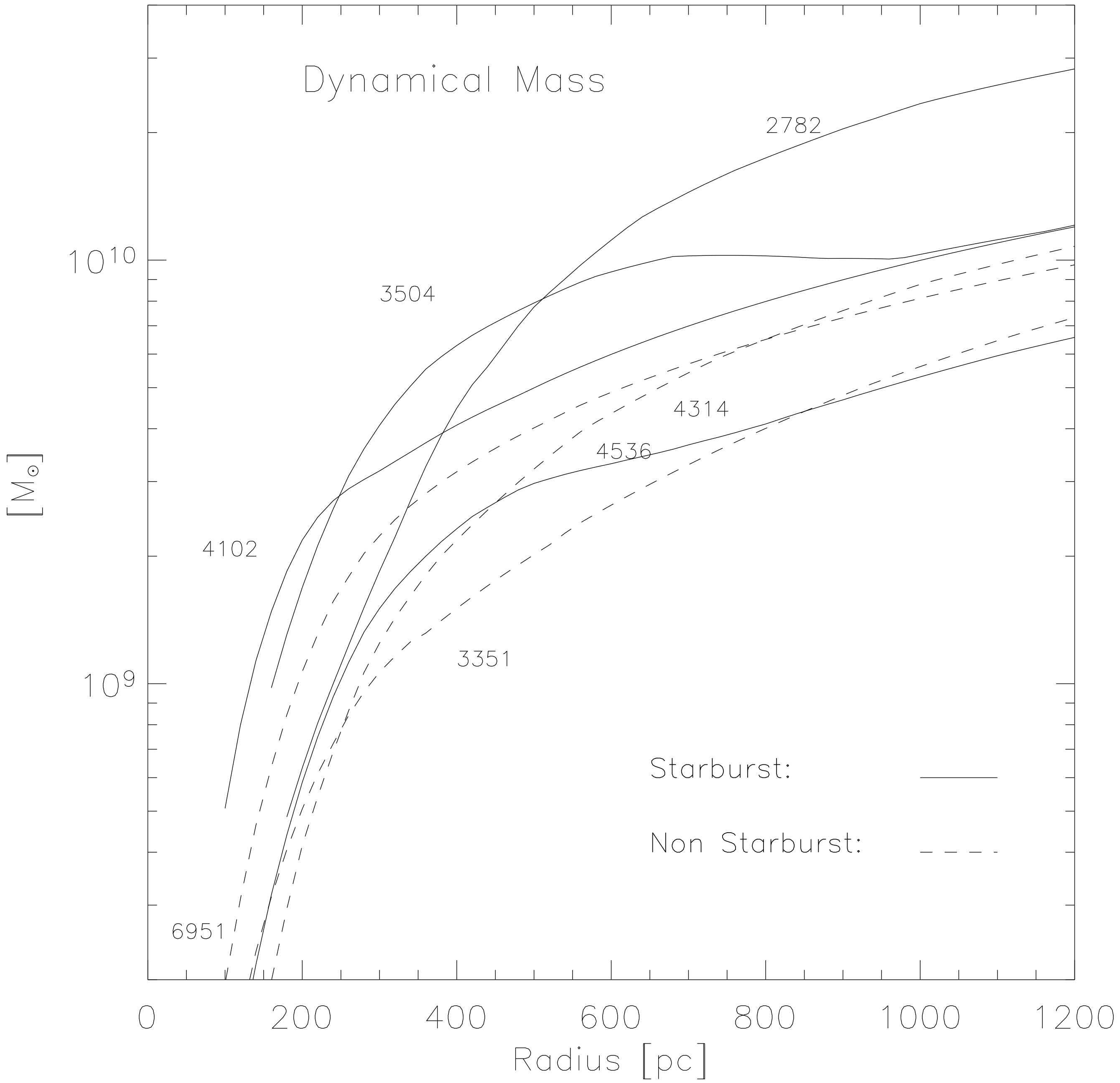

Fig. 12— The enclosed dynamical mass within the inner kpc: The dynamical mass (M_{dyn}) enclosed within a given radius R is estimated from the rotation curve, assuming a spherically symmetric gas distribution. Values are shown only for sample barred galaxies where a reliable rotation curve can be derived. For R=1 kpc, M_{dyn} has a range of 6–30 $\times 10^9$ $M_\odot$

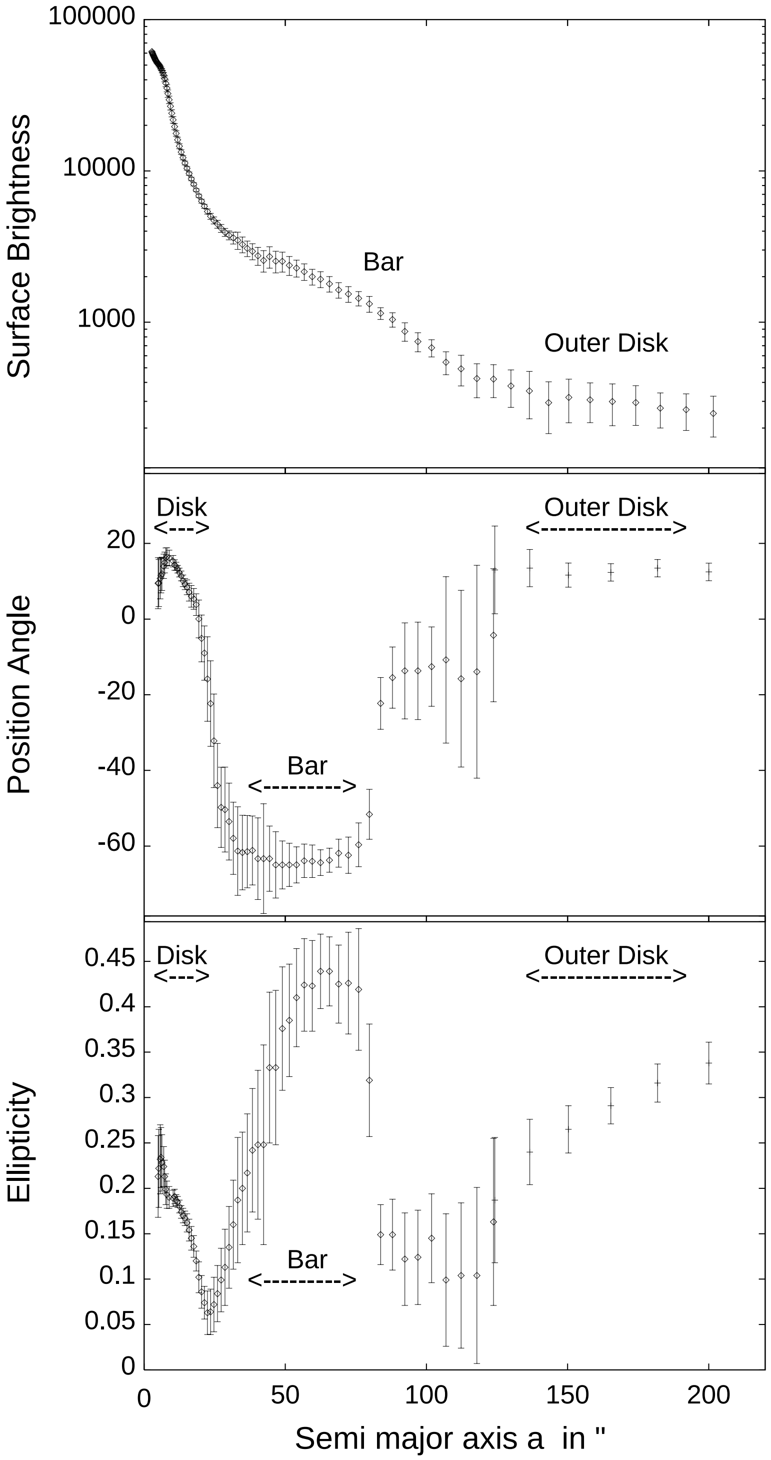

Fig. 13— Evidence for a pseudo-bulge or compact disk in NGC 3351? The isophotal analysis of the K-band and R-band images of NGC 3351 is shown. Inside the inner kpc radius, the ellipticity rises from a minimum value of 0.05 at r $\sim$ 1 kpc to a maximum of $\sim$ 0.2 at a radius of $5''$ (250 pc). The position angle (P.A.) of the isophotes change from -60deg in the region of the large-scale stellar bar to a value between 5 and 20deg in the central $5''$ (250 pc) radius. The central component has an ellipticity and P.A. which is similar to that of the outer disk, and a published high ratio of rotational to random motions.

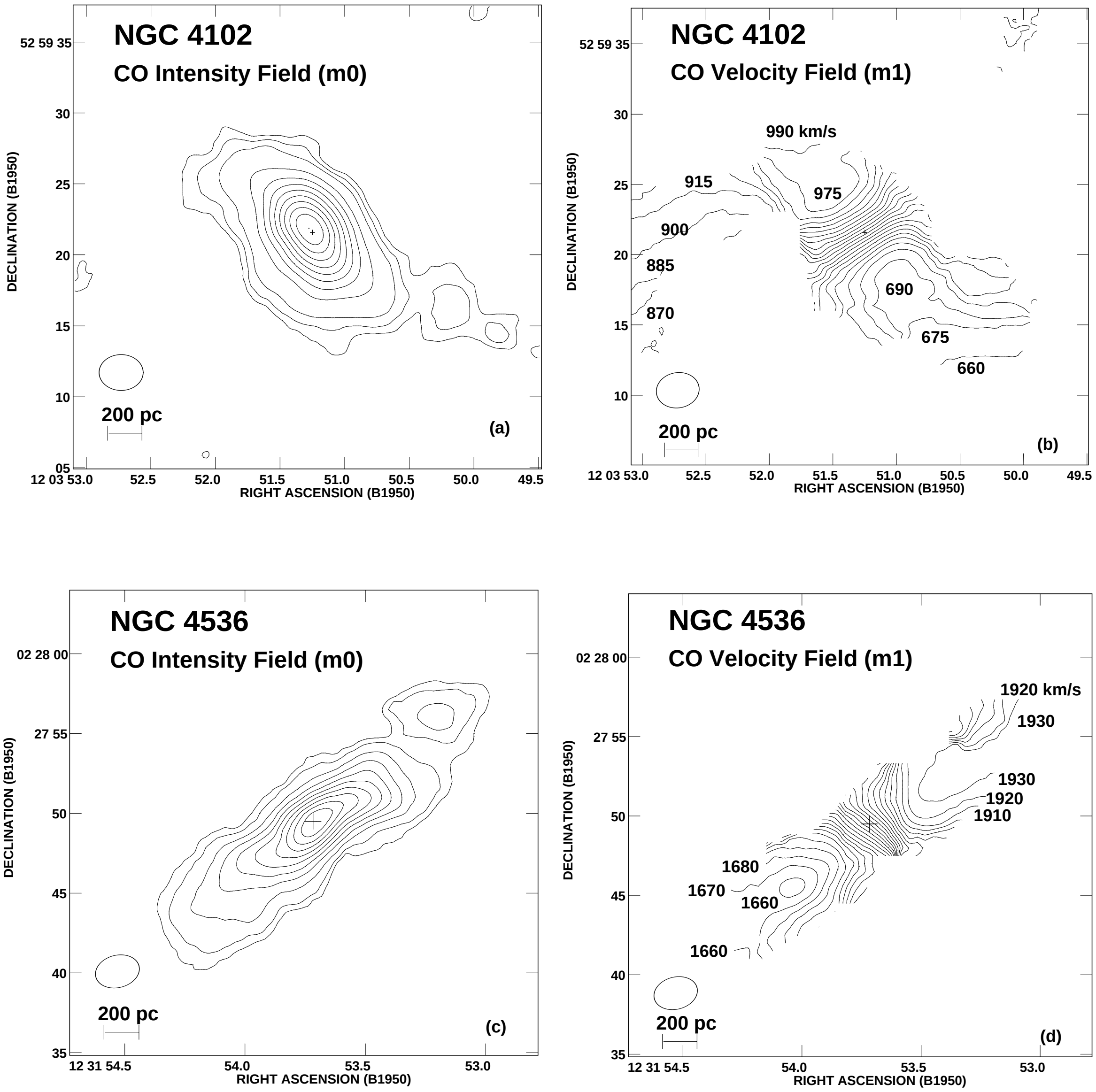

Fig.14— Molecular gas kinematics and distribution in individual starbursts: The CO intensity-weighted velocity (moment 1) fields and the CO total intensity (moment 0) maps of the starbursts NGC 4102 (a-b), NGC 4536 (c-d), NGC 3504 (e-f), NGC 470 (g-h), and NGC 2782 (i-j) are shown. The size of the synthesized beam is shown next to each map. Relatively axisymmetric annuli or disks (NGC 4102, NGC 3504, NGC 4536) and elongated double-peaked morphologies (NGC 2782) are seen. The velocity field in the inner 500 pc radius is generally dominated by circular motions, with weaker non-circular components. In NGC 4102 and NGC 4536, there are faint gas streams which extend out, intersect the dust lanes on the leading edges of the large-scale stellar bar, and show non-circular motions. In NGC 2782, there are weak bar-like streaming motions in the inner 400 pc radius, on the leading side of a nuclear stellar bar.

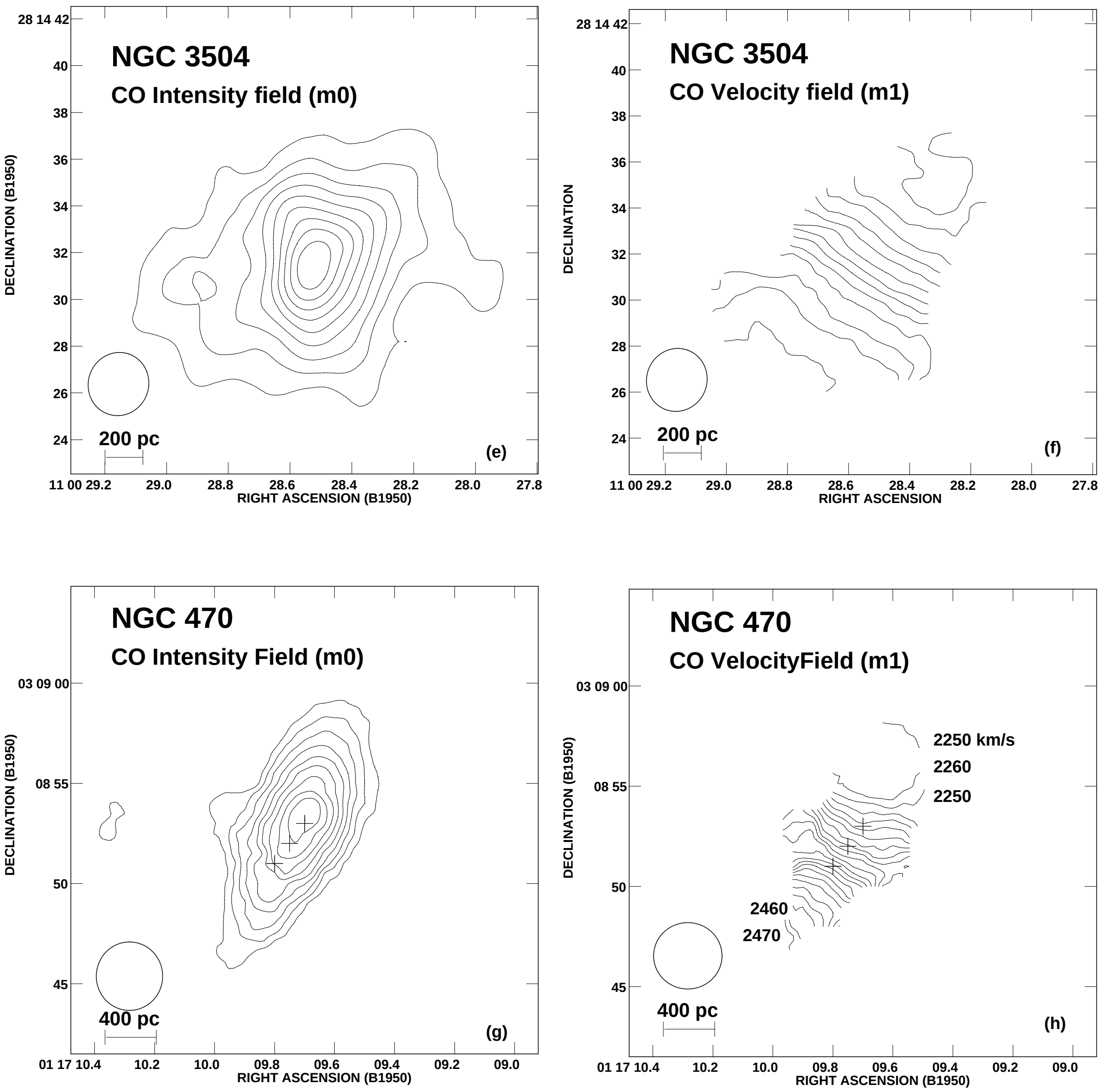
NGC 3504
CO Intensity field (m0)
DECLINATION (B1950)
RIGHT ASCENSION (B1950)
200 pc
(e)
NGC 3504
CO Velocity field (m1)
DECLINATION
RIGHT ASCENSION
200 pc
(f)
NGC 470
CO Intensity Field (m0)
DECLINATION (B1950)
RIGHT ASCENSION (B1950)
400 pc
(g)
NGC 470
CO VelocityField (m1)
2250 km/s
2260
2250
2460
2470
DECLINATION (B1950)
RIGHT ASCENSION (B1950)
400 pc
(h)

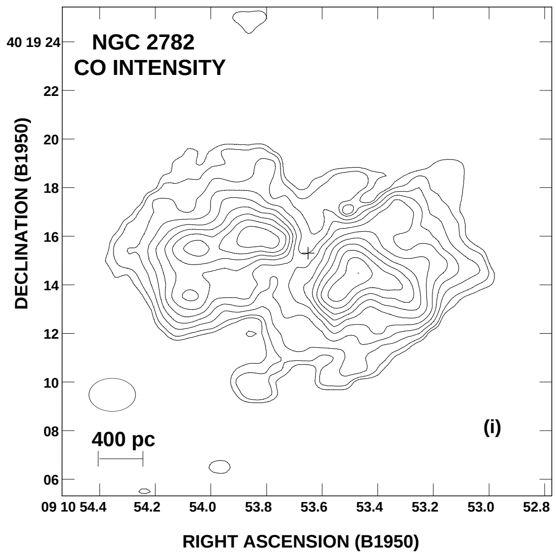
NGC 2782
CO INTENSITY
40 19 24
22
20
18
16
14
12
10
08
06
DECLINATION (B1950)
400 pc
(i)
09 10 54.4
54.2
54.0
53.8
53.6
53.4
53.2
53.0
52.8
RIGHT ASCENSION (B1950)

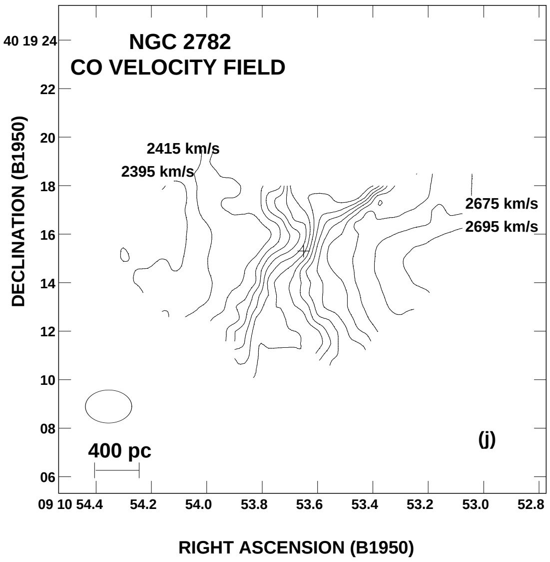
NGC 2782
CO VELOCITY FIELD
40 19 24
22
20
18
16
14
12
10
08
06
DECLINATION (B1950)
2415 km/s
2395 km/s
2675 km/s
2695 km/s
400 pc
(j)
09 10 54.4
54.2
54.0
53.8
53.6
53.4
53.2
53.0
52.8
RIGHT ASCENSION (B1950)

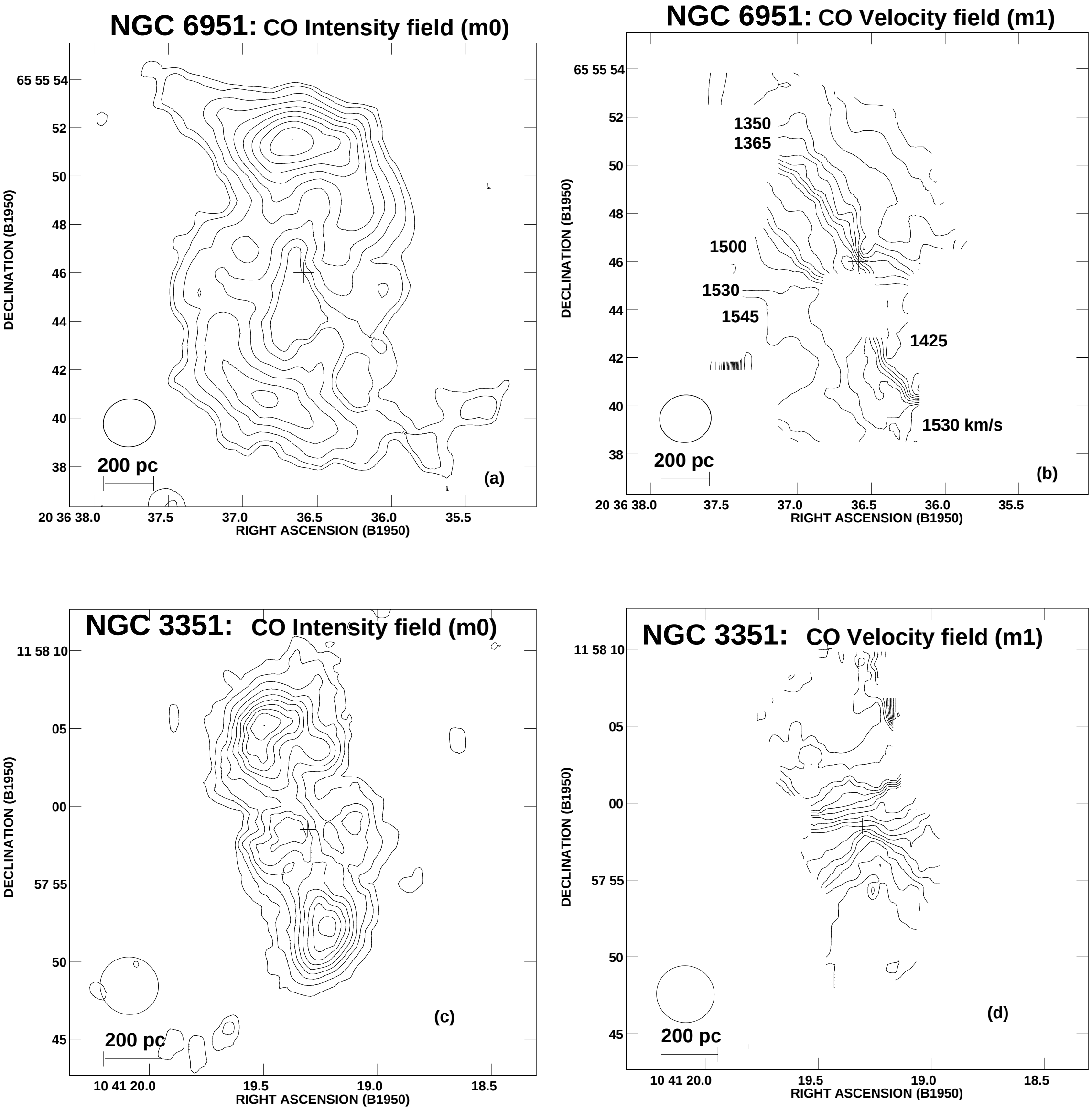

Fig. 15— Molecular gas kinematics and distribution in the individual non-starbursts: As in Fig. 14, but for non-starbursts NGC 6951 (a-b), NGC 3351 (c-d), and NGC 4314 (e-f). NGC 6951 has two spiral-shaped CO arms where the CO emission peaks at a radius r $\sim 6''$ (570 pc). NGC 3351 hosts two CO peaks at a radius r $\sim 7''$ (350 pc). In NGC 4314, there is a relatively circular CO ring of $8''$ (400 pc) radius from which extend two CO spurs/streams. The CO peaks in both NGC 6951 and NGC 3351 lie almost along the minor axis of the large-scale stellar bar. The CO arms in NGC 6951, the fainter emission around the CO peaks in NGC 3351, and the two CO spurs in NGC 4314 intersect the dust lanes on the leading edge of the large-scale stellar bar and show non-circular motions.

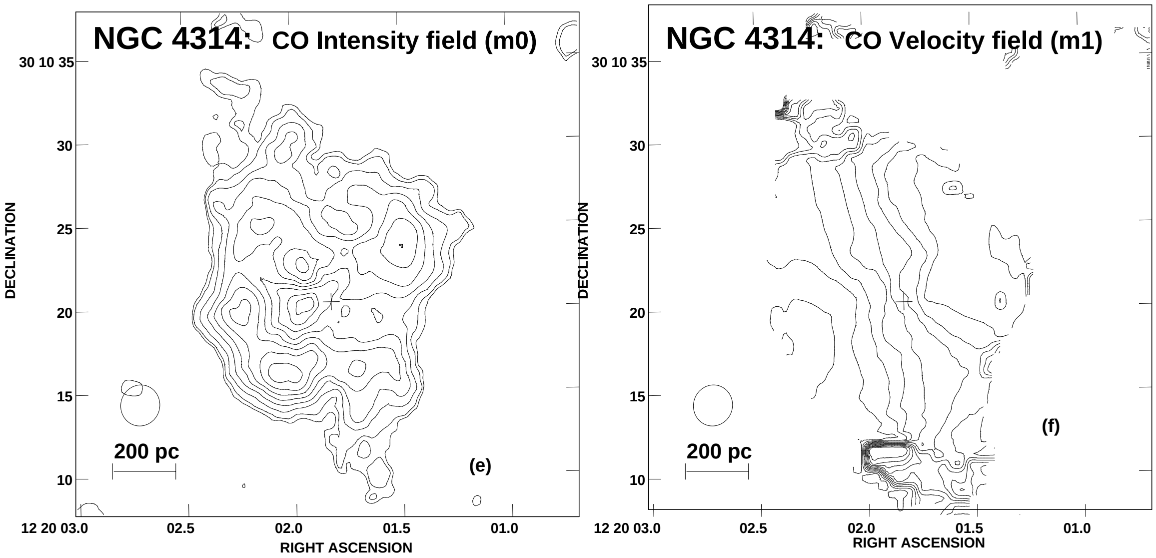
NGC 4314: CO Intensity field (m0)
30 10 35
30
25
20
15
10
DECLINATION
200 pc
(e)
12 20 03.0
02.5
02.0
01.5
01.0
RIGHT ASCENSION
NGC 4314: CO Velocity field (m1)
30 10 35
30
25
20
15
10
DECLINATION
200 pc
(f)
12 20 03.0
02.5
02.0
01.5
01.0
RIGHT ASCENSION

TABLE 1
THE SAMPLE

NGC (1)	R.A. (1950.0) (2)	Dec (1950.0) (3)	Type (RC3) (4)	i (deg) (5)	D (Mpc) (6)	D_{25} (') (7)	$m_{\rm B}$ (8)	Notes (9)
				CIRCUMNUCLEAR STARBURSTS				
NGC 470	01:17:10.5	03:08:53	SABb(rs)	57	30.5	3.2	12.37	D,HII
NGC 2782 (Arp 215)	09:10:54.1	40:19:18	SABa(rs)pec	30	34	3.9	12.0	D,HII
NGC 3504	11:00:28.1	28:14:35	SABab(s)	22	20.0	2.6	11.74	D,HII
NGC 4102	12:03:51.6	52:59:23	SABb(s)	52	17.0	3.1	12.13	D,L
NGC 4536	12:31:53.6	02:27:50	SABbc(rs)	66	18.0	6.3	10.60	HII,L
				CIRCUMNUCLEAR NON-STARBURSTS				
NGC 3351	10:41:19.7	11:58:00	SBb(r)	46	10.1	7.5	10.28	HII
NGC 3359	10:43:21.1	63:29:11	SBc(rs)	55	19.2	7.2	10.83	HII
NGC 4314	12:20:2.1	30:10:25	SBa(rs)	21	9.7	4.2	11.28	L
NGC 4569	12:34:18.7	13:26:20	SABab(rs)	64	16.8	8.8	9.86	HII,L
NGC 6951	20:36:37.7	65:55:48	SABbc(rs)	44	18.8	3.7	11.18	SEY2

NOTE.— Columns are : (1) NGC number; (2) (3) Right Ascension and Declination (Equinox 1950.0) of the optical center, from the Third Reference Catalog of Bright Galaxies, hereafter RC3 (de Vaucouleurs et al. 1991); (4) Hubble types from RC3; (5) i in degrees, the inclination of the galaxy. Sources are : NGC 2782 (Jogee et al. 1998, 1999), NGC 3351 (Grosbol 1985), NGC 3359 (Martin & Roy 1995), NGC 6951 (Grosbol 1985), NGC 4314 (Benedict et al. 1996), and the Nearby Galaxies (NBG) Catalogue (Tully 1988) for the remaining galaxies. (6) D, the adopted distance in Mpc. Sources are : NGC 4536 (Saha et al. 1996), NGC 3504 (Kenney et al. 1993), NGC 2782 (Jogee et al. 1998, 1999), and for the remaining galaxies, the NBG Catalogue (Tully 1988) which assumes a Hubble constant of 75 km s^{-1} Mpc^{-1}; (7) D_{25} in arcminutes, the diameter of the isophote where the surface brightness is 25 magnitude arcsecond^{-2} in blue light. Values are from the NBG Catalogue (Tully 1988). (8) $m_{\rm B}$, the blue apparent magnitude corrected for reddening, from the NBG Catalogue (Tully 1988); (9) Description of the nuclear activity and optical emission line spectrum of the galaxy. D denotes a galaxy belonging to Devereux's (1989) sample of circumnuclear starbursts. H denotes an HII region-like spectrum (Giuricin et al. 1994), L denotes a LINER (Guiricin et al. 1994), and SEY2 denotes a Seyfert 2 (Guiricin et al. 1994; Wozniak et al. 1995).

Table 2
Single Dish CO Luminosities and Tracers of Star Formation

NGC	$S_{\rm CO,S}$ 45″ (Jy kms^{-1})	$L_{\rm CO}$ 45″ ($L_\odot$)	$L_{\rm RC}$ 45″ ($L_\odot$)	$L_{10\mu{\rm m}}$ 5″ − 10″ ($L_\odot$)	$L_{\rm FIR}$ Global ($L_\odot$)	$L_{\rm RC}/{\rm L_{CO}}$ 45″
(1)	(2)	(3)	(4)	(5)	(6)	(7)
CIRCUMNUCLEAR STARBURSTS						
470	68	3.83	4.17	9.12	10.21	2.10
2782	266	4.50	4.72	9.02	10.42	1.60
3504	450	4.30	4.60	9.11	10.31	1.99
4102	572	4.26	4.50	9.23	10.55	1.74
4536	607	4.33	4.35	8.77	10.32	1.03
CIRCUMNUCLEAR NON-STARBURSTS						
3351	479	3.73	3.28	7.51	9.52	0.35
3359	162	3.82	3.19	–	9.90	0.23
4314	251	3.41	2.62	<7.38	8.78	0.16
4569	870	4.43	3.62	8.48	9.98	0.15
6951	496	4.28	3.85	–	9.95	0.37

Note.— Columns are : (1) NGC number; (2) $S_{\rm CO,S}$ in Jy km s^{-1}, the single dish CO flux measured in the central 45″ for all galaxies, except NGC 4314 where the aperture is 55″. $\rm S_{CO,S}$ was estimated from observations with the Five College Radio Observatory (FCRAO) 14-m dish (Young et al. 1995) and NRAO 12-m single dish observations (Sage 1993). To derive flux densities $\rm S_{CO,S}$ in units of Jy km s^{-1} from the integrated intensity $\rm I_{CO}$ in units of K($\rm T_A{}^*$) km s^{-1}, we adopted a main beam efficiency of 42 Jy K^{-1} and 35 Jy K^{-1} respectively for the FCRAO (Young et al. 1995), and NRAO (e.g., Maiolino et al. 1997) observations, and a source-beam coupling efficiency of 0.7; (3) $L_{\rm CO}$ in logarithmic units of $L_\odot$, the single dish CO luminosity determined from $S_{\rm CO,S}$; (4) $L_{\rm RC}$ in logarithmic units of $L_\odot$, the RC luminosity at 1.5 GHz in the central 45″ (Condon et al. 1990); (5) $\rm L_{10_{\mu m}}$ in logarithmic units of $L_\odot$, the nuclear 10 μm luminosity in a central 5″-10″ aperture (Giuricin et al. 1994); (6) $L_{\rm FIR}$ in logarithmic units of $L_\odot$, the far-infrared luminosity from the whole galaxy , measured in a bandpass 80 μm wide centered on a wavelength of 82.5 μm, from the IRAS Bright Galaxy Sample (Soifer et al. 1989); (7) $L_{\rm RC}/L_{\rm CO}$, the ratio of the RC luminosity at 1.49 GHz to the CO luminosity. Both luminosities are measured within the same 45″ aperture, except for NGC 4314.

Table 3
External Disturbances and Large-Scale Stellar Bars

NGC (1)	Bar Type[f] (2)	Evidence for External Disturbances (3)
		CIRCUMNUCLEAR STARBURSTS
470	SAB	Outer disk has asymmetric Hα emission[h] and shows evidence for warping. A recent interaction with 474[b] is likely.
2782	SAB	Outer galaxy shows HI tails, optical tails, and ripples.[c,d,e]. A close and intermediate mass-ratio interaction with a disk galaxy[c] is likely.
3504	SAB	Belongs to a group. [k] Possibly interacting with the small galaxy 3512.
4102	SAB	Belongs to a group whose brightest member is NGC 3992.[j]
4536	SAB	Is in the Southern Extension of the Virgo cluster.[l] Possibly interacting with 4527.
		CIRCUMNUCLEAR NON-STARBURSTS
3351	SB	Belongs to a group. [k]
3359	SB	Shows evidence[m,n] for a bar which is young and possibly tidally triggered. Has a possible small bound companion.[g]
4314	SB	Belongs to a group.[11] Outer disk is unusually gas poor. The total HI to H_2 mass ratio is unusually low (~ 0.02)
4569	SAB	Is located in projection within 2 deg of the center of the Virgo Cluster. Has anemic spiral structures[o] and a truncated HI disk.[i] Optical images [a] suggest an outer warped disk. In the inner 3.5 kpc radius, the K-band image[h] shows an asymmetric bar, and the molecular gas has very disturbed kinematics[h] .
6951	SAB	Isolated galaxy.

Note.— Columns are : (1) NGC number; (2) Bar Type according to RC3 (de Vaucouleurs et al. 1991); (3) Evidence for External Disturbances

References.— a. Sandage & Bedke 1994; b. Schweizer & Seitzer 1988; c. Smith 1994; d. Jogee et al. 1998 ; e. Jogee et al. 1999; f. RC3 (de Vaucouleurs et al. 1991); g. Ball 1986; h. Jogee 1999 ; i. Giovanelli & Haynes 1983; j. Geller & Huchra 1983 ; k. Tully 1988; l. Bingelli, Sandage, & Tammann 1985; m. Friedli, Benz, & Kennicutt 1994; n. Martin & Roy 1995; o. van den Bergh 1976;

Table 4
CO (J=1-> 0) observations & channel maps

NGC (1)	Synthesised Beam (2)	Weight (3)	R.m.s. noise (mJy/Beam) (4)	T_B for 1 Jy/Beam (K) (5)
470	3.61"x3.46"= 550x530 pc	U	22.0	7.4
2782	2.14"x1.52"= 364x258 pc	U	13.0	28.2
	2.62"x1.98"= 445x337 pc	N	10.5	17.7
3504	2.50"x2.40"= 250x240 pc	U	35.0	15.3
4102	2.40"x1.96"= 204x167 pc	U	15.0	19.5
	3.12"x2.56"= 265x218 pc	N	13.0	11.5
4536	2.63"x1.88"= 235x170 pc	U	15.0	18.6
	2.82"x2.37"= 255x215 pc	N	12.0	13.7
3351	2.38"x2.34"= 120x118 pc	U	30.0	16.5
3359	3.38"x2.91"= 324x279 pc	N	16.0	9.3
4314	2.29"x2.17"= 110x105 pc	U	28.0	18.5
	3.12"x2.70"= 150x130 pc	N	22.0	10.9
4569	2.65"x2.01"= 225x170 pc	U	16.0	9.7
	3.22"x2.95"= 275x251 pc	N	14.0	17.4
6951	2.28"x2.11"= 110x102 pc	U	19.2	19.1

Note.— Columns are : (1) NGC number; (2) The size of the synthesized beam ; (3) The weighting used for the channel maps: 'U' refers to uniform and 'N' to natural weighting; (4) The r.m.s. noise in mJy beam^{-1} for the channel maps; (5) The equivalent brightness temperature (T_B) in K for 1 Jy beam $^{-1}$.

Table 5
Cicumnuclear Molecular Properties

NGC (1)	$S_{\rm CO,I}$ (Jy kms^{-1}) (2)	$M_{\rm H2}$ ($M_{\odot}$) (3)	$V_{\rm sys}$ (km s^{-1})) (4)	$f_{\rm SD}$ (%) (5)
		CIRCUMNUCLEAR STARBURST		
470	53	5.0E8	2350	80
2782	184	2.3E9	2555	65
3504	280	1.2E9	1535	71
4102	450	1.4E9	835	80
4536	355	1.2E9	1800	60
		CIRCUMNUCLEAR NON-STARBURSTS		
3351	241	2.7E8	780	60
3359	20	8.0E7	-	12[1]
4314	248	2.6E8	983	92
4569	550	1.7E9	-235	65
6951	299	1.2E9	1431	60

Note.— Columns are : (1) NGC number; (2) $S_{\rm CO,I}$ in Jy km s^{-1}, the flux detected by the OVRO interferometric observations; (3) $\rm M_{H2}$ in solar units, the mass of molecular hydrogen corresponding to $S_{\rm CO,I}$, if one assumes a standard Galactic CO-to-H_2 conversion factor; (4) $V_{\rm sys}$ in km s^{-1}, the systemic velocity estimated from the moment 1 map. (5) $f_{\rm SD}$, the fraction of the single dish flux detected by the interferometric observations. See text for a discussion of the low $f_{\rm SD}$ for NGC 3359.

Table 6
Molecular Environemnts in the Circumnuclear Region vs. the Outer Disk

Quantities [a]	Outer Disk of Normal Sa-Sc Spirals	Inner 500 pc radius of Sample Starbursts and Non Starbursts	Inner 500 pc radius of ULIRG Arp 220
(1) $M_{\rm gas,m}$ [$M_\odot$]	$\leq$ few $\times 10^9$ [b]	Few $\times$ (10^8-10^9) [c]	3×10^9 [d]
(2) $M_{\rm gas}/M_{\rm dyn}$ [%]	< 5 [e]	10 to 30 [c]	40 to 80 [d]
(3) SFR [$M_\odot$ yr^{-1}]	-	0.1-11 [c]	> 100[g]
(4) $\Sigma_{\rm gas,m}$ [$M_\odot$ pc^{-2}]	1-100 [f]	500 to 3500 [c]	4×10^4 [d]
(5) σ [km s^{-1}]	6-10[h]	10 to 40[i]	90[g]
(6) κ [km s^{-1} kpc^{-1}]	< 100[j]	800 to 3000 [c]	> 1000[g]
(7) $\Sigma_{\rm crit}$ [$M_\odot$ pc^{-2}]	< 10 [k]	500-1500 [l]	2200 [m]
(8) $t_{\rm GI}$ [Myr]	>10 [k]	0.5-1.5 [l]	0.5 [m]
(9) $\lambda_{\rm J}$ [pc]	Few $\times$ (100-1000) [k]	100-300 [l]	90 [m]
(10) $M_{\rm J}$ [$M_\odot$]	Few $\times$ (10^7-10^6) [k]	Few $\times$ (10^7-10^8) [l]	8×10^8 [m]

Note.—Rows are : (1) $M_{\rm gas,m}$ in $M_\odot$, the molecular gas content including hydrogen and helium. A standard CO-to-H_2 conversion factor and a solar metallicity are assumed; (2) $M_{\rm gas,m}/M_{\rm dyn}$ in %, the ratio of molecular gas mass to dynamical mass; (3) $\Sigma_{\rm gas,m}$ in $M_\odot$ pc^{-2}, the molecular gas surface density; (4) Σ_{SFR} in $M_\odot$ yr^{-1} pc^{-2}, the SFR per unit area; (5) σ in km s^{-1}, the gas velocity dispersion; (6) κ in km s^{-1} kpc^{-1}, the epicyclic frequency; (7) $\Sigma_{\rm crit}$ in $M_\odot$ pc^{-2}, the critical density for the onset of gravitational instabilities as defined in § 5.3.1, with $\alpha = 0.7$; (8) $t_{\rm GI} = Q/\kappa$ in Myr, the growth timescale of the most unstable wavelength associated with gravitational instabilities, assuming $Q \sim 1$; (9) $\lambda_{\rm J}$ in pc, the Jeans length (10) $M_{\rm J}$ in $M_\odot$, the Jeans mass.

Note.— [a] Typical values are quoted for the quantities. Individual cases may vary; [b] Young & Scoville 1991; [c] This work; [d] Sakamoto et al. (1999), for a self-gravitating gas disk. Quoted mass is the sum for Arp 220 W and E; [e] Binney & Tremaine 1987; [f] Devarheng et al. 1994; [g] Scoville, Yun, and Bryant 1997 [h] Dickey et al. 1990; [i] The upper limit for the velocity dispersion is quoted after correcting for beam smearing; [j] Larson 1988; [k] For the outer disk, (7) to (10) are computed for $\kappa <$ 100 km s^{-1} kpc^{-1}, $\sigma \sim 6$ km s^{-1}, and $\Sigma_{\rm gas,m}$ = 10-100 $M_\odot$ pc^{-2}; [l] Quantities (7) to (10) are computed at r=250 pc in the circumnuclear starbursts and non-starbursts NGC 4102, NGC 4536, NGC 3504, NGC 3351 and NGC 4314; [m] Quantities (7) to (10) are computed for Arp 220 W assuming $\kappa \sim 2000$ km s^{-1} kpc^{-1}, $\sigma \sim 90$ km s^{-1}, and $\Sigma_{\rm gas,m} \sim 4 \times 10^4$ $M_\odot$ pc^{-2}.

Table 7
SF Rates from FIR, RC, and Brγ data

NGC (1)	Based on global $L_{\rm FIR}$ $L_{\rm FIR}$, SFR$_{\rm FIR}$ ($L_\odot$, $M_\odot$ yr^{-1}) (2)	Based on RC ν, S_ν, $R_{\rm RC}$, SFR$_{\rm RC-N}$ (GHz, mJy, pc, $M_\odot$ yr^{-1}) (3)	Based on Brγ $R_{Br\gamma}$, $N_{\rm Ly}$, SFR$_{Br\gamma}$ (pc, s^{-1}, $M_\odot$ yr^{-1}) (4)
	CIRCUMNUCLEAR STARBURSTS		
470	10.21, 6.3	1.5, 26.6[a], 1680, 2.8	-
2782	10.42, 10.2	1.5, 107[a], 2210, 13.8	1650, 5.0E53[g], 5.6
		4.9, 40[e], 1700, 11.6	
3504	10.31, 8.0	1.5, 230[a], 800, 10.2	945, 1.5E53[g], 2.8
4102	10.55, 13.8	1.5, 227[a], 1105, 7.3	945, 9.2E52[g], 1.1
4536	10.32, 8.1	1.5, 149[a], 1800, 5.4	840, 4.0E53[g], 4.8
		4.9, 61[f], 900, 4.9	
	CIRCUMNUCLEAR NON-STARBURSTS		
3351	9.52, 1.3	1.5, 28[b], 1000, 0.3	490, 6.0E52[g], 0.5
3359	9.90, 3.1	1.5, 50[a], 20160, 2.1	-
4314	8.78, 0.2	1.5, 12.5[c], 3640, 0.1	-
4569	9.98, 3.7	1.5, 83[c], 8420, 2.5	-
6951	9.95, 3.5	4.9, 14[e], 750, 1.2	-

Note.— Columns are : (1) NGC number; (2) $L_{\rm FIR}$ in logarithmic units of $L_\odot$, the global FIR luminosity; SFR$_{\rm FIR}$ in $M_\odot$ yr^{-1}, the global SFR for the entire galaxy; (3) ν in GHz, the frequency of the RC observations; S_ν in mJy, the RC flux density; R_{RC-N} in pc, the radius within which more than 90 % of the RC emission is concentrated; SFR$_{RC-N}$ in $M_\odot$ yr^{-1}, the SFR within R_{RC}, estimated from the non-thermal component of the radio continuum flux density; (4) $R_{Br\gamma}$ in pc, the aperture radius for the Brγ observations; N_{Ly} in s^{-1}, the number of Lyman continuum photons per seconds from Puxley et al. (1990); SFR$_{Br\gamma}$ in $M_\odot$ yr^{-1}, the SFR within $R_{Br\gamma}$

References.—a. Condon et al. 1990; b. Condon, Anderson, & Broderick 1995; c. Condon 1987 ; d. Hummel et al. 1985; e. Saikia et al. 1994; f. Villa et al. 1990; g. Puxley et al. 1990

TABLE 8
ADOPTED CIRCMUNUCLEAR SFRS OVER RADIUS OF CO EMISSION

NGC (1)	$R_{\rm CO}$ (pc) (2)	$M_{\rm H2}$ ($M_\odot$) (3)	$\rm SFR_{CO}$ ($M_\odot$ yr^{-1}) (4)	$\rm SFR_{CO}/M_{H2}$ (yr^{-1}) (5)	$t_{\rm SFR}$ (10^8 yrs) (6)
		CIRCUMNUCLEAR STARBURST			
470	1100	5.0E8	3	6E-9	2
2782	1530	1.8E9	11	6E-9	2
3504	1300	1.2E9	10	8E-9	1
4102	1275	1.4E9	7	5E-9	2
4536	1300	1.2E9	5	4E-9	2
		CIRCUMNUCLEAR NON-STARBURSTS			
3351	600	5.3E8	0.5	9E-10	11
4314	590	2.3E8	<0.1	< 4E-10	> 25
4569	1680	1.6E9	<1.2	> 7E-10	> 14

NOTE.— Columns are : (1) NGC number; (2) $R_{\rm CO}$ in pc, the radius of CO emission; (3) $M_{\rm H2}$ in $M_\odot$, the mass of molecular hydrogen within a radius $R_{\rm CO}$; (4) $\rm SFR_{CO}$ in $M_\odot$ yr^{-1}, the SF rate within $R_{\rm CO}$; (5) ($\rm SFR_{CO}/M_{H2}$) in yr^{-1}, the SFR per unit mass of molecular hydrogen; (6) $t_{\rm SFR}$) in 10^8 years, the average gas consumptiuon timescale by SF given by ($M_{\rm H2}/\rm SFR_1$)

TABLE 9
PRIMARY BAR PROPERTIES AND DYNAMICAL RESONANCES

NGC (1)	Bar (2)	ϵ_1 (3)	PA_1 (4)	a_1 (5)	$M_{\rm gas,m}$ (6)	$\frac{M_{\rm gas,m}}{M_{\rm dyn}}$ (7)	$\Omega_{\rm p}$ (8)	R_{OILR} (9)	R_{IILR} (10)
470	AB	0.55^a	14^a	4.8^a	2E8	30	···	···	···
3504	AB	0.58^b	135^b	3.0^e	8E8	20	< 76	> 900	< 200
4102	AB	0.45^e	62^e	1.8^e	8E8	25	< 115	>500	< 250
4536	AB	0.40^b	$140^{b,c}$	3.1^c	1E9	30	< 50	> 800	< 200
3351	B	0.57^d	115^c	$2.2^{c,d}$	2E8	17	< 85	> 300	< 300
3359	B	0.68^d	24^c	2.9^d	···	···	···	···	···
4314	B	0.69^a	143^a	3.6^a	2E8	9	< 78	> 700	< 200
4569	AB	···	15^e	···	2E8	···	···	···	···
6951	AB	0.59^a	85^a	5.2^a	3E8	21	< 43	> 650	< 300

NOTE.— Columns are : (1) NGC number; (2) Bar type from RC3 (de Vaucouleurs et al. 1991): B denotes a strong bar, and AB a bar of intermediate stength; (3) (4) (5) ϵ_1, PA_1 in deg, a_1 in kpc, the ellipticity, position angle, and semi-mjor axis of the large-scale stellar bar; (6) $M_{\rm gas,m}$ [r=300] in $M_\odot$, the molecular gas mass enclosed within a 300 pc radius. A standard CO-to-H_2 conversion factor and a solar metallicity are assumed; (7) $\frac{M_{\rm gas,m}}{M_{\rm dyn}}$ [r=300], the ratio of molecular gas mass to dynamical mass within a 300 pc radius; (8) Upper limit on $\Omega_{\rm p}$ in km s^{-1} kpc^{-1}, the primary bar pattern speed; (9) Upper limit on R_{OILR} in pc, the radius of the Outer Inner Lindblad Resonance; (10) Lower limit on R_{IILR} in pc, the radius of the Inner Inner Lindblad Resonance.

REFERENCES.— a. Friedli et al. 1996; b. Pompea & Rieke 1990; c. Shaw et al. 1995; d. Martin 1995; e. This work.